Università Politecnica delle Marche
Scuola di Dottorato di Ricerca in Ingegneria dell'Informazione
Curriculum in Ingegneria biomedica, elettronica e delle telecomunicazioni

Optofluidic microlasers based on femtosecond micromachining for LAB-ON-CHIP technology

Ph.D. Dissertation of:

Paolo Spegni

Advisor:

Prof. Francesco Simoni

Curriculum supervisor:

Prof. Francesco Piazza

XVI edition – new series

Acknowledgements

First and foremost I want to thank my supervisor Francesco Simoni for providing me the opportunity to complete this Ph.D. at Department of Sciences and Engineering of Matter, of Environment and Urban Planning (SIMAU) at the Polytechnic University of Marche. It has been an honour to work in a dynamic and creative group composed by heterogeneous group of students, technicians, researchers and professors. Your hard work and passion has always been an example and an inspiration in this three-year period.

It was a great honour to collaborate with Dott. Luigino Criante and the staff of the FemtoFab laboratory at the Centre for NanoScience and Technology of the Italian Institute of Technology (CNST-IIT) in Milan, where several powerful facilities are present and great guys such as Silvio Bonfadini who realized all the characterized samples and whom a close friendship is growing with.

The final thanks to the COST action MP1205 that allowed me to attend two great and interesting Summer schools, and allowed me to meet visiting students, but also to visit the Institute for Optics and Nanophotonics (IONAS) at the Karlsruhe University of Applied Science in Germany and the Department of Micro and Nanotechnology at the Technological University of Denmark where clever Professors and students have increased the desire for working in science and maintain international friendship.

Abstract

In this thesis work I report the realization and characterization of different optofluidic microlasers based on Fabry-Perot and hemispherical cavity fabricated by exploiting two fabrication techniques: the femtosecond laser micromachining and the inkjet printing technology.

In this way a standard Fabry-Perot cavity has been integrated into an optofluidic chip. The microlasers were tested with different laser dyes such as Rhodamine 6G, Pyrromethene and DCM. The best result was an emission bandwidth below ~0.6 nm and a quality factor $Q \sim 10^3$ measured when using Rhodamine 6G dissolved in ethanol at concentration of 5mMol as active medium. Laser emission was detected at a threshold energy density as low as $1.8\ \mu J/mm^2$ about one order of magnitude lower than state-of-the-art optofluidic lasers. These performances and mechanical and chemical robustness of these devices fully embedded in glass make them promising for future development in optofluidic chips to be exploited in biosensing applications.

Contents

Introduction

The lab-on-chip technology is growing very quickly because of the wide range applications in the biomedical area and sensing for environment control and security. In this frame, it is a challenge to realize a complete optical lab in a single chip. This chip should contain the optical source (laser), the optical control elements (waveguides, lenses, polarizers, etc.), the sample analysis channels and the light detector. The advantages of developing of such technology will be to get high sensitivity, use of low testing volumes, low cost and device portability. In order to get these results, it is important to develop a suitable microfluidic laser that acts as a light source in this optical lab in a chip.

The first microfluidic laser has been realized at the Technical University of Denmark by Anders Kristensen and coworkers using a transversal Fabry-Perot (F-P) resonator of $10um$ with a Rhodamine 6G solution in ethanol at concentration of $10mMol$. After this demonstration several different devices were developed using DFB (Distributed Feedback) to get narrow light emission. Fabry-Perot resonators have also been proposed and tested with cavity mirrors coated either on optical fiber surfaces or on the side of microfluidic channels. Most of the proposed microfluidic lasers were fabricated in polymeric materials thus presenting lack robustness and mechanical stability. The motivation of the present work is to overcome these problems realizing an optofluidic laser full embedded in glass chip with state of the art performances.

This work has been carried out in collaboration with the group led by Dott. Luigino Criante at the Center for Nano Science and Technology at Italian Institute of Technology (CNST-IIT). We have designed different cavities in collaboration with the IIT group where devices were fabricated. All the measurements and tests of the characteristics of the devices were performed at the SIMAU Department of the Polytechnic University of Marche.

This presentation is organized as follows. In chapter 1 a background of laser properties has reported according with the main books in the field. Some details are also given on the laser dyes which have been used in this work. In the second chapter the different fabrication techniques for microfluidic chips are described with particular emphasis on

the Femtosecond Micromachining technology that has been exploited to fabricated the devices used here. Chapter 3 deal with design and fabrication of our devices describing the different resonator geometries which have been characterized in chapter 4. The chapter 5 reports the experimental details and the results obtained for the different tested devices. After a short conclusion the appendix presents a report of the activities performed during the stages in the group of Prof. Christian Karnutsch at the Institute of Optofluidics and Nanophotonic (IONAS) of the Applied Science University (Karlsruhe, Germany November 2015) and in the group of Prof. Anders Kristensen at the Department of Micro and Nanotechnology (DTU Nanotech) at the Technical University of Denmark (Lyngby, Denmark, August-September 2016 and September 2017). These activities concerned the development of technologies correlated to the main subject of this work and more in general to the area of microfluidic devices. Finally a copy of the published papers is reported.

1 Background on lasers

In this chapter the basic concepts describing the laser emission will be summarized. They are important both for a proper design of the laser cavity and to better understand the behaviour of the optofluidic microlasers characterized in this thesis.

The word ‘Lasers' is the acronym for Light Amplification by Stimulated Emission of Radiation. It is an oscillator at optical frequencies realized coupling a positive feedback to an amplifying medium. Many books deal with the physics of lasers, among them I refer to “Principle of Lasers” by O. Svelto and “Optical Electronics” by Amnon Yariv.

The light amplification is the consequence of stimulated emission. It is the process occurring when one electron is stimulated by an incident photon to make a downward transition from a high-energy state to a low-energy state. The result is the emission of a photon with the same characteristics of the incident one, that is coherent with it. Coupling this process with the feedback mechanism produced by the optical cavity laser radiation is generated with a high degree of coherence that is shown by the typical collimated monochromatic beam.

The achievement of the amplification condition in the medium requires a population inversion between the two energy levels involved in the process, since under thermal equilibrium the electron population in the low energy state is higher than in the high energy state. Therefore, it is necessary to provide energy to the medium through a pumping mechanism. Different pumping methods are found for different types of active media. The most common are electrical and optical methods. In this work Rhodamine 6G is used as active medium and it is optically pumped with external lasers. More information about Rhodamine 6G and pumping method are given in section 1.5.

A basic element of lasers is the optical cavity that provides the positive feedback mechanism necessary to get oscillations. The simplest optical resonator is realized by two highly reflecting flat and parallel mirrors. In this case the light travels orthogonal of them. Photons bounce from and back in the cavity and every time the electromagnetic wave passes through the active medium it increases the intensity. Increasing the pumping energy the population inversion increases until the optical amplification compensates the losses, thus achieving the oscillation condition.

1.1 Laser oscillator

The basic scheme of a laser (the electromagnetic oscillator at optical frequency) is depicted in Figure 1.1

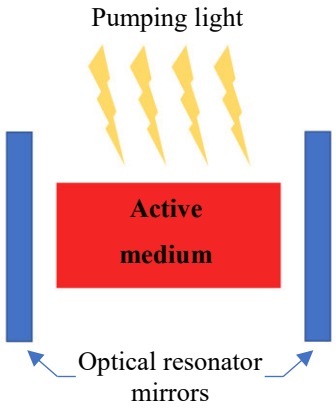

Figure 1.1 - Basic scheme of a laser: gain medium where population inversion take place by a pumping effect, and the optical cavity that allow that the part of the emetted light remain in the cavity

The oscillator is made by an active medium located inside an optical resonator. Active medium means: a medium where a population inversion is achieved my providing energy through a pumping mechanism. Under these conditions the material acts as optical amplifier. If a suitable method of feedback is provided, the amplifier may turn into an oscillator. Feedback is given by the optical cavity, that can be simply realized by two parallel flat mirrors (Fabry-Perot cavity). It is useful to recall the basic oscillation conditions for the mentioned Fabry-Perot resonator.

1.2 Fabry-Perot resonator

As already mentioned this oscillator is realized by a couple of flat mirrors with an active medium of length d located in between. One mirror is semi-transparent, so that a small part of the incident field can come out from the cavity, while the reflected part traveling through the active medium is amplified. Starting from the incoming field E_i we calculate the transmitted electric field E_t considering the multiple reflections and the phase contribution of the active media. Defining as: t_1, r_1 and t_2, r_2 the beam transmission and reflection coefficients for the field of the two mirrors; $e^{-ik'd}$ the propagation factor corresponding to a cavity transit, where k' is the complex wavevector that takes into account both gain and losses.

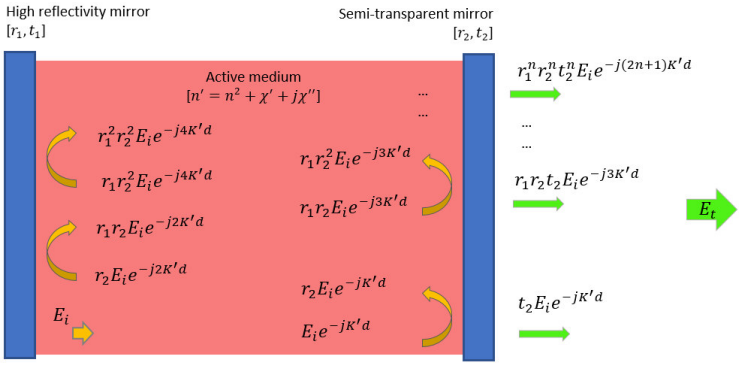

Figure 1.2- Model used to analyse a laser oscillator. Gain material with inverted atomic population and complex propagation constant k'(ω) located between two reflecting mirrors

The complex constant propagation can be written as:

$$k'(\omega) = k + k\,\frac{\chi'(\omega)}{2n^2} - ik\frac{\chi''(\omega)}{2n^2} - i\frac{\alpha}{2} \tag{1.1}$$

Where $k - i\alpha/2$ is the propagation constant of the medium at frequencies well removed from that of the laser transition in which α accounts for the distributed passive losses of the medium and $\chi(\omega) = \chi'(\omega) - i\chi''(\omega)$ is the complex dielectric susceptibility at the considered resonance [2].

The total outgoing wave is the sum of all the partial waves that come out from the semitransparent mirror after each round trip of the wave in the cavity; looking at Figure 1.2 the transmitted field E_t is easily calculated as:

$$E_t = t_1 t_2 E_i e^{-ik'd}\left[1 + r_1 r_2 e^{-i2k'd} + r_1^2 r_2^2 e^{-i4k'd} + \cdots\right] \tag{1.2}$$

The term inside square brackets is a well-known geometric series, therefore:

$$E_t = E_i\left[\frac{t_1 t_2 e^{-ik'd}}{1 - r_1 r_2 e^{-ik'd}}\right] = E_i\left[\frac{t_1 t_2 e^{-i(k+\Delta k)d} e^{(\gamma-\alpha)d/2}}{1 - r_1 r_2 e^{-i(k+\Delta k)d} e^{(\gamma-\alpha)d}}\right] \tag{1.3}$$

where

$$k' = k + \Delta k + i\,(\gamma + \alpha)/2$$

with [2]

$$\Delta k = k\frac{\chi'(\omega)}{2n^2} \tag{1.4}$$

$$\gamma = -k\frac{\chi''(\omega)}{n^2} = (N_2 - N_1)\frac{\lambda^2}{8\pi n^2 t_{spont}}g(\nu) \tag{1.5}$$

Under population inversion ($N_2 > N_1$) then $\gamma > 0$ the denominator of (1.3) decreases by increasing the power gain $|E_t/E_i|^2$. This ratio becomes infinite when the denominator of (1.3) becomes zero:

$$r_1 r_2 e^{-i(k+\Delta k)d} e^{(\gamma-\alpha)d} = 1 \tag{1.6}$$

This corresponds to a finite transmitted wave E_t with a zero incicent wave, $E_i = 0$ and represents the case of a wave that, after a round trip, keeps the same amplitude and the same phase excepts for some integral multiple of 2π. In fact, from (1.6) we get two separate conditions. From the real part we can take out the *gain condition*:

$$r_1 r_2 e^{(\gamma(\omega)-\alpha)d} = 1 \tag{1.7}$$

Therefore, the threshold gain is:

$$\gamma_t(\omega) = \alpha - \frac{1}{d}\ln(r_1 r_2) \tag{1.8}$$

Combining (1.5) and (1.8) it is possible write the population inversion density at threshold:

$$N_t \equiv (N_2 - N_1)_t = \frac{8\pi n^2 t_{spont}}{g(\nu)\lambda^2}\left(\alpha - \frac{1}{d}\ln(r_1 r_2)\right) \tag{1.9}$$

Where the lineshape $g(\nu)$ represents the a priori probability for a given spontaneous emission with photons whose frequency is ν; t_{spont} indicate the spontaneous emission lifetime [1, 2]. The expression (1.9) is also often written in a different form:

$$N_t = \frac{8\pi n^2 t_{spont}}{g(\nu)\tau_c\lambda^2} \tag{1.10}$$

where τ_c is the cavity decay constant which takes into account both the average losses and reflectance of mirrors [2].

The physical meaning of this condition is very simple: after each round trip in the cavity gain must compensate the energy losses, thus making possible the stable oscillation of a wave with constant amplitude.

From the imaginary part of (1.6) we get the condition for the phase of the oscillating wave. By neglecting the small correction Δk , we have:

$$2kd = 2\pi m \quad m = 1,2,3, \ldots \tag{1.11}$$

Therefore, the wavelength of the oscillating modes must fulfil the condition:

$$d = m \ \frac{\lambda_m}{2} \quad with \ \ m = 1,2,3, \ldots \tag{1.12}$$

Then we can write the cavity modes in the frequency domain:

$$\nu_m = m \ \frac{c}{2nd} \quad with \ \ m = 1,2,3, \ldots \tag{1.13}$$

being *n* the refractive index of the medium. Therefore the distance between two modes is:

$$\Delta\nu = \nu_{m+1} - \nu_m = \frac{c}{2nd} \tag{1.14}$$

That can be also written in term of wavelength as:

$$\Delta\lambda = \frac{\lambda^2}{2nd} \tag{1.15}$$

Cavity length [μm]	**$\Delta\lambda$ (nm)**
50	2
150	0.7
700	0.15
1550	0.07

Table 1.1 The mode distance for F-P resonator at different cavity length

In the table below is shown the calculation of this parameter for different cavity lengths in the range of interest for our optofluidic laser, by taking as central emission wavelength $\lambda = 560nm$.

1.3 Output power of laser

The emitted power of laser strongly depends on the energy level structure of the active medium. For our optofluidic system, the active medium is given by a dye solution in ethyl alcohol or other fluids. This laser medium provides a four levels system as depicted in Figure 1.3.

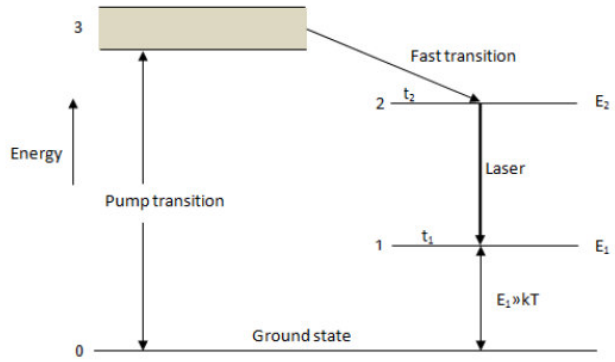

Figure 1.3 - Idealization scheme of the energy level model for a four-level laser

As described above, a threshold population inversion is required for the laser emission. This is achieved by optical pumping. An external light source excite electrons from the ground state 0 to some excited state 3 from where they decay by nonradiative emission to the upper laser level 2, in this way it is possible to get the necessary population inversion between the levels 2 and 1. Due to stimulated or spontaneous emission electrons transit from level 2 to level 1 by emission of a photon with frequency ν_{12}. Finally fast and nonradiative emission from level 1 to the ground state 0 allow keeping negligible population of level 1. As a consequence, the population inversion is $\Delta N = N_2 - N_1 \approx N_2$

By solving the rate equations for this four-level system is possible to get the emitted power written as [2]

$$P_e = P_s \left(\frac{R}{R_t} - 1 \right) \tag{1.16}$$

The equation indicates the total power generate by stimulated emission, when the pumping rate R is higher then the threshold pumping rate defined as $R_t = N_t\omega_{21}$; P_S indicates the power going into spontaneous emission at threshold. The equation 1.16 is plotted in Figure 1.4

It usually represents the signature of the onset of the laser action where the characteristic threshold behaviour is made clear by the sudden change of the slope of the emission power versus R.

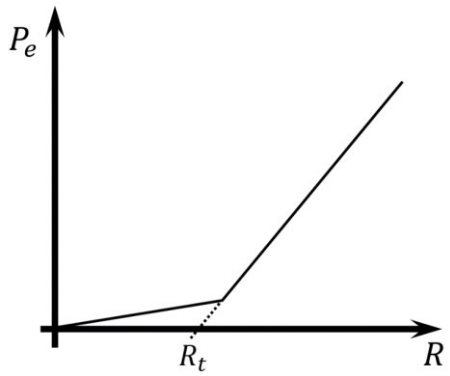

Figure 1.4 - Plot of typical output power versus pumping rate.

The curve shows how the weak linear rise of the emitted power below threshold (spontaneous emission) and a sudden change in the growth of the emitted power as the threshold condition, is reached due to the prevalence of the stimulated emission. The change of the slope is combined with the narrowing of the emitted spectrum in favour of one mode or a reduced set of modes selected by the cavity. As mentioned above, the spontaneous emission process generates photons with any frequency of the characteristic emission spectrum of the material and random phase, while during the stimulated emission, photons are emitted with the same frequency and same phase of the electromagnetic wave that stimulated the transition.

1.4 Optical resonator stability

The oscillation condition has been found for the Fabry-Perot cavity under the approximation of ideal flat and parallel mirrors with an infinite number of reflections of the oscillating field. From a geometrical point of view, this is possible only for a ray travelling in a direction orthogonal to the mirror surface. In facts, any other ray would exit from the cavity after some reflections. From this geometrical point of view, the stability of the cavity can be discussed in a more general way by taking into account

both the curvature radius of the mirror surface and the distance between the mirrors. In this way, it is possible to work out a stability condition for optical cavities made by two mirrors with curvature radii R_1 and R_2 located at a distance d. Stability is achieved if the following condition is fulfilled [2]

$$0 \leq \left(1 - \frac{d}{R_1}\right)\left(1 - \frac{d}{R_2}\right) \leq 1 \tag{1.17}$$

The stability condition is presented by the curved plotted in Figure 1.5. The shaded areas indicate the high losses where the stability condition (1.17) is violated and the clear areas are those where it is fulfilled.

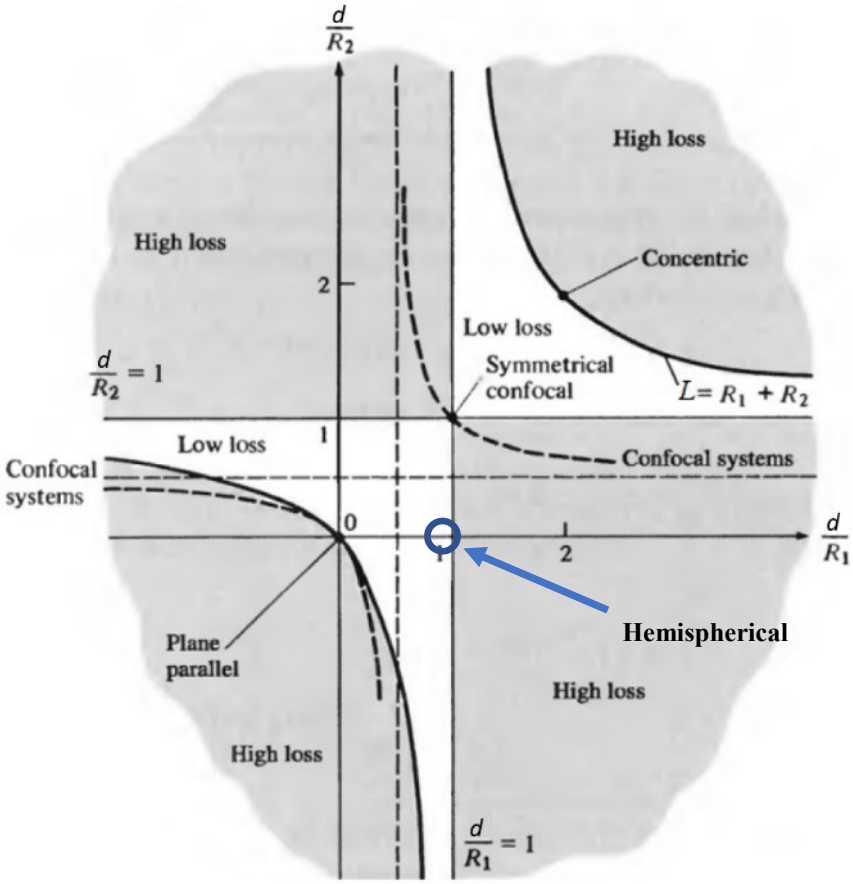

Figure 1.5 - Stability diagram of optical resonators.

It is observed that Fabry-Perot cavity falls on the edge of the stability curve. Use of curved mirror may provide less critical stability conditions.

1.5 Dye as active media

Organic dye molecules solved in different kind of liquids are frequently used as active media for lasers. Dye molecules have a broad emission spectrum that is very interesting to realize tunable lasers. Pumping is usually achieved by optical excitation, often are realized by other laser beams. The laser dye molecules are composed of organic

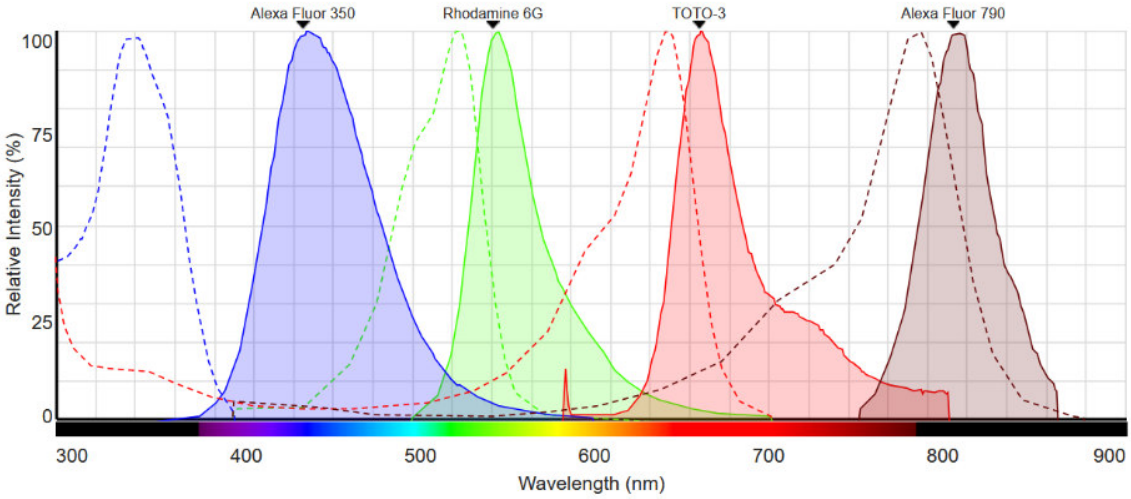

Figure 1.6 Absorption and emission spectra of some commercial dye laser. The dotted lines represent the absorption spectra and the continuous and filled curves show the emission spectra. Image from Thermo Fischer Scientific web page.

molecules where alternating single and double carbon bonds form long molecular chains. The results is a complex molecular structure due to the large molecular size, and the chemical bonds that give a very large dipole matrix element μ. These circumstances lead to many vibrational and rotational levels for each electronic state. Usually light coefficient is found in ultraviolet and visible region. [2, 3]. In Figure 1.6, are reported absorption and emission spectra of four commercial laser dyes, where is it also shown the typical Stokes shift between absorption and emission band. Moreover, absorption and emission spectra are lightly superimposed, this means that the emitted light is lightly self-absorbed by the dye molecules.

Figure 1.7 reports the scheme of the energy levels of a typical dye molecule. The useful four level system is provided by singlet states (S_0 and S_1in Figure 1.7) while the presence of triplet states may affect the working condition by reducing the efficiency of the laser emission. This occurs when energy transfer from singlet to triplet state reduce the population inversion of the singlet states. We will describe the transition process involved in a laser system and the energy levels using the rate-equation model.

Assuming that we can describe the photophysical property of the dye molecules with four-energy levels system shows in Figure 1.7 wherein every electronic state reports a set of vibrational levels (heavy lines) and rotational levels (light lines). S_0 and S_1 represent the fundamental and the first singlet excited state in which the total spin quantum number is $S_{sing} = 0$. T_0 and T_1 are the first and the second excited triplet state with total spin number $S_{trip} = 1$. By the selection rules that require $\Delta S = 0$ the singlet-triplet transition is forbitten, thus, when molecules are subjected to electromagnetic radiation the dye molecules absorb the pump light rising from the level S_0 to one of the S_1 vibrational levels. To minimize the system energy, molecules decay in a very short time to the lowest vibrational level of the S_1 level. This nonradiative process is in the picosecond time order, $\tau_{nr} \sim 10^{-12} sec$ and generates a thermal process heating the dye and the solution. From there (S_1) molecules decay emitting light by spontaneous or stimulated emission. In both of cases molecules decay to a vibrational level of S_0, and finally returns to the lower S_0 level by another nonradiative process. An important condition about the S_0 levels involved in the laser process it is far enough from ground level. In this way at thermal equilibrium its population density can be negligible. The photon energy, neglecting the molecular loss that generate the heating process, can be calculated as $vh = \left(E_{S_1} - E_{S_0}\right)$.

Even if it is a forbitten transition, some electrons in the lowest level of the S_1 may decay to the first excited triplet state. These processes, give rise to undesired losses. The

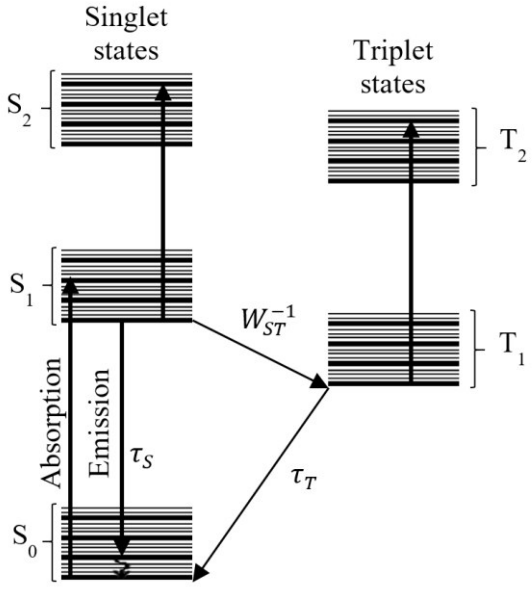

Figure 1.7 - Typical energy level for a dye solution. the singlet and triplet levels are shown in separate columns

emission band is characterized by homogeneous broadening, therefore is suitable for realising tunable laser emission. The large number of available dye molecules allow covering a broad range of emission in the visible depending on the usable pumping wavelengths. One of the most popular dye molecule for this purpose is Rhodamine 6G that we have used to test on our device. In addition to Rhodamine 6G, Pyrromethene 597 and DCM were also used for lasing tests. Usually, as solvent was used ethyl alcohol, but also Cinnamaldehyde and Quinoline was tested.

2 Fabrication technology in Optofluidics

The great majority of microfluidic lasers are realized with lithographic techniques, using polymers such as SU-8 or polydimethylsiloxane (PDMS). In particular, the SU-8 allows a flexible and inexpensive realization of devices exploiting the well-known technique of lithography, lamination and the use of sacrificial materials to realize single or multilayer devices. It can also be used to realize a master mould to imprint a microfluidic circuit on PDMS. It is really suitable to realize mould for the high aspect ratio achievable and because PDMS and SU-8 have low mutual adhesion. A high resolution "moulding" technology is Nanoimprinting Lithography that allows to replicate nanometric structure in polymers from a high precision mould, for instance made by electron beam lithography.

These processes are largely used also for multilayer devices, but the developing process require (expensive) masks and fine alignments between layers and masks. On the other hand, it is a challenge to realize a circular channel section, curved walls or variable section aperture. A flexible and innovative technique that allows a mask free, 3D fast microstructure fabrication and other is the Femtosecond Micromachining Technology that will be deeply described in section 2.3.

2.1 Soft lithography

It can be viewed as an evolution of photolithography. Originally, standard photolithography, was developed for semiconductor in the microelectronics industry. In the lasts decades, it was adapted to process a family of polymers called photoresist that interact with light and/or heat to drive, or activate, the polymerization process. This interest was driven by the optical and chemical properties and by the biocompatibility of polymers, that, combined with low cost and high mass-producible devices make them an ideal candidate for mass production of single use biosensors.

One of the most used polymers to realize biochip is PDMS (polydimethylsiloxane). It is liquid at room temperature, polymerize at low temperature ($60 - 75°C$), it is transparent up to UV light ($> 280nm$), it has good elasticity (it belongs to elastomer category), biocompatibility and gas permeability. It is also cheap and largely used to realize microfluidic chip for bio-applications. The realization requires to cast a

prepolymer mixture of PDMS and its curing agent against a master mold that, for example, can be realized by SU-8, a photopolymer largely used to realize MEMS and NEMS that is characterized by high aspect ratio of the final structures. SU-8 structure on a silicon substrate is a perfect mold since allows the realization of fine structures and the PDMS has low adhesion on them that can be easily peeled off after polymerization.

The procedure to realize PDMS samples using a SU-8 master mold is sketched in Figure 2.1. (1) The process starts with the deposition of a layer of photoresist on a substrate (as glass or silicon). Commonly a spin-coater is used to spun the substrate with a controlled speed and uniformly distribute the liquid polymer deposited in the center of its surface. The final thickness depends on the viscosity of the material and the value of the rotation speed. (2) The second step consist in placing a mask made by a transparent material and that includes a fine drawing of the microfluidic structure to be realized. Under this condition the system is irradiated by UV light to active the polymerization process on the areas not covered by the mask. (3) In the other parts, the film keeps be fluid and can be removed by immersion in a solvent. Photoresists are indicated as positive or negative depending on whether or not they are polymerized in the next step after exposure to light. UV exposure is preceded and followed by a baking process that removes solvent and activates cross-link between polymer's molecules. The sealing process can be achieved by direct or indirect techniques: one of the most common one is bond the PDMS stamps on glass after an oxygen plasma treatment of both surfaces [17].

An alternative way to realize microfluidic devices is the use of standard lithography. Standard lithography it is also used to realize microdevices or sensors with polymers because it allows realizing multilayer devices combining the steps (1), (2), (3) N-times, that can be integrated by using sacrificial material or laminating process to close structures depositing a layer of polymers as represented in Figure 2.1 (B) [4].

The drawbacks of soft lithography are: it realize structures layer by layer limiting the possibility to obtain complex 3D structures (such as circular channels or spherical shape walls); (II) an alignment procedure is necessary between two successive layers; (III) sealing of open structures sometime becomes a critical step in the fabrication process;

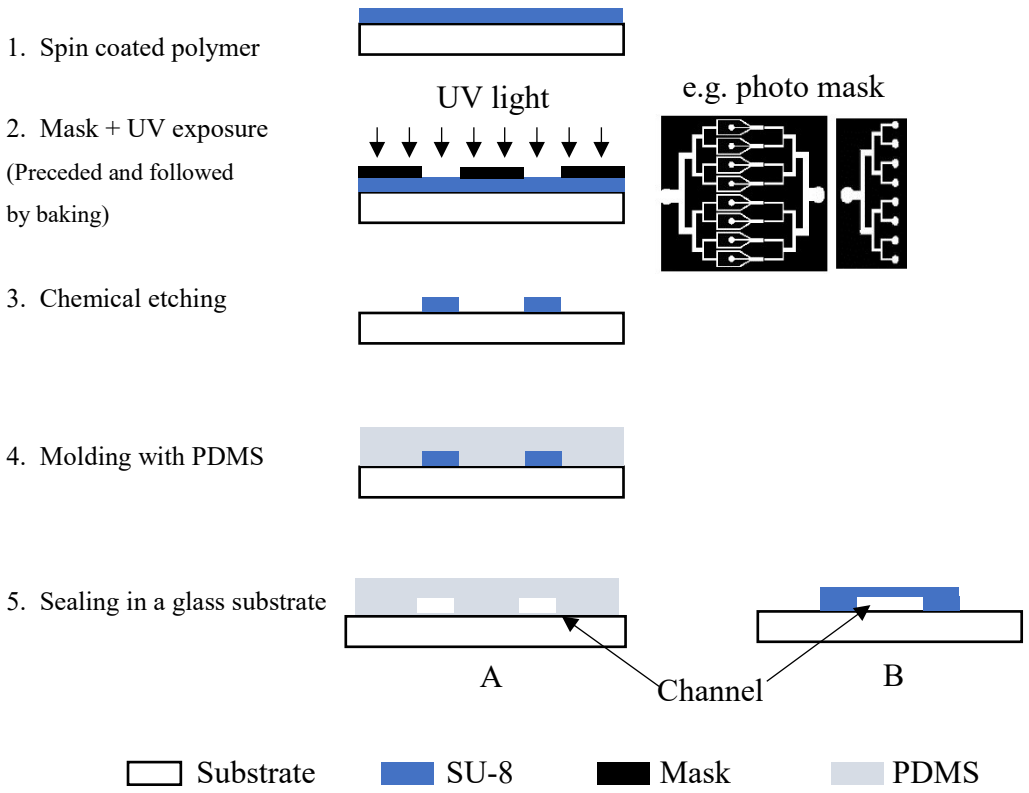

Figure 2.1 - Soft lithography steps processes that are required to realize PDMS or SU-8 microfluidic devices.

(IV) the high sensitivity to mechanical stress in polymers, consequence of the elasticity of the materials, can generate structure deformation during its use.

2.2 Replicant methods

Another common fabrication method to realize low-cost and high-volume polymers microfabrication field is the replicant method. This technology requires a master structure; the success and the replicated structure quality depend basically by four parameters: (i) the geometrical accuracy of the master, (ii) the ability to separate mould and moulded part, (iii) the surface roughness of the master (that should be as low as possible), and (iv) a suitable interface chemistry between master and substrate. All the microfabrication methods are available to generate the master structure that represent the crucial part in this fabrication method. Among the many technologies available are: wet (or dry) silicon etching, photoresist, laser ablation & electroforming, and others, the best is the electron beam lithography (EBL) (especially for micro and nanostructure).

2.2.1 Electron-Beam Lithography and Nano Imprinting Lithography (NIL)

Electron-beam Lithography is a photolithography technology where a focused beam of electrons is scanned across a substrate covered by an electron-sensitive material. It changes the solubility properties of the resist according to the energy dose of the electron-beam. After a developing process, the areas exposed (or not exposed) according with the resist family (positive or negative) are removed and the final drawn structure will appear. The main advantage of EBL is that it is a direct writing process, further no mask is required. Additional to and it is possible draw custom structures with a resolution below 5 nm [5, 6]. The main limits of EBL are: a low volume production and is the time-consuming process. For these reasons, commonly it is used to realize master molds and samples are fabricated with a replicant method. A sketch of the electron beam systems is shown in Figure 2.2.

EBL masters can be used in NanoImprinting Lithography (NIL), that is an attractive, high throughput, high-resolution and parallel patterning of polymer micro- and nanostructures. A mold that contain a surface pattern is impressed to polymer material by direct mechanical deformation of the resist due to a temperature effect. This process allows to replicate very high resolution, (5 nm feature has been demonstrated) [6]. The NIL requires thermoplastic polymers that can be softened by heating. Basically, the process can be described in the following steps: (i) master mold is mounted in the mold

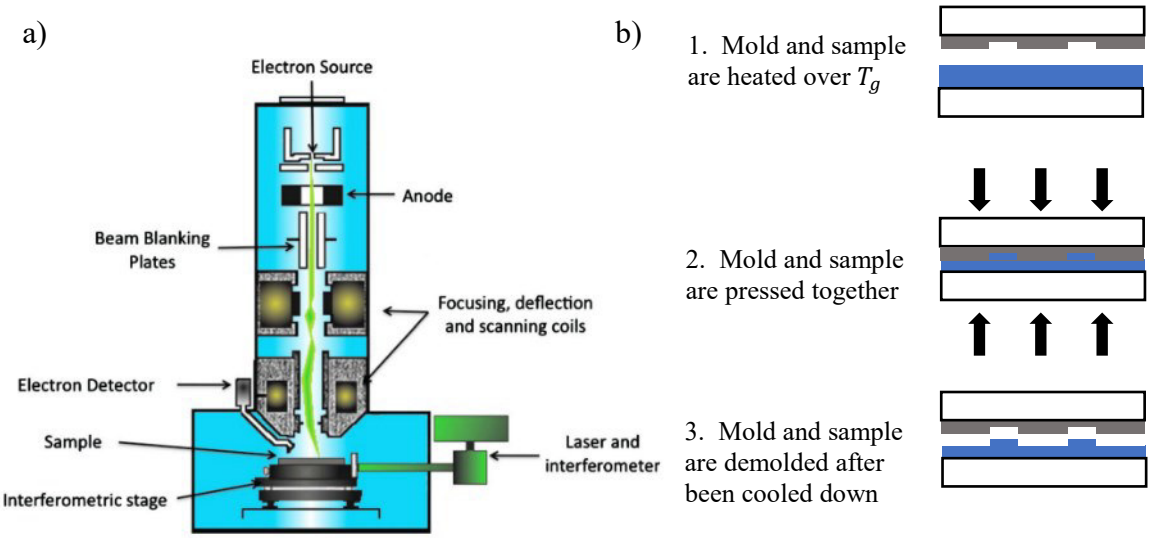

Figure 2.2 - (a) Typical EBL system consist of a chamber, an electron gun, a culomn including all the electron optics needed to focus, scan and turn on or of the electron beam [16]; (Right) The principal steps to relize a sample by using NIL with hot embossing.[]

holder; (ii) a substrate with a thermoplastic polymer layer is located into NIL machine and heated just above the polymer glass temperature (T_g); (iii) the master mold is heated at T_g (or few degree higher); (iv) master and polymer structure are pressed together with several tents of kN (in according with the sample dimension and complexity); (v) Mold and substrate are isothermally cooled down to a temperature few degree below the T_g of the polymer; (vi) mold and sample are separated. New samples can be obtained repeating the process from step (iii).

Critical issues for the success of the replication process are the temperature distribution in mold and sample, the presence of air bubbles during the compression step and the chemical compatibility between the involved materials.

2.3 Femtosecond Laser Micromachining Technology

Femtosecond Laser Micromachining Technology (FMT) represent a different fabrication technique with several advantages over soft lithography, the main are:

- 3D fast fabrication of microstructures inside transparent materials
- Maskless and flexible fabrication process;
- Quick prototyping;
- Device robustness and micrometric precision;
- No post fabrication processes

It actually consists in writing on the chip substrate the microfluidic circuit with a focused light beam originated by a laser emitting ultrashort pulses in the femtosecond range.

During the writing process, ultrashort laser pulses modify both the chemical and physical properties of the material because the high pulse energy activate absorption processes that occur by non-linear processes such as: (a) multiphoton ionization, (b) tunneling and (c) avalanche effect that are schematically depicted in Figure 2.3. This

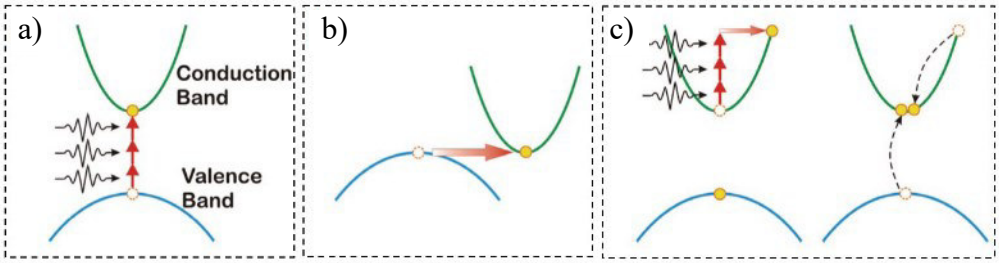

Figure 2.3 - Schematics of the nonlinear absorption process: a) multiphoton absorption; b) tunnelling ionization; c) advance ionization [15]

allows the material interaction with the laser beam in correspondence of the beam focus, where the intensity is enough to active the absorption effects. The irradiated material changes chemical structure of the substrate that became soluble on acid or basic bath (usually hydrofluoric -HF- acid or potassium hydroxide - KOH-). This allows removing selectively the irradiated material with a small and predicable effect on the remaining parts of the substrate, then, reproducing a negative structure with empty microchannel in the correspondence of the irradiated areas. This technique is successful with transparent materials such as fused silica glass and it is still under study when considering different substrates.

Actually, femtosecond pulsed lasers can induce three different modifications in transparent materials, effects that can be controlled by the laser fluence used during the irradiation process. At low fluence (Regime-1) smooth homogeneous structural modification are imprinted in the substrate. Mainly it results as refractive index variation; for instance, the refractive index increase ($\Delta n \sim 10^{-3}$) therefore direct 3D waveguide can be obtained. For this type of waveguide, the losses are less than 1dB/cm [18]. For higher fluence values (Regime-2) self-ordered nanogratings with average period $\sim \lambda/2n$ and perpendicular to the electric field make a periodic density modulation. This periodic structure is composed on “dark” (low density) and white (high density) regions. In the case reported in Figure 2.4 the width of these structures are $\sim 20nm$ and $\sim 200nm$ respectively, but they depend on laser parameters such as wavelength, energy dose, pulse width and accumulation rate. In case of high fluence (Regime-3), the focal spot generates high temperature and pressure that produced

internal micro explosions. This produce micro voids surrounded by densified material. The realization of nano voids without the presence of surrounding cracks is due to the ultrashort pulses that ends before the workpiece feels the excitation avoiding thermal effects.

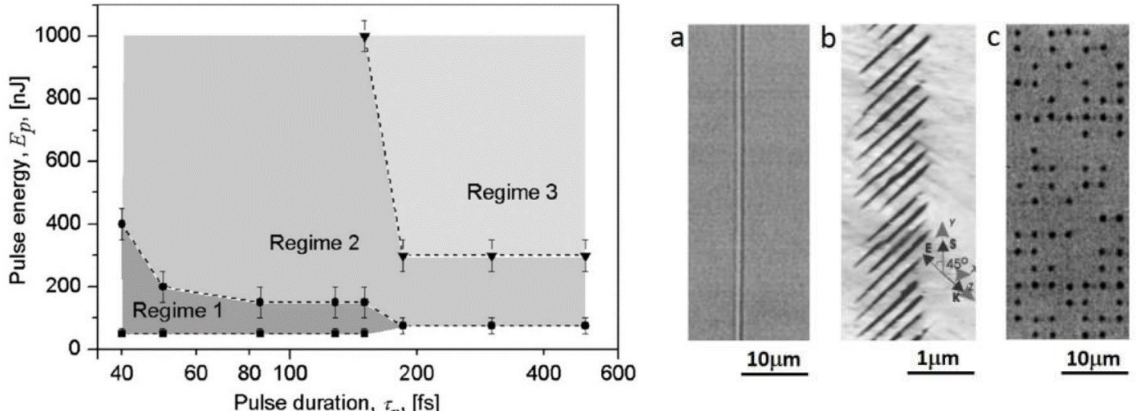

Figure 2.4 (Left) Different types of femtosecond laser modification in transparent materials depending on pulse energy, and pulse-width. Regime-1) smooth refractive index increase leading to internal 3D waveguides; Regime-2) periodic arrangement emerging in nanogratings generation; Regime-3) disruptive nanocraks and void formation. (Right) Microscope images of different type of modification in fused silica: a) waveguide [16], b) nanogratings perpendicular to the E field of laser beam [17]; c) array of micro-voids [18]

In silica glasses the femtosecond irradiation in the working Regime-2, with moderate fluence, modify the structure by reducing the angle of the bond between silicon (Si) and oxygen (O). This change not only increases the refractive index of the irradiated area but also make it more reactive to acids (or bases) increasing the etching-rate, that become 40 times higher with respect of the not irradiate areas.

A typical system for femtosecond micromachining is reported in Figure 2.5 and consists by a laser source, the laser beam manipulation equipment, the focusing system and the 3D micro positioning of the sample. The micromachining equipment used to realize glass embedded microlasers to the aim of this thesis work use a Pharos laser, (Light

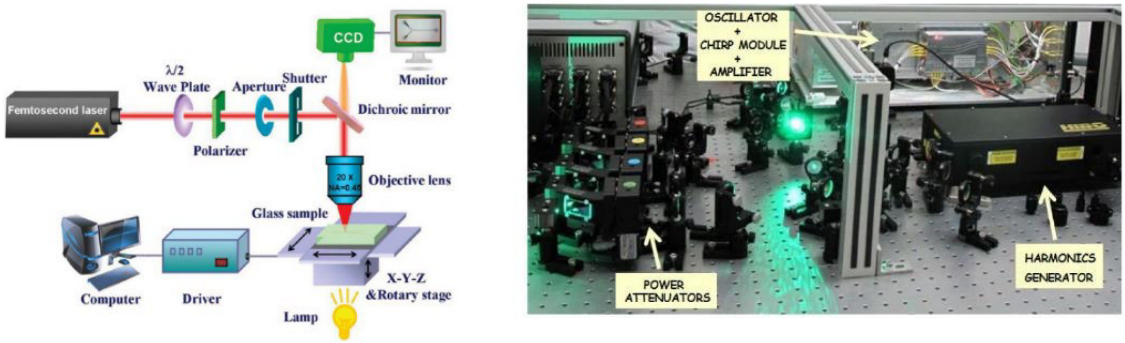

Figure 2.5 – (Left) Typical femtosecond micromachining set-up [7]; (Right) Main parts of the FemtoFab micromachinig setup showing the laser source, the high harmonic generator and power attenuators. [8]

Conversion) where is possible control the pulse duration ($240fs - 10ps$), repetition rate ($1kHz - 1MHz$), pulse energy (up to~$0.2mJ$) and average power (up to~$10W$) [p5]. The high power and ultrashort pulsed-mode relies on the conventional chirped-pulse amplification technique, which is based on: (1) a mode locked oscillator; (2) a stretcher/compressor module; (3) and a cascade regenerative amplifier. Both the oscillator and the regenerative amplifier are based on Yb:KGW lasing medium, emitting in the near-IR ($\lambda = 1030nm$), and laser diodes are used as high-efficiency pumping modules. In particular the Kerr-lens mode-locked oscillator is the core of stable 80fs-pulse generation with a repetition rate of 67MHz. Only a small fraction of the emitted pulse is selected by the BBO electro-optic Pockels cell and seeded into the amplifier cavity (1MHz maximum repetition rate). Before this step, the pulse must be temporally stretched (in order to avoid pules distortion passing through the cascade laser cavity) and after amplification the pulse is back-compressed by means of a grating-pair allowing the pulse-width tuning from a minimum value of $240fs$ up to $10ps$. Apart from the laser source, the system is equipped with a harmonic generation (HIRO, Light Conversion) that generates the second, third and fourth harmonic ($515nm$, $343nm$, $257nm$ respectively).

	SH ($515nm$)	TH ($343nm$)	4H ($257nm$)
η	21%	12%	2%

Table 2.2 - Conversion efficiency of the high harmonic generator[8]

The laser beam, before illuminating the sample, pass through a proper section of focusing lenses equipped with different objectives in order to select the suitable spot size. In particular the used system is equipped with three infinite corrected NIR-extended objectives (20X 0.4NA, 50X 0.42NA, 100X 0.5NA, Mitutoyo), one oil-immersion objective for VIS region (100X 1,25NA, Olympus) and few lenses designed for the UV wavelengths. These objectives allow setting a working distance from $12mm$ to $20mm$ ($0.15mm$ in case of oil-immersion) and an elliptical spot size form $3\mu m$ x $3\mu m$ and $10\mu m$ long to $0.8\mu m$ x $0.8\mu m$, $4\mu m$ long. A CMOS camera, located before the objective allows looking out the surface to control the writing process. The camera vison can be used to set manually the substrate surface distance but it can be also set automatically by using an integrated AutoFocus system. The sample movement are

made by a 3D motorized air-bearing translator stage (FiberGlide3D, Aerotech) that ensures low friction and high precision even at high translation speeds. In microfabrication it is better to move the sample in order to avoid affecting the beam quality and alignment, to have higher translation range. FiberGlide3D consists of three linear stages (X-Y-Z) controlled and programable by a dedicated computer software (Automation 3200, Aerotech) able to control the relative position, velocities and acceleration modes. The sample is fixed to the stage by vacuum-valves. Several integrated feedbacks ensure a real-time monitoring and allow to uniform translation along any 3D path ensured by the constant tangential velocity. A control software (SCA, Altechna) offers a more user-friendly programming environmental and convert the instructions in the G-Code that drives the motion stage (Figure 2.5). This stage ensures repeatability of $\pm 100nm$ with $5nm$ resolution within a large travel range of $150mm$ x $100mm$ x $50mm$ (X-Y-Z) and high maximum velocity of $300mm/s$.

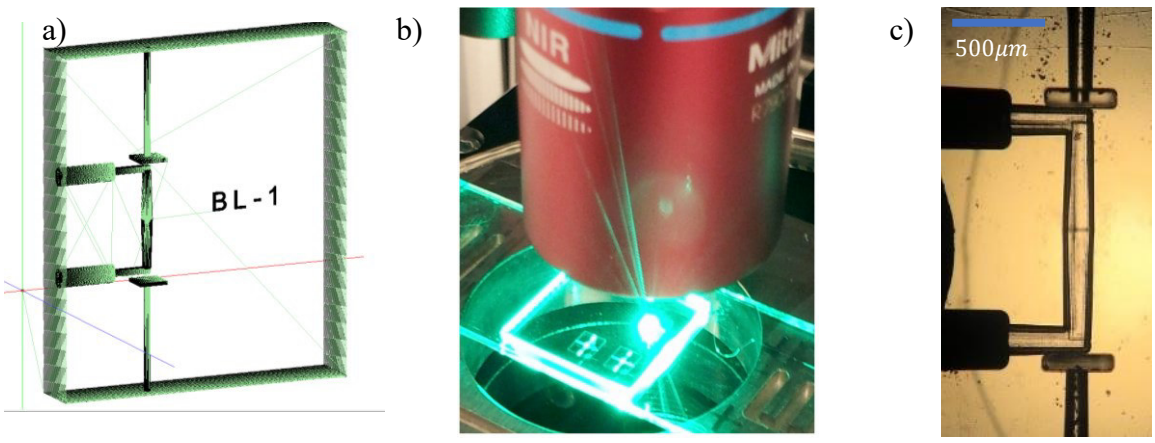

Figure 2.6 – a) 3D sketch for the writing process: it reports path the laser follows to realize the design device. b) Picture during the chip fabrication c) Optical microscope image of a final sample.

The chemical etching concludes the fabrication process. It can be achieved by a solution of HF or KOH in deionized water in a performed and dedicated environment. Since the irradiated area are etched 40 times faster than the fused silica glass, the glass etching can be compensated during the sample design introducing a "conical shape" compensation that taking into account the different etching velocity allowing to realize uniform final structures. The etching rate is also dependent on the beam polarization: the etching rate is faster when the electric field $\bar{E}$ of the writing beam is perpendicular to the writing direction $\bar{S}$ compared to the case parallel polarization (Figure 2.7). This behaviour is due to the different nanograting orientation formed in the irradiated area that affects the etching process.

The duration of the etching treatment is about one hour; during this time, the structure formation can be monitored by visual inspections; at the end samples are cleaned in a bath in deionized water and isopropyl alcohol to eliminate potential acid residues.

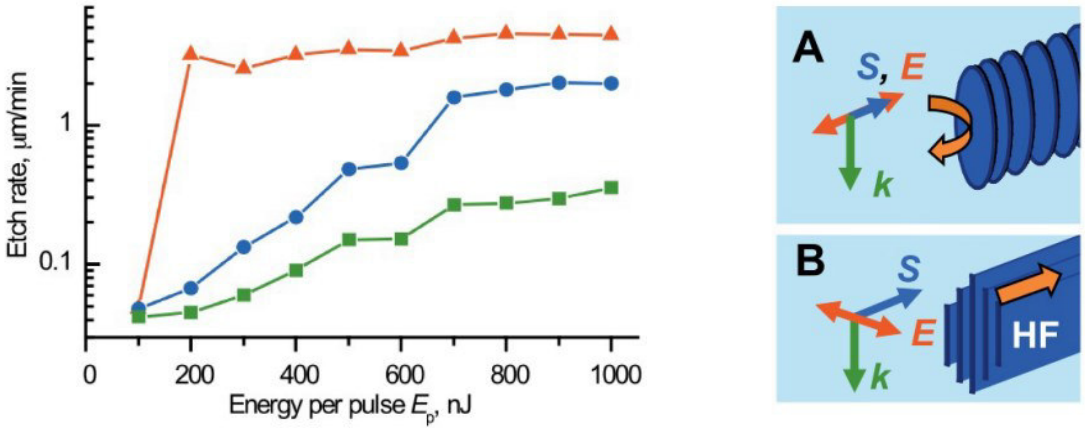

*Figure2.7– Polarization dependence of etching rate versus pulses energy and writing beam polarization: electric field **(E)** perpendicular to the writing direction **(S)** **E ⊥ S** (orange triangles); **E** oriented at 45° to **S** (blue dot); **E** ||**S**; A: sketch of the grating orientation in case of **E** ||**S**; B: sketch of the grating orientation in case of **E ⊥ S** [9]*

3 Design and fabrication of the optofluidic resonators

The difficulty of realizing a Fabry-Perot micro-resonator is due to the critical alignment of the two mirrors with respect to each other and of achieving suitable mechanical stability. It is a key issue when the cavity is made by two parts that need to be bounded together [11, 12, 13], or if it is made by a soft material, as PDMS [15] that it is characterized by a high softness.

In this work, all the investigated microlasers have been realized by using the Femtosecond Micromachining Technology (FMT) described in the former section (2.3).

In the next sections will be described how combining two fast prototyping technology such as femtosecond micromachining and Ink-Jet, is possible realize a high performance Fabry-Perot resonator embedded in a glass chip.

3.1 Mirror fabrication by Ink-Jet technology

The Ink Jet printing technology was initially developed as a low-cost solution to standard lithographic processes and to print other material in electronics and integrated circuits [10]. To the aim of this thesis work we have used a Fujifilm DIMATIX printer (in future *DIMATIX*) designed for high resolution and non-contact jetting of functional fluids in a broad range of applications and a commercial ink, Inktek *IJ* 010, that is based on Ag-nanoparticle solved in organic complex solvent. DIMATIX works like a standard colour printer where a head moves in a XY plane and “print” ink droplets (Figure a, b).

A fluidic module (bag, valve, pressure system) and jetting module (MEMS jetting structure, heater, thermistor, electrical connection, fluid connection) compose the printer head. In order to work in high-resolution regime, the printer was tested with 1pL and 10pL cartridges. In both cases an electric field acts a piezoelectric membrane that allows the ink to flow out from the needle and be ejected. Figure 3.1(c) reports a scheme of the steps that allow the droplet generation: (Step 1) the standby position and the relative electric field applied; (Step 2) and (Step 3) the droplet releasing is leaded by

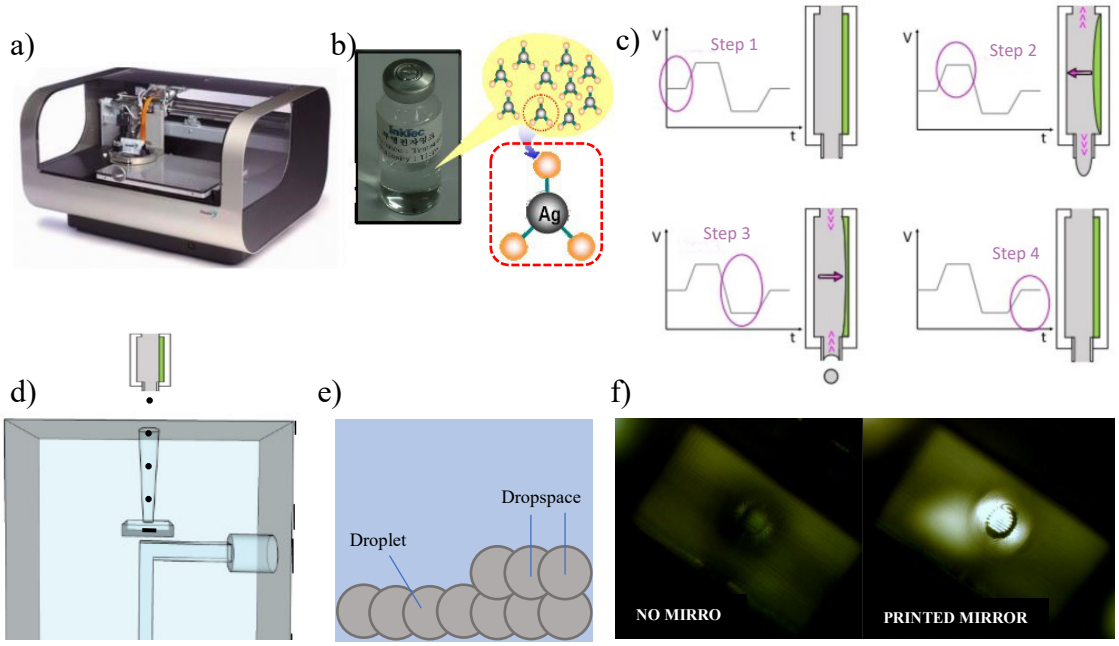

Figure 3.1 – a) Picture of the Fujifilm Dimatix printer; b) picture of the Inktek IJ010 and a sketch of the molecules formula; c) The four steps required to the droplet generation: Step 1 standby position, Step 2-3 the droplet releasing is leaded by the membrane contraction and distress due to the applied electric field; Step 4 standby position; d) Mirror realization: the ink's droplet reach the basin surface travelling through the lateral basin access; e) mirror realized droplets array where "dropspace" means the distance between the centre of two droplets f) picture of the basin trough the lateral basin access before and after the mirror realization

the membrane contraction and distress due to the applied electric field; (Step 4) the membrane returned to the standby position and it is ready to generate a new droplet. Mirrors are printed in the bottom surface of the specially designed basin realized close to dye microchannel.

As shown in the Figure 3.1(e), the droplets pass through the access channel that connects the basin with the external side of the sample. The mirrors have a diameter higher than $100\mu m$, double of the core of a multimodal optical fiber. In order to control the mirror thickness, then the final reflectivity, the distance between two successive droplets, called "dropspace", is fixed This allows to determine the final volume of the printed ink, thus the mirror performances. In order to obtain high density and uniform surface, curing the ink at 150°C for 5 min is needed, in this way the solvent evaporates causing silver nano-particle sintering [15]. Figure 3.1(f) shows the printed mirror before and after the curing process. In the printed mirror, on the right, the reflecting surface is clearly visible; the parallel dark lines represent the intrinsic roughness and are due to the MFT process that realizes surfaces as a sequence of parallel layer. In order to realise the surface as smoothest as possible, the bottom surface of basin (where mirror is printed) is written as "vertical wall".

	Value
Mirror reflectivity	40 ~95%
Ink volume [nL/mm²]	$6.67 - 102$
Metal film thickness	$230 - 1000nm$

Table 3.1 – The table reports the mirror reflectivity, the ink volume and the metal film thickness achievable by using the Fujifilm Dimatix Ink-Jet printer and Inktek IJ010 ink.

A careful mirror calibration has been carried out in order to have a correlation between the, used ink volume, the resulting film thickness and the final mirror reflectivity. In this way the mirror reflectivity was adjusted by controlling the total volume of the ink droplets to get a high reflectivity mirror (~90.5%) and an output mirror with reflectivity in the range 65%-90.5%.

The mirror reflectivity has been measured using the spectrophotometric method shown in Figure 3.2 where the bright signal from a white source was collected by an optical fiber to the fabricated mirror; the reflected optical signal was detected by a coupled spectrometer (Black-Comet, StellarNet).

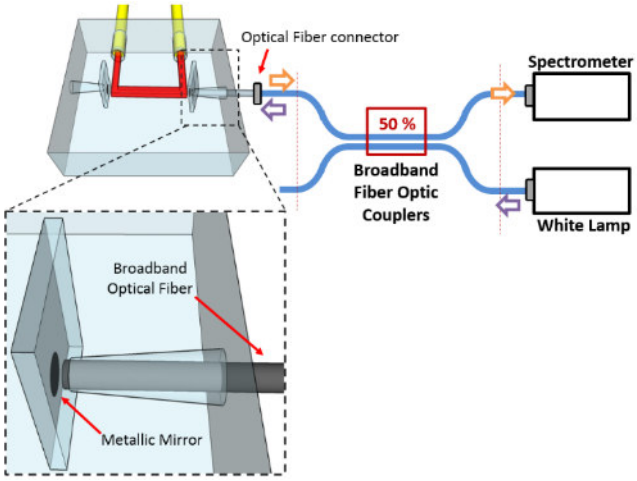

Figure 3.2- Sketch of the set-up used to measure the mirror reflectivity. A halogen light source is collect by optical fiber to a broadband fiber optic coupler to the fabricated mirror. The reflected light is signal was detected by a coupled spectrometer.

3.2 Connection of the samples

The step after the sample realization is providing it with two microtubes for inlet and outlet of the gain medium and an optical fiber close to the output mirror to deliver the emitted light to an external detector. The flexibility offered by FTM has allowed to make all the correspondent channels aperture with conical shape that simplify and ensure best alignment during the integration steps. the sample chip is glued on a glass substrate in order to protect the optical fiber from bending and to keep the optofluidic chip in the sample holder for the optical characterization.

A picture of the final sample, ready to be tested:

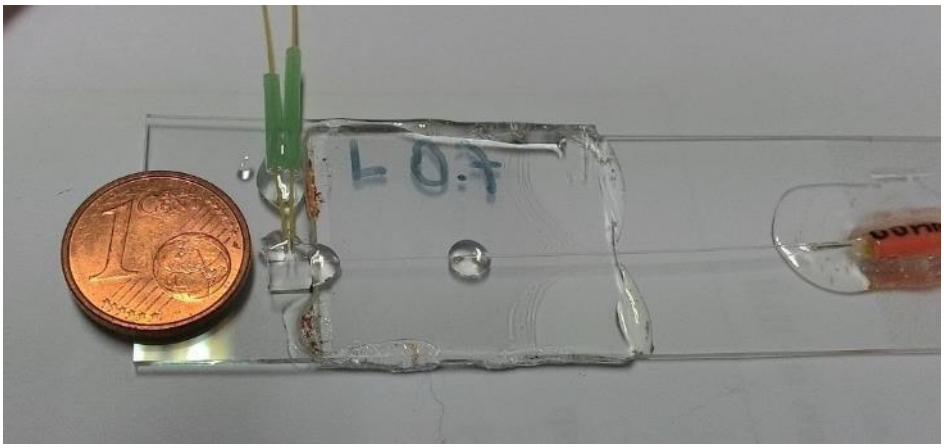

Figure 3.3 Picture of microfluidici sample glued on a glass substrate to protect the optical fiber from bending and to lock into the sample holder. The microlaser is in between the yellow microtubes used to recirculate the gain medium.

4 Optofluidic microlaser realized by FMT

4.1 Previous works

There are only two sample of optofluidic microlasers realized by other researchers before beginning of this thesis work.

The first demonstration of optofluidic microlaser fabricated by FMT was reported by Midorikawa and co-workers in 2004 [18]. The authors realized a ring microresonator fully embedded in a glass chip. Since a used metal-ions rich structure, additional baking was necessary after chemical etching. The realized device is shown in Figure 4.1. The resonator is made by four mirrors (actually based on total internal reflection between glass and air voids) placed at 45° with respect to the oscillating beam. In this way a ring cavity is obtained with a gain medium flowing in through a channel in the transversal direction.

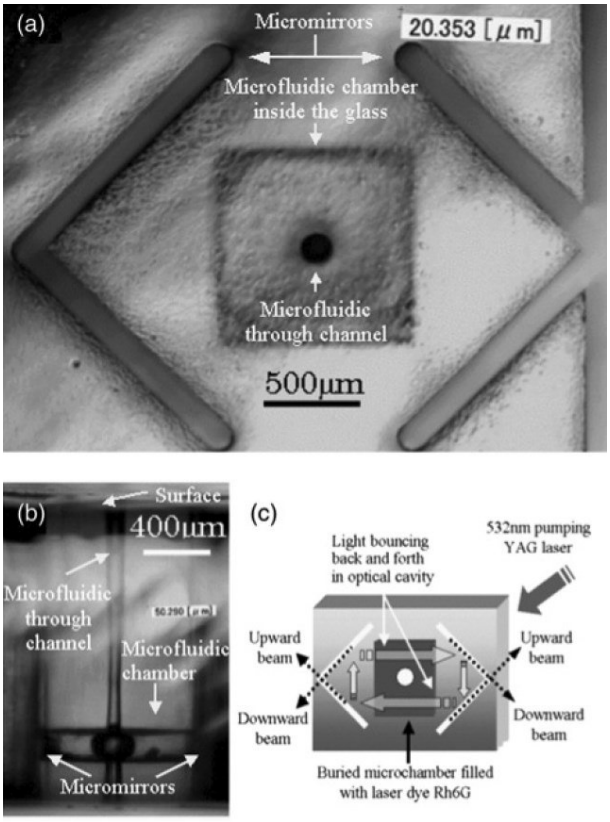

Figure 4.1 – The first microfluidic laser realized by FMT; optical micrograph of the top view of the resonator, b) optical micrograph of the side view of the whole structure including the cavity chamber and the microfluidic channel; c) sketch of the ring cavity resonator with light path and output beams [18]

Critical issues in this design are the smoothness of micromirror surfaces and their reciprocal alignment. Moreover, laser output was obtained just exploiting the light

leakages tangential to the mirror surfaces as shown in the Figure 4.1(c). The laser emission by a solution of Rhodamine 6G in ethanol ($20mMol$) pumped by the second harmonic ($\lambda = 532\ nm$) of a Nd:YAG laser pulse ($5ns$) is shown in Figure 4.2 with typical bandwidth $5nm$ and a threshold of pump energy density of below $20mJ\ /\ mm^2$.

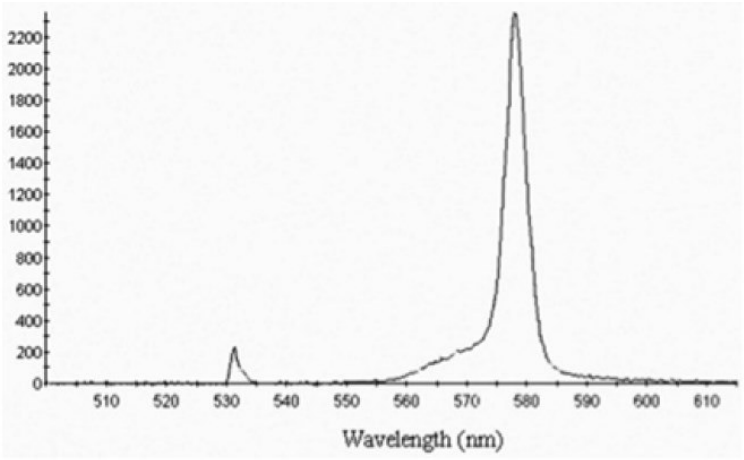

Figure 4.2 Typical emission spectrum of the microfluidic laser described in the text [18]

The main drawbacks are the low efficiency of the output coupling and resulting broad emission bandwidth.

The second example of the use of FMT to realize optofluidic microlaser was reported in 2015 by the Fan group [19]. In this case, the resonator is defined by a ring shaped channel, that is connected to conventional microfluidic circuit needed to get gain medium flowing. All the resonator parts where buried into the glass chip. A sketch of it is shown in Figure 4.3.

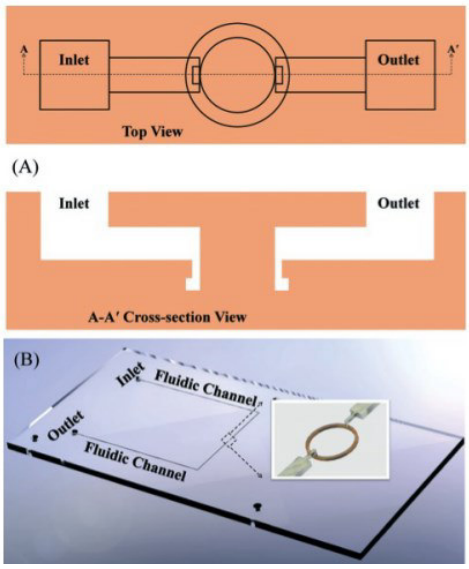

Figure 4.3 Design of the ring resonator based on the Whispering Gallery Modes realize by FMT: top view (A), cross section (A-A') and overall scheme (B) [19]

Exploiting the 3D capability of FMT the microfluidic channels were connected to the ring resonator, in this way there was no degradation of the Q factor of the cavity. The fabrication process required a third step after laser writing and chemical etching necessary to bond the two substrates in order to get a single monolithic optofluidic platform, shown in Figure 4.4. This optofluidic laser was tested with a quinoline solution of Rhodamine 6G ($1mMol$) pumped by nanosecond pulses at 532 nm. The lasing threshold was measured at pumping energy density of about $5\ \mu J/mm$ with a quality factor $Q \approx 3.3 \cdot 10^4$. These excellent results show the capability of FMT as powerful tool to fabricate optofluidic microlasers with state-of-the-art performances.

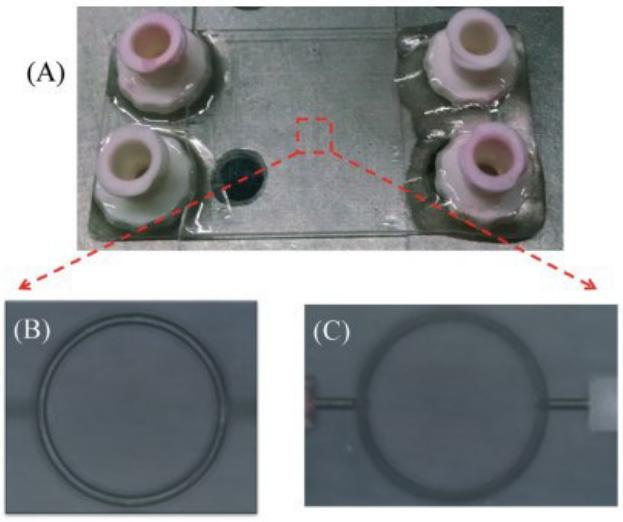

Figure 4.4 Practical realization of the ring resonator described in the text: (A) the whole optofluidic chip; (B) the ring resonator embedder in glass (C) microchannels providing the gain medium

4.2 Our cavity design

All the optofluidic microlasers based on Fabry-Perot cavity, fabricated up to now, could not reach a high quality factor leading to an emission linewidth of about $3-4\ nm$. In fact, alignment of the two mirror surfaces with respect to each other and the mechanical stability of such alignment represented critical issues in microlasers fabricated by coating a metallic films on the side of microfluidic channels or on the edge of the fibers used to collect the signal, where the soft-lithography technique was used for the fabrication of the microfluidic chip [13, 20, 21, 22].

These alignment problems can be overcome if the cavity is fabricated as a rigid structure embedded in glass, since FMT provide high resolution writing allowing to get good parallelism between mirrors without any need of further adjustment. As described in section 2.4 mirrors have been realized using a high-resolution ink-jet printing technique on previously fabricated basins in the glass structure. We have designed and realized different resonator cavity which are described below.

4.2.1 Transversal cavity

In this configuration two mirrors have been realized on the opposite side of the microfluidic channel to get a resonator with optical axis perpendicular to the gain medium flow. The separation between the mirror surface and the channel is made by thin glass layer of $15\mu m$. The microfluidic channel has a rectangular section with height between $50\ and\ 150\mu m$, depth of $150\ \mu m$.

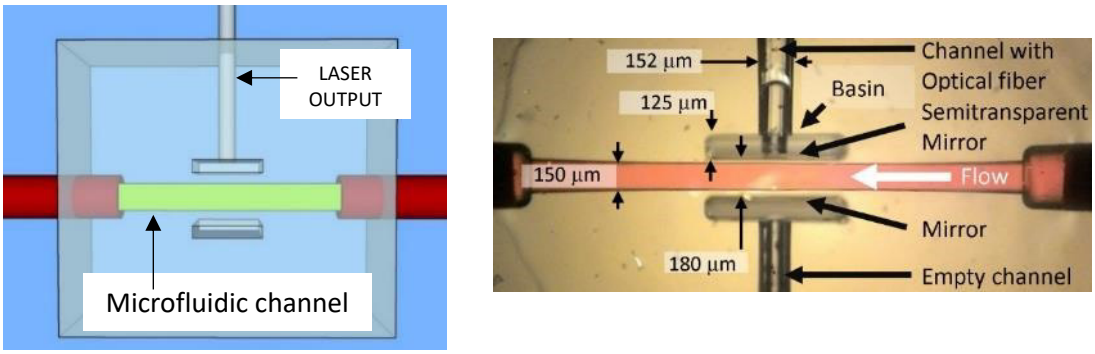

Figure 4.5 - Sketch and microscope picture of the transversal Fabry-Perot resonators realized in glass chip. The picture reports the main dimension of the cavity parts.

In this configuration the channel is pumped by an orizontal focused beam and the light coming out by the semitransparent mirror is collected by an optical fiber located close

to it. On the sides the microtubes allow the active medium recirculation. In Figure 4.5 it is shown a schetch of the cavity and a microscope image reporting the actual dimensions of the different parts.

4.2.2 Longitudinal cavity

In order to increase overall gain, the empty basins were built close to the edges of the microchannel realizing the laser cavity along the gain medium flow. In this way, the cavity length has been increased from $0.7mm$ to $2.6mm$. Pumping and gain resirculation have realized as in the previous design.

In Figure 4.6 it is shown a schetch of the cavity and a microscope image reporting the actual dimensions of the main parts.

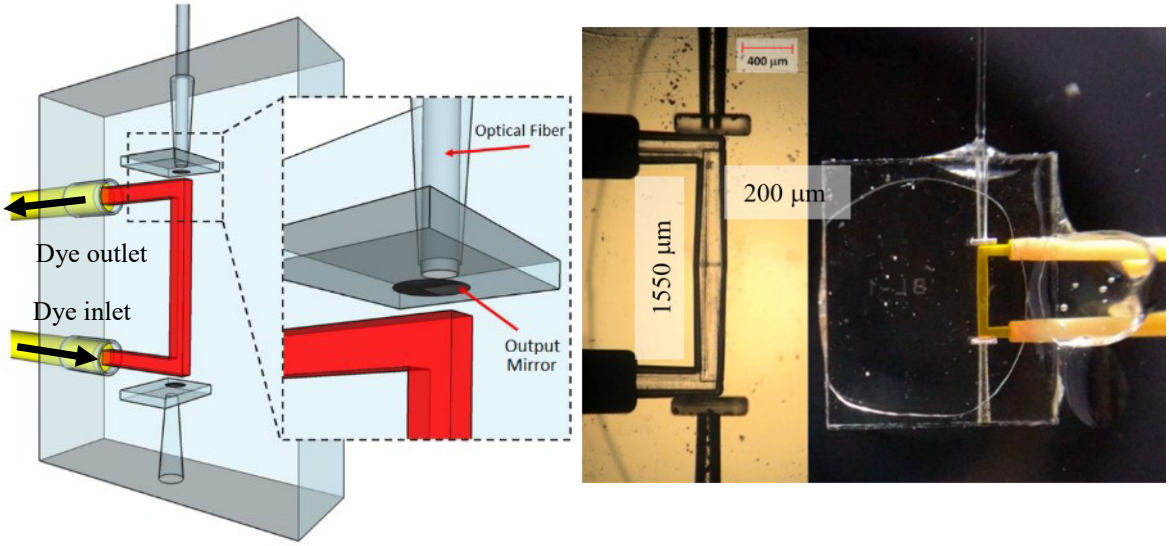

Figure 4.6 - Sketch and microscope picture of the longitudinal Fabry-Perot resonators realized in glass chip. The picture reports the main dimension of the cavity parts.

4.2.3 Hemispherical cavity design

The hemispherical cavity has been developed with the purpose to have a higher confinement of the electric field in the cavity and to reduce in this way the pumping threshold by increasing cavity stability. For this purpose, two mirrors were made: one is flat and perpendicular to the channel, the other has spherical shape with radius of curvature $R = 1.64\,mm$; the stability condition is fulfilled since $d = 1.5mm$, thus being $R > d$. In Figure 4.7 it is shown a schetch of the cavity and a microscope image reporting the actual dimensions of the main parts.

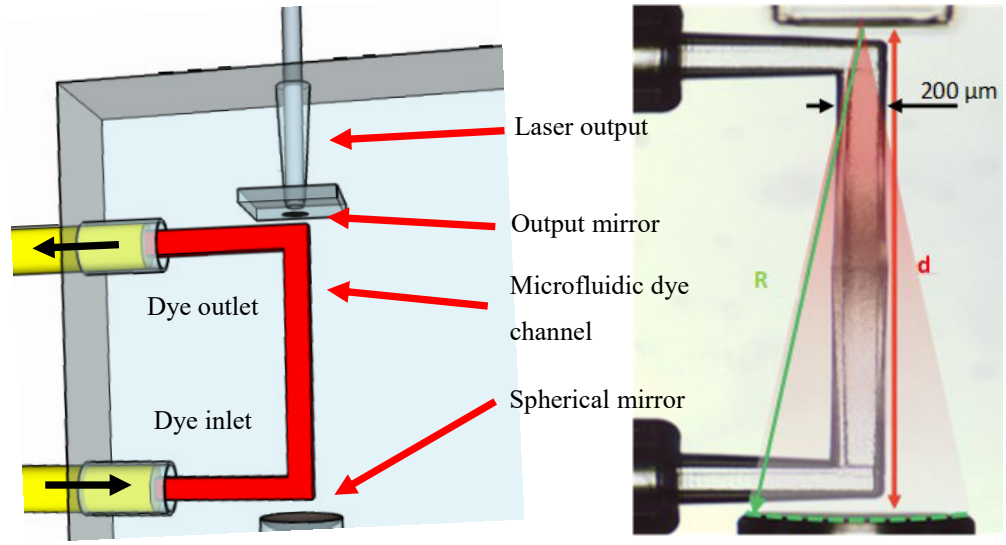

Figure 4.7 - Sketch and microscope picture of the hemispherical resonators realized in glass chip. The picture reports the main dimension of the cavity parts.

4.2.4 Cavity with control channel

This cavity is based on the longitudinal design in which a second channel is added. It passes through the resonator and can be used (i) to tune the laser wavelength, (ii) deliver materials under test that modifying the cavity condition (increasing the losses) changing the emitted spectrum. In Figure 4.8 it is shown a schetch of the cavity and a microscope image reporting the actual dimensions of the main parts.

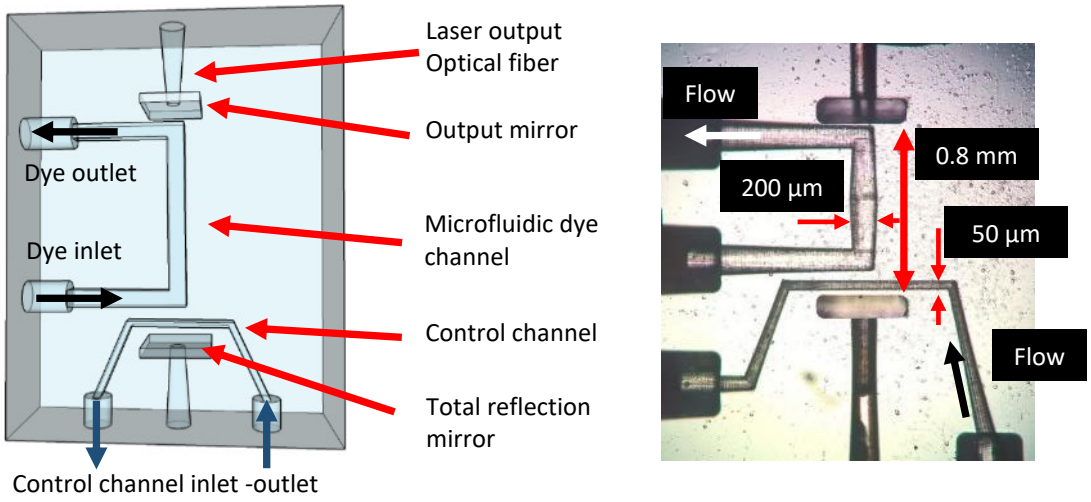

Figure 4.8 – Sketch and microscope picture of the longitudinal Fabry-Perot resonators with a control channel realized in glass chip. The picture reports the main dimension of the cavity parts.

5. Device characterization

5.1 Experimental set-up

The expreimental set-up used for the characterization is shown in Figure 4.1. The optical pumping source is a pulsed Nd:YAG laser (*Continuum Surelite SL-20*) that generates a fundamental wave at $\lambda_I = 1064\ nm$ with duration of $\sim 5\ ns$. This wavelength is located into the infrared spectrum and cannot be used to pump dyes that emit in the visible range. A second harmonic crystal is used to double it to $\lambda_{II} = 532\ nm$. The visible emission is separated and filtered from the infrared one by a second harmonic separator and a KG filter. The pulse energy is controlled by a double stage of attenuators: neutral density filters, and a $\lambda/2$ plate placed before a polarizer provide a vertical polarization and the fine control of the energy density. To monitor the energy of each pulse a beam splitter redirect part of the beam intensity to a fast photodetector connected to a fast oscilloscope. A diaphragm and a cylindrical lens with a focal length of 5cm generate a rectangular spot that overlap the optical cavity of the sample, mounted in a x-y-z micrometric translator (Thorlabs). The dye flow into the microfluidic channel of the samples with a stable flow rate of $3.3\mu l/min$ thanks to a high-performance syringe pump (NE-1002X, SyringePump) connected to the microtubes plugged to the glass chip. The constant flow rate guarantees the complete replacement of dye molecules in the cavity volume between two successive pumping pulses avoiding bleaching and quenching effect. The fiber optic coming from the glass chip is connected to a high-resolution spectrometer with resolution of $0.2\ nm$ (Ocean Optics HR4000) and the signal, is analyzed by a computer. The conversion of the pulse energy into the energy density was made possible by measuring the beam spot size in the focal plane by the knife-edge technique using a razor blade in front of a detector. With the described set-up the available energy density range from $0.3\mu J/mm^2$ to $275mJ/mm^2$.

All the fabricated devices were characterized using Rhodamine 6G solution in ethyl alcohol as gain medium with concentration ranging from $0.5mMol$ to $10mMol$. Some test has been done changing both laser dye and solvent. In the following sections, typical experimental results are reported for each cavity design.

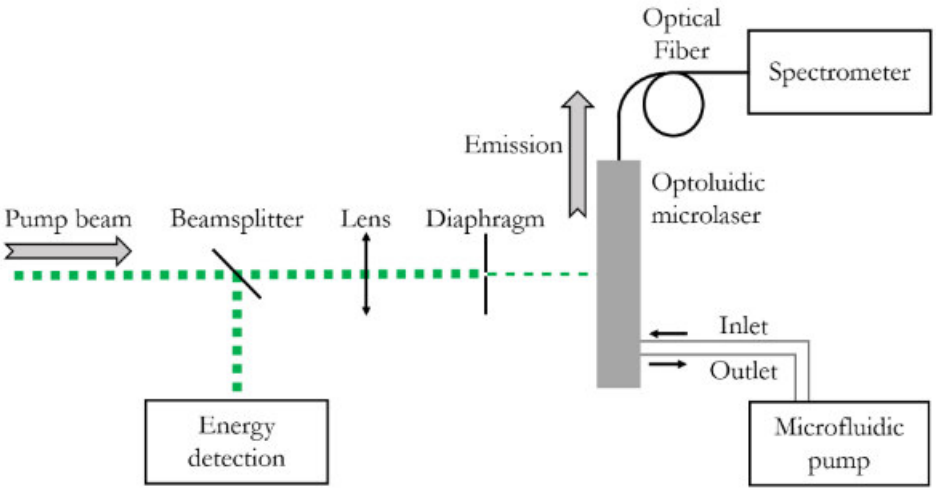

Figure 5.1 – Experimental set-up for optofluidic microlaser analysis

5.2 Results of measurements

5.2.1 Transversal cavity

In Figure 5.1(a-b) the evolution of the emission spectrum is reported by increasing the pumping energy density for 1mMol Rh6G solution in ethyl alcohol. It is also reported the spectrum (red line) of the emission from a chip with the same channel geometry without mirrors (in this case the correspondence basin has not been coated by metallic ink). It is clear the effect of the resonant cavity in using a clear narrowing of the emission up to a full width bandwidth (FWHM) of $3.4nm$. This data refers to a cavity length of $50um$. A second test has been performed with a chip where the cavity length was $150\mu m$ at the same concentration of Rh6G. In this case narrowing effects is improved with the achievement of a FWHM of $2.5nm$; Figure 5.1(c-d). The plot of the FWHM for both samples, reported in Figure 5.2, point out the onset of the threshold laser action,

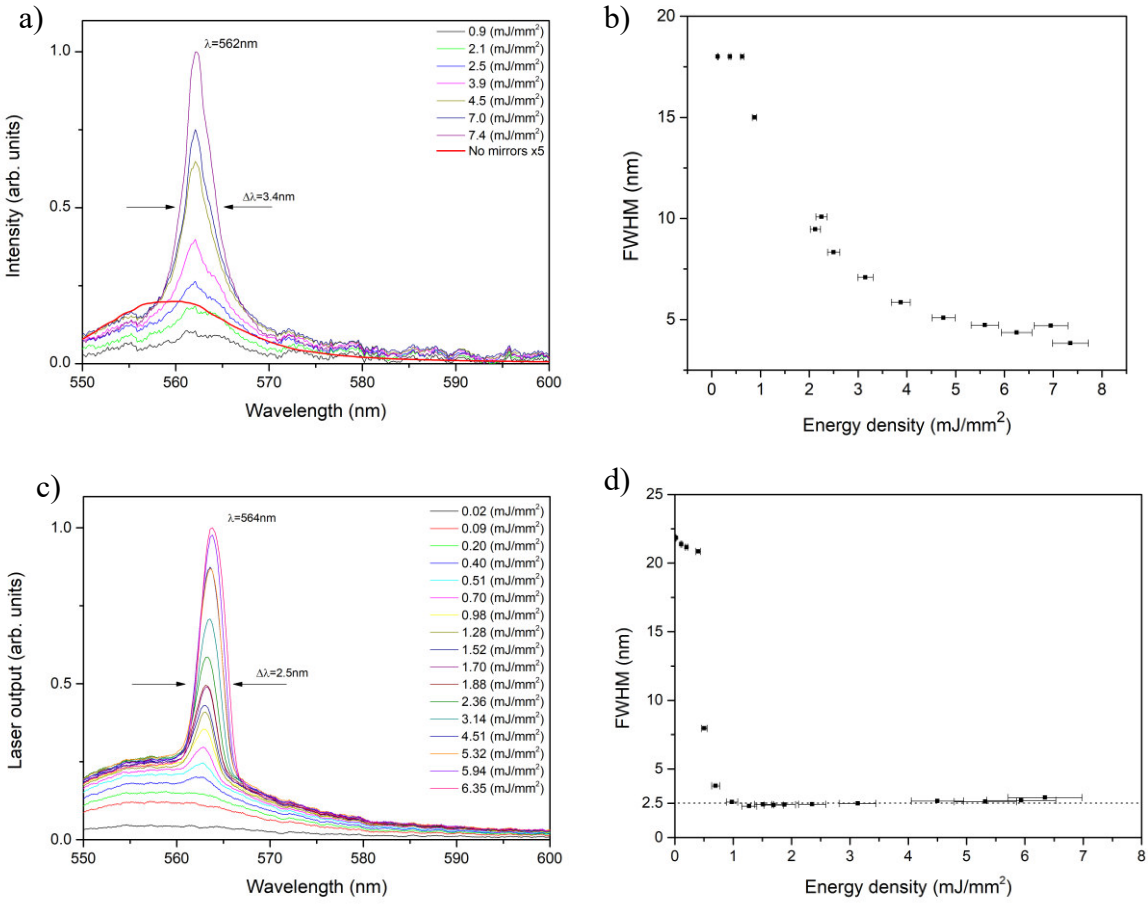

Figure 5.1 – a) Typical emission spectrum increasing the pump power and b) Full width half maximum of the stimulated emission bandwidth versus pumping energy density. Data correspond to a channel width of $50\mu m$. *c) represent the typical emission spectrum increasing the pump power, and d) report the Full Width Half Maximum of the stimulated emission. Data correspond to a channel width of* $150\ \mu m$. *In both of cases a solution of R6G solved in ethyl alcohol at a concentration of* $1mMol$.

since the suddenly reduction of the emission bandwidth is clearly observed. This is confirmed by plotting the output signal versus the pumping energy density.

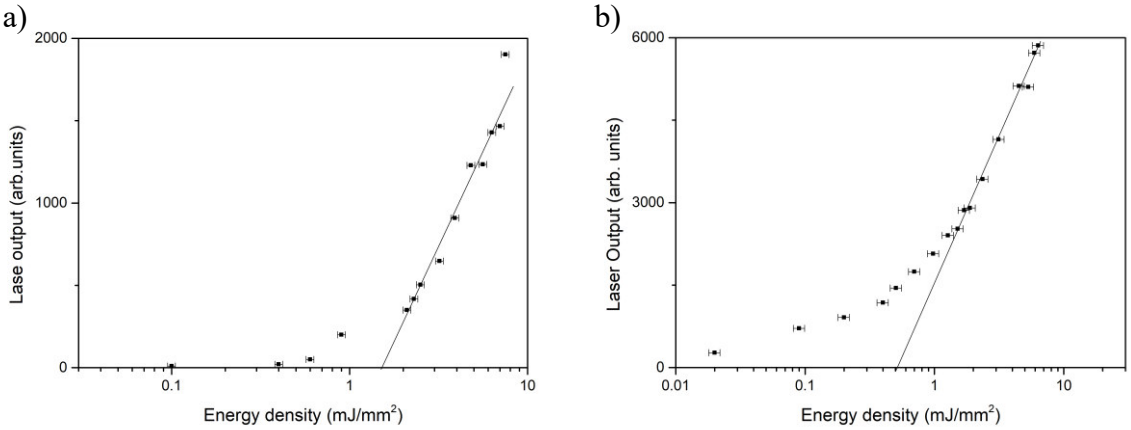

Figure 5.2 - Laser output versus energy density of the pumping pulse in case of: a) channel width of $50\mu m$*, and b) a channel width of* $150\mu m$*. In both cases the gain medium was a solution of R6G solved in ethyl alcohol at a concentration of* $1mMol$*.*

The classical threshold behaviour is evident in both cases. The increase of the interaction length in the $150\mu m$ cavity shows a clear reduction of the threshold with respect to the $50\mu m$ cavity.

5.2.2 Longitudinal cavity

In this configuration chip with three different lengths: $0.7mm$, $1.5mm$ and $2.5mm$ were tested. In this case the device behaviour was characterized using the following laser dyes. Rhodamine 6G, Pyrromethene 597, DCM. Ethyl alcohol as solvent.

Measurements were performed at different pumping power and different dye concentrations. As an example, we report data obtained with the cavity length of $1.5mm$ that showed the best performances. The appearance of the laser action over the dye spontaneous emission band is clear from Figure 5.3 for 0.5mMol Rh6G concentration. The transition from the spontaneous to the laser emission can be easily observed. The correspondent plot of FWHM and laser output versus energy density are also shown.

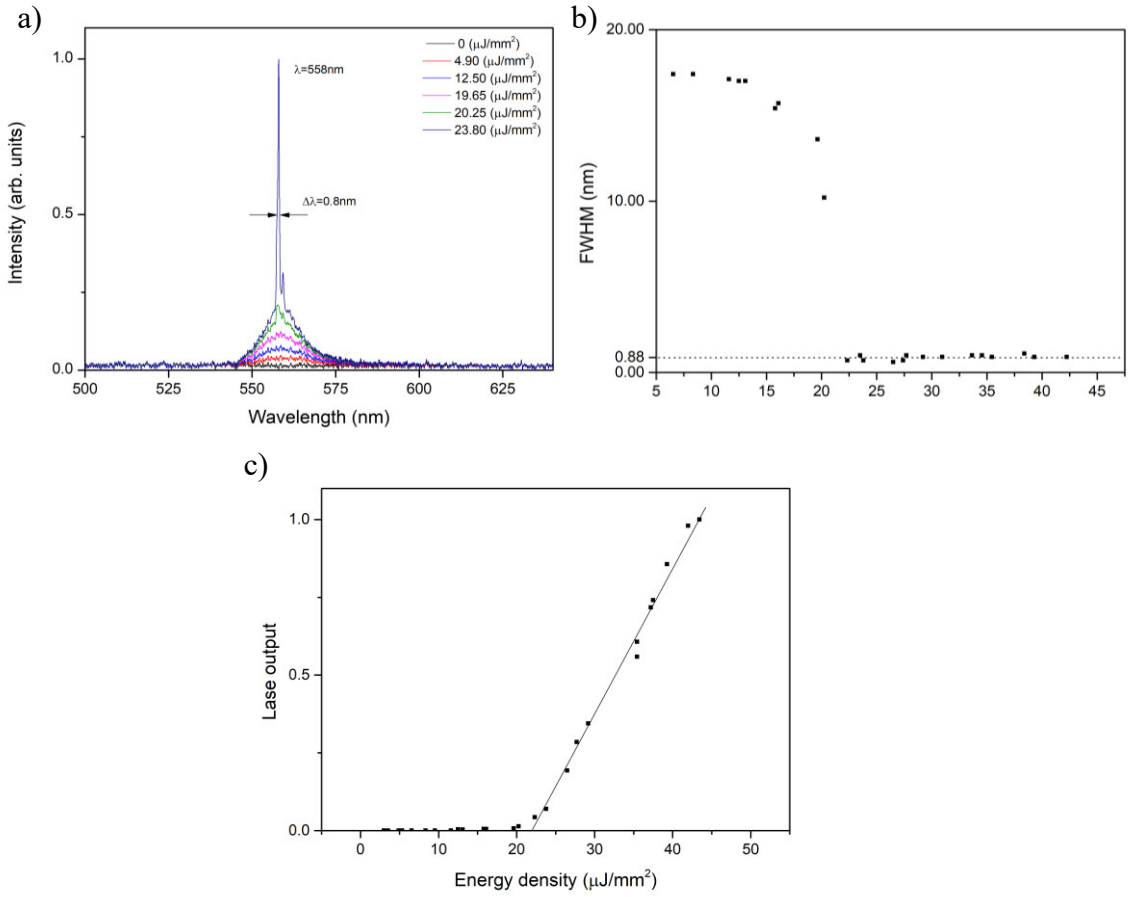

Figure 5.3 – a) Typical emission spectrum increasing the pumping energy; b) Full Width Half Maximum of the stimulated emission vs pumping energy; c) Laser output versus energy density of the pumping pulse for a solution of Rh6G in ethyl alcohol at concentration of $0.5mMol$.

Using $5mMol$ R6G solved in ethyl alcohol the lowest threshold has been obtained $1.8mJ/mm^2$, as shown in the Figure 5.4. In this case a nice laser spike is measured at 572nm with a FWHM below 0.6nm. This data shows the achievement of a quality factor $Q \sim 10^3$, that is a remarkable result for a Fabry-Perot microlaser. Figure 5.4(b) shows a bandwidth always lower than 1nm is obtained in this case well below the values reported for other optofluidic based on F-P resonator.

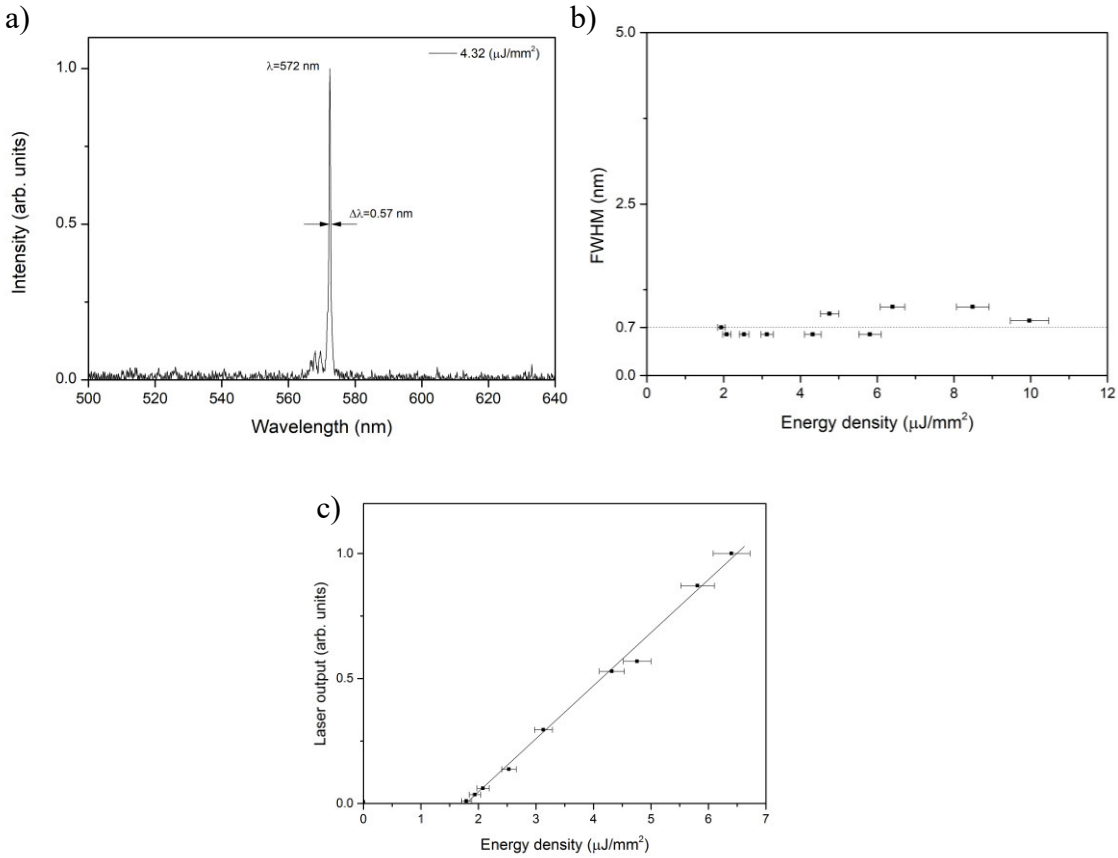

Figure 5.4 – a) Typical emission spectrum increasing the pumping energy; b) Full Width Half Maximum of the stimulated emission vs pumping energy; c) Laser output versus energy density of the pumping pulse for a solution of Rh6G in ethyl alcohol at concentration of $5mMol$.

Several measurements were carried out by changing the dye concentration. The dependence of the pumping threshold and the correspondence emission wavelength versus concentration are reported in Figure 5.5. The chips with different cavity length ($0.7mm$ and $2.5mm$) have been tested using Rh6G as laser dye. Figure 5.6 shows that the expected threshold decrease is observed from 0.7mm to 2.5mm length while no additional improvement in the pumping threshold is associated to the increase of the cavity length up to 2.5mm. On the other hand, the longest F-P cavity shows a broader bandwidth.

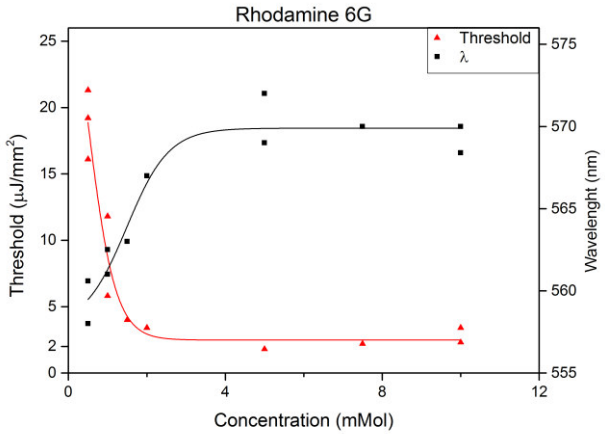

Figure 5.5 - Dependence of the pumping threshold and the correspondence emission wavelength versus concentration for a longitudinal cavity $1.5mm$ *length.*

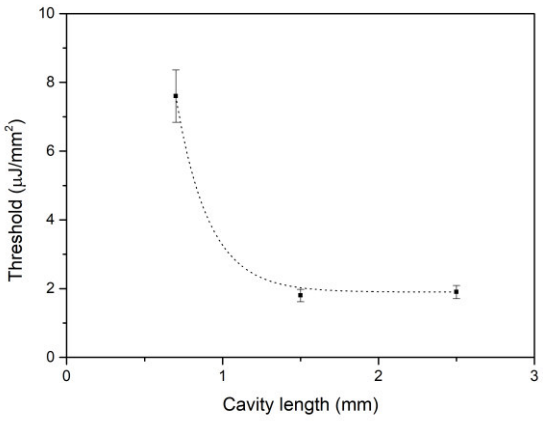

Figure 5.6 – Dependence of the pumping threshold versus longitudinal cavity length.

The $1.5\ mm$ long cavity has also been tested using Pyrromethene 597 (PM 597) and DCM as laser dyes. Similar performances (or even better) in case of PM 597 has been achieved for the emission bandwidth, however with some increase the required threshold. The Figure 5.7 correspond to the laser emission of this cavity when PM 597 is used at a concentration of $5mMol$ solved in ethyl alcohol.

On the contrary using DCM we have a remarkable increase of the threshold as shown in Figure 5.8(b) while the emission bandwidth is interesting as shown in Figure 5.8(a).

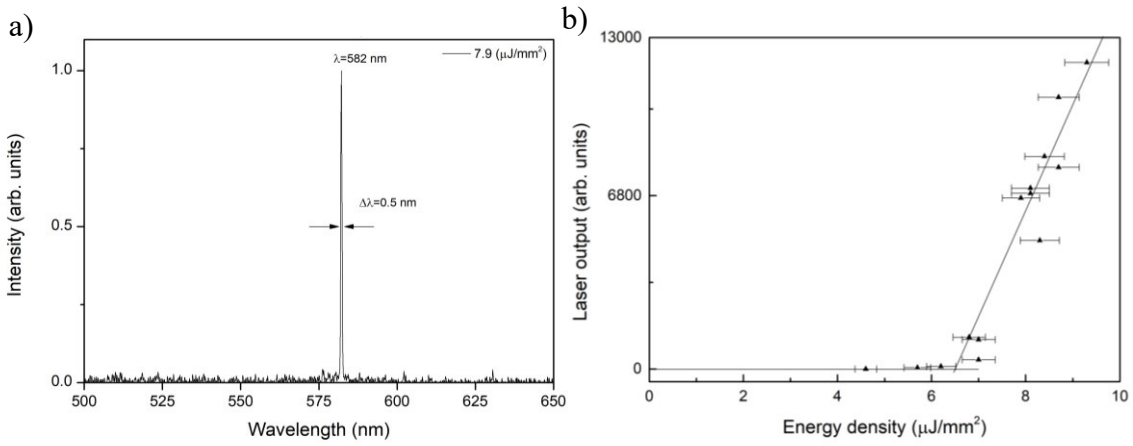

Figure 5.7 – a) Typical emission spectrum above threshold; b) Laser output versus energy density of the pumping pulse for a solution of PM597 in ethyl alcohol at concentration of $5mMol$.

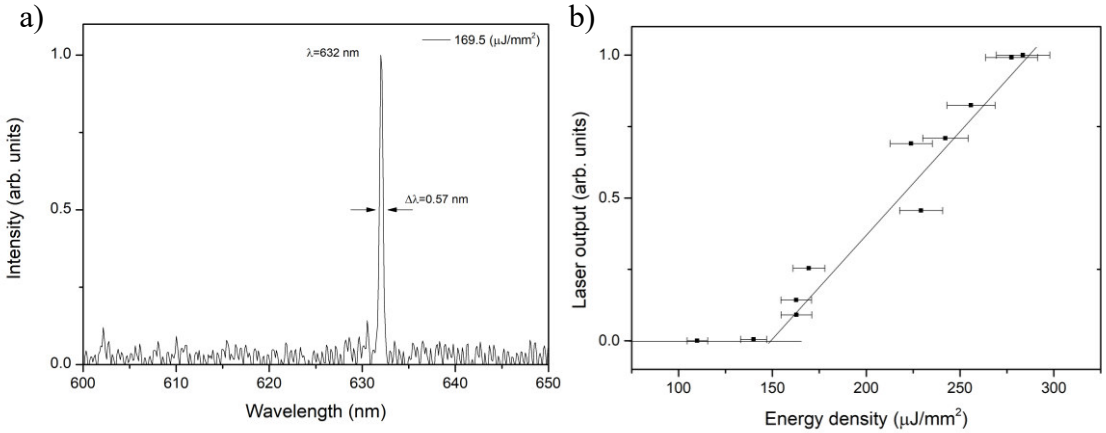

Figure.5.8 – a) Typical emission spectrum above the threshold; b) Laser output versus energy density of the pumping pulse for a saturated solution of DCM in ethyl alcohol.

Similar studies have been done with cavities length of $0.7\,mm$ and $2.5\,mm$: the performances in terms of linewidth has been confirmed and was achieved for both spectra with $\Delta\lambda < 0.9\,nm$ while the threshold value obtained define the trend reported in Figure 5.6.

It is also important to observe that the spectrometer (HR4000, Ocean Optics) used to acquire the light coupled out by the chip has a resolution of $0.12nm$ that is higher than the distance between two consecutive modes (0.07nm, Table 2). It means that the cavity does not select a single mode emission, but amplify a small range of modes.

5.2.3 Hemispherical cavity

Hemispherical cavity was realized with a cavity length of 1.5 mm as shown the best performances in F-P resonator. To study the behaviour of this device has been tested with Rhodamine 6G ($5mMol$) and Pyrromethene 597 ($1mMol$) at concentration of $5mMol$ in ethyl alcohol.

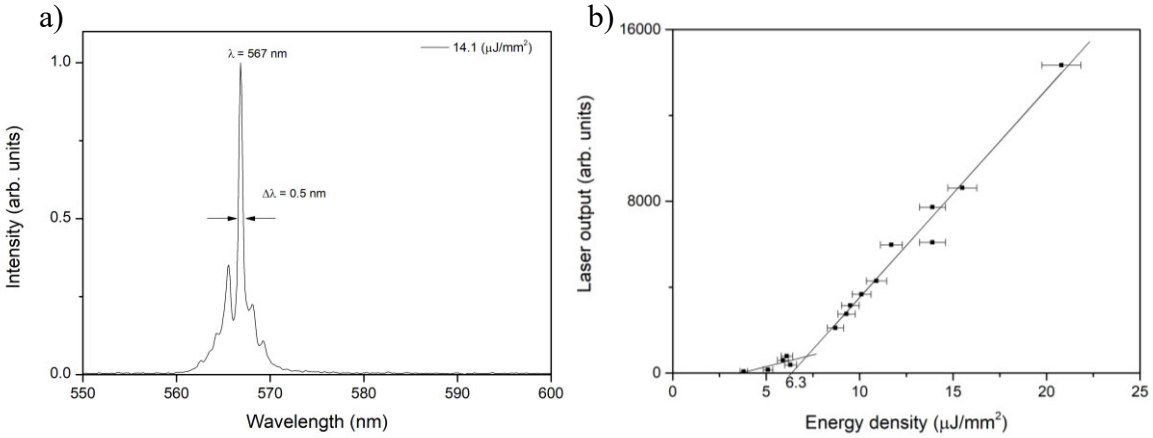

Figure 5.9 - Typical emission spectrum above the threshold; b) Laser output versus energy density of the pumping pulse for a solution of RH6G in ethyl alcohol at a concentration of $5mMol$.

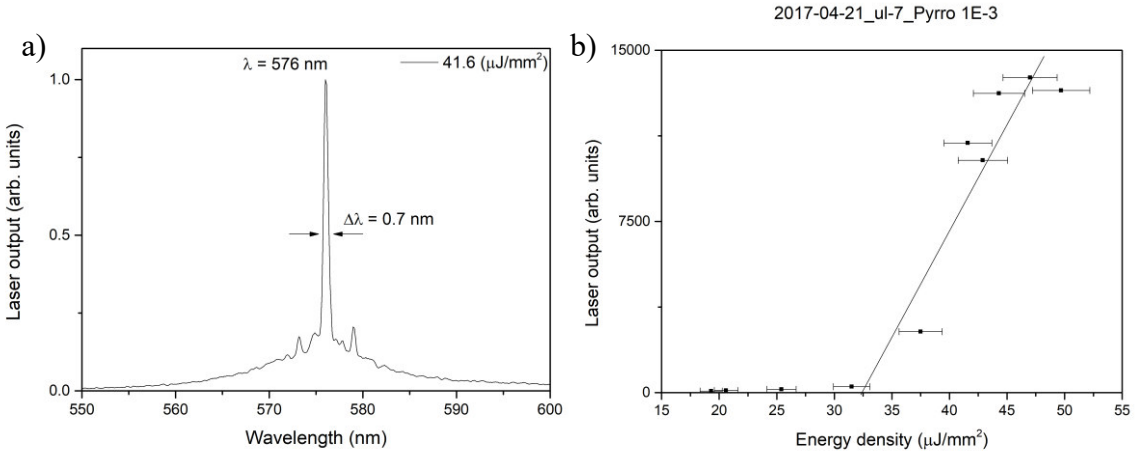

Figure 5.10 - Typical emission spectrum above the threshold; b) Laser output versus energy density of the pumping pulse for a solution of PM 597 in ethyl alcohol at a concentration of $1mMol$

Emission spectra and pumping energy density shown for Rh6G in Figure 5.9 and for Pyrromethene in Figure 5.10. In this case emission is characterized by a narrow peak with a bandwidth in same order of the previous cases. However, a broader background is present. Threshold is increased in comparison to the flat mirror cavity.

A further comparison between the hemispherical and the Fabry-Perot laser resonators have been carried out concerning the dependence of the device performances on the

alignment of the pump beam with respect to the active channel. Data reported in Figure 5.11 shown the emission spectra obtained by translating in the vertical plane the sample with respect to vertical plane of the focal spot of the pump beam. In case of F-P cavity (flat mirrors) we observe a critical dependence of the emission spectrum on the sample position. Translation leads to the appearance of additional spikes and to a wavelength shift of the main emission line. On the contrary, the hemispherical cavity looks less sensitivity to this translation: emission is always characterized by a broad background but the emission peak is always located at the same wavelength. This latter effect is clearly shown in Figure 5.12 where the laser emission corresponded to three different positions are superimposed

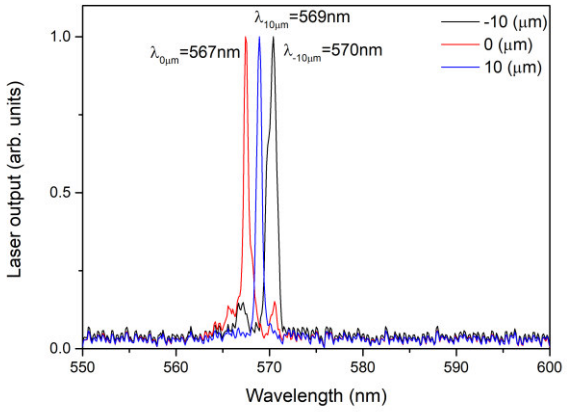

Figure 5.11 - Emission spectra above the threshold for a Fabry-Perot cavity length of 1.5mm*. The spectra are obtained by translating in the vertical plane the sample with respect to vertical plane of the focal spot of the pump beam, for a solution of Rh6G in ethyl alcohol at a concentration of 5mMol*

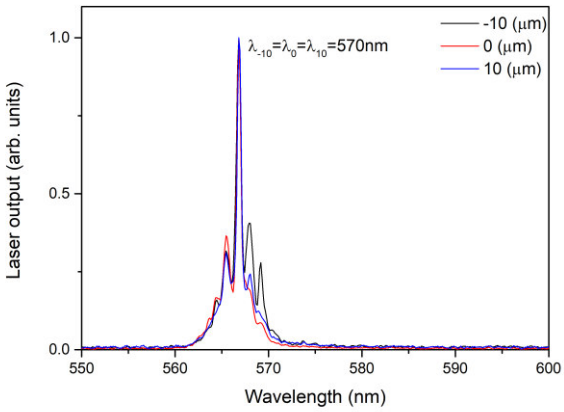

Figure 5.12 - Emission spectra above the threshold for a Hemispherical cavity with a length of 1.5mm*. The spectra are obtained by translating in the vertical plane the sample with respect to vertical plane of the focal spot of the pump beam, for a solution of Rh6G in ethyl alcohol at a concentration of 1mMol*

Wider sequence of measurement taken by changing the mutual position of focal spot and active channel by $100um$ are repoerted in Figure 5.13, for the Fabry-Perot cavity, an in Figure 5.14, for the hemisferical cavity, and confirm the behavioru just described.

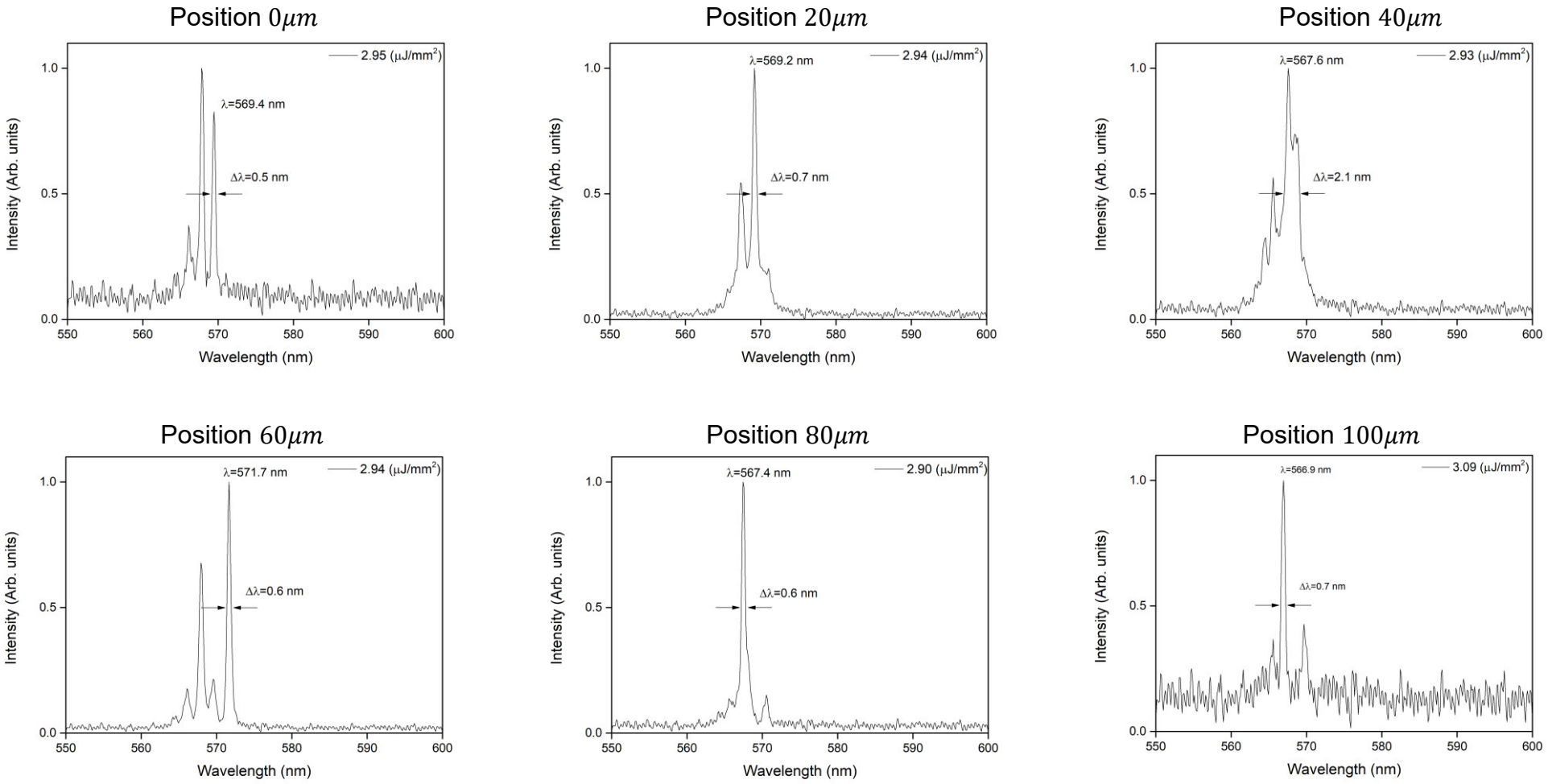

Figure 5.13 – Emission spectra above the threshold for a longitudinal cavity with a length of 1.5mm. The spectra are obtained by translating in the vertical plane the sample with respect to vertical plane of the focal spot of the pump beam by steps of 20μm*, for a solution of Rh6G in ethyl alcohol at a concentration of 5mMol*

While translating the hemispherical cavity with $1.5mm$ cavity length where flows a concentration of R6G $5mMol$ by steps of $10\mu m$, the following spectra are obtained:

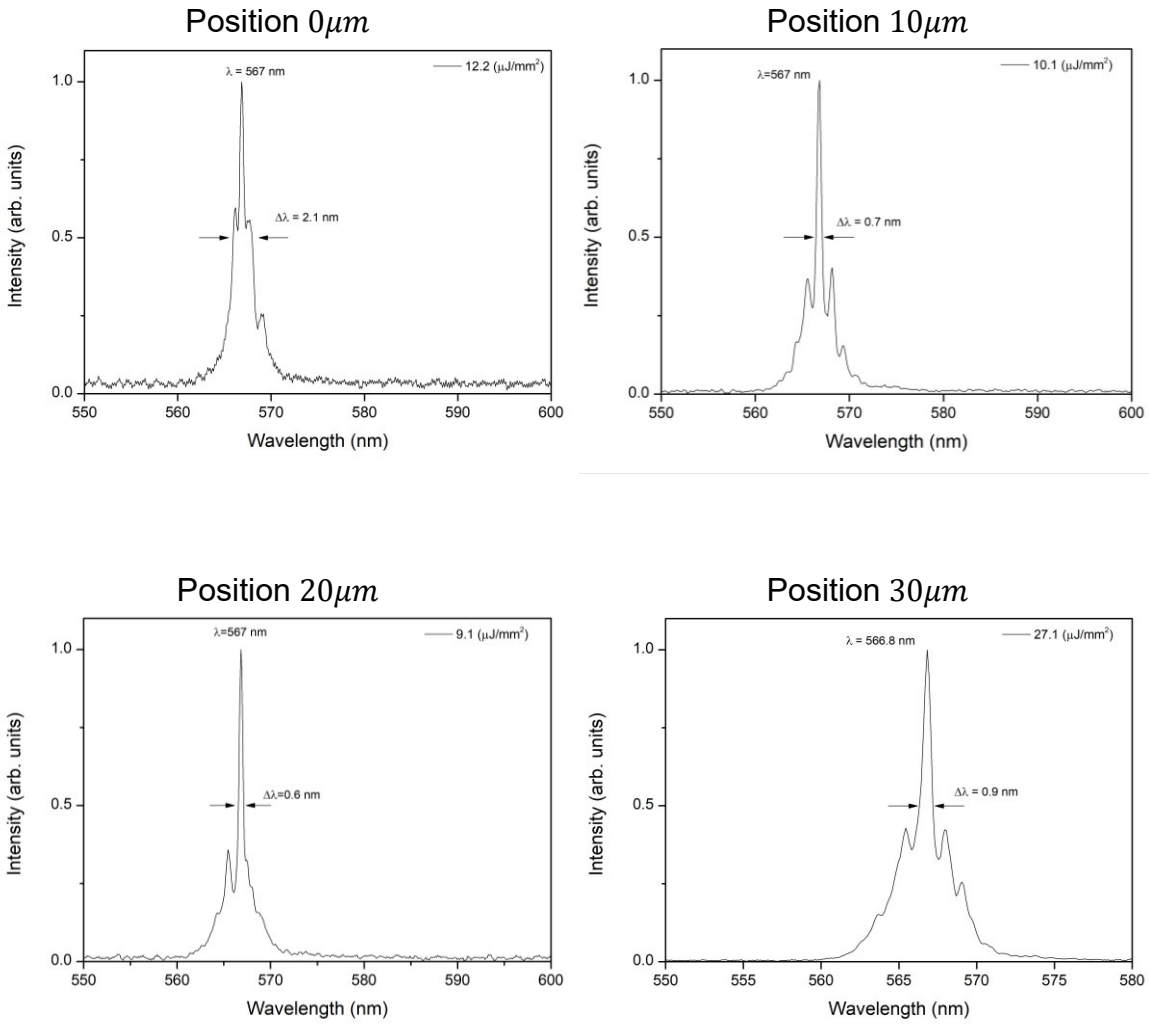

Figure 5.14– Emission spectra above the threshold for a hemispherical cavity with a length of 1.5mm. The spectra are obtained by translating in the vertical plane the sample with respect to vertical plane of the focal spot of the pump beam by steps of $10\mu m$*, for a solution of Rh6G in ethyl alcohol at a concentration of 5mMol.*

5.2.4 Cavity with control channel

The cavity with an internal control channel (see section 4.2.4) has been realized with the aim of exploiting the channel either to control the laser emission band or to investigate a sample fluid for sensing application. Firstly, we have characterized the device by using pure ethyl alcohol in the control channel and Rhodamine 6G at a concentration of $4mMol$ as active medium.

In this case the laser performance is shown in Figure 5.15. We can observe that we have just increased the threshold with no major change in the emission spectrum.

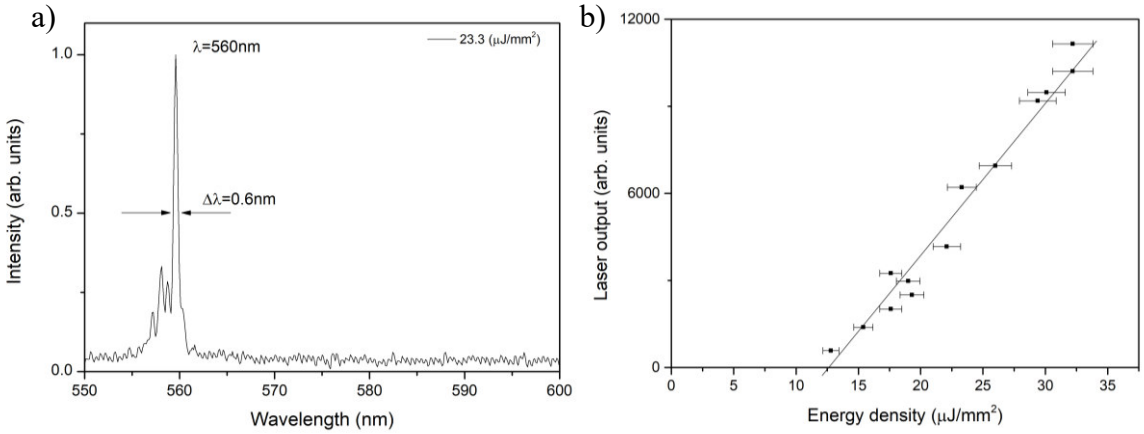

Figure 5.15 - a) Laser emission spectrum of for a solution of Rh6G in ethanol (0.4mMol) and pure ethanol in the control channel; b) Output vs energy density of the pump beam for the same condition

Additional experiments have been performed using pure solution of chloroform ($n = 1.4455$), and Cinnamaldehyde ($n = 1.6209$) in the control channel. No significant effect was observed as compared to was previously reported with ethyl alcohol.

Finally, we report an experiment has been performed including in the control channel an adsorbing medium. We have used Oxazine in ethyl alcohol at a concentration of $0.1mMol$. The absorption spectrum of the solution is shown in Figure 4.17 (a) where it is highlighted the 72.4% of transmission on the emission peak of the optofluidic laser. This measurement was performed with a 1cm thick cuvette and correspond to a 98% of transmission for the $52um$ transversal channel. In this case the laser emission spectrum is shown in Figure 5.16 (b) showing the expected cleaning of the background with respect Figure 5.15 (a)

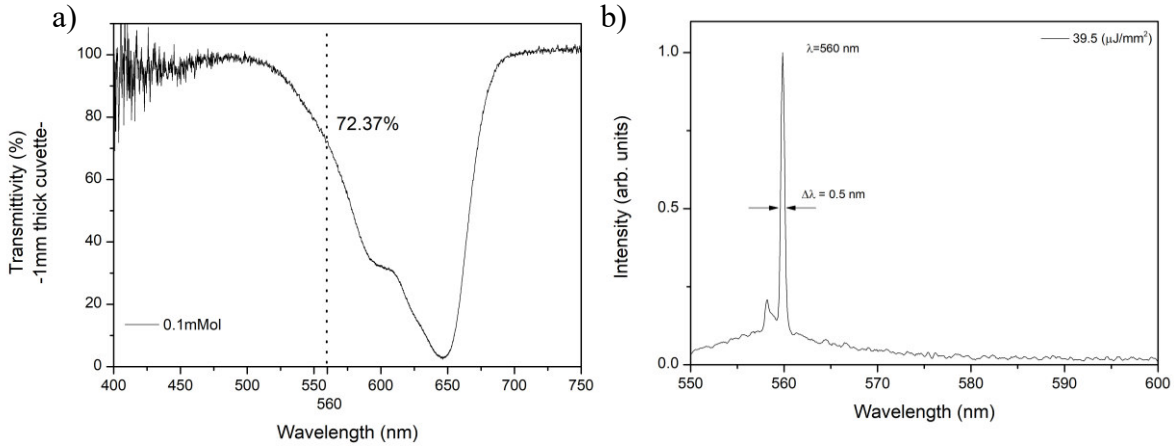

Figure 5.16 - a) Transmittivity of a low absorption material: Oxazine solved in ethanol at a concentration of 0.1mMol; b) Emitted spectra when a low absorbing material fill the control channel 52μm thick and. Rh6G in ethanol was the gain material (0.4mMol)

5.2.5 Use of different solvents

Some experiment has been carried out in the longitudinal cavity with length $0.7mm$ and solution of Rh6G in Cinnamaldehyde. The interest of trying this solution is in the high index of the solvent ($n = 1.62$) thus providing guiding conditions in the channel due to lower refractive index of the glass support ($n = 1.55$). The Figure 5.17(a) below shows the fluorescence of the used solution with a peak at $\lambda \approx 570nm$ for different pumping power when the concertation is 1mMol. No laser emission is observed. By increasing the concentration up to $5mMol$ a narrow laser peak ($0.5nm$) for energy density about $12\mu J/mm^2$ is clearly observed in Figure 5.17(b). It is quite remarkable the emission occurs on the edge of the luminescence spectrum.

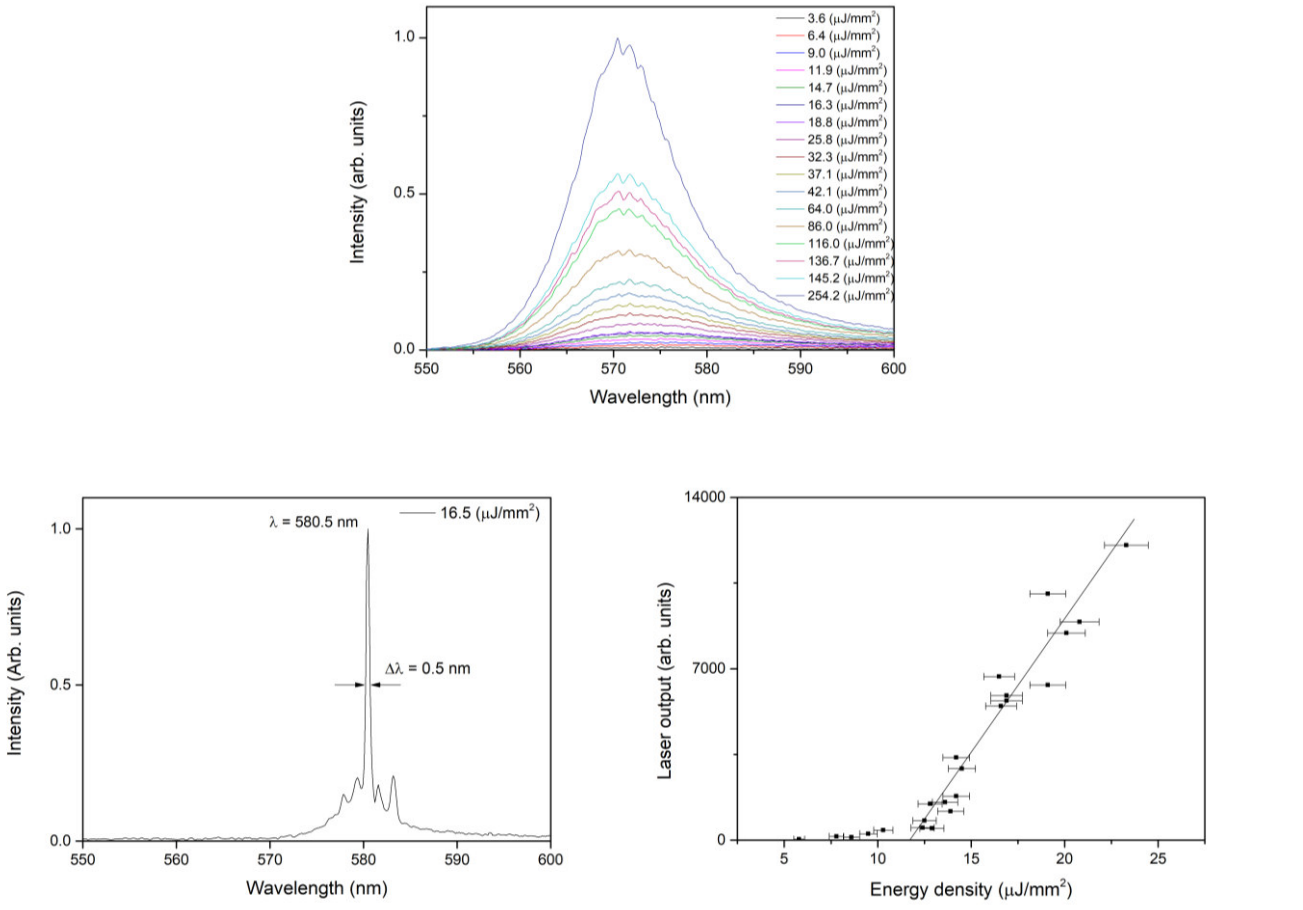

Figure 5.17 – a) Emission spectrum on transversal F-P cavity with Rh6G in cinnamaldehyde (1mMol); b) laser emission spectrum of Rh6G solved in Cinnamaldehyde (5mMol); c) Laser output vs energy density of the pumping pulse for the same dye concentratinon

Conclusion

The main achievements of the present work are: (i) realization of optical resonators fully embedded in glass; (ii) laser characteristics over the state of the art for optofluidic lasers based on Fabry-Perot cavities.

(i) Coupling FMT with high resolution Ink-Jet technology has been demonstrated to be a suitable method to realize robust optical resonator for the microfluidic technology. The powerful FMT allowed the fabrication of cavities with different geometries suitable for realization of dye lasers, exploiting the real 3D writing capabilities and the high resolution of the writing process by the femtosecond laser beam. The use of Ink-Jet technology allowed, for the first time, the coating of mirrors with controlled reflectivity inside a glass chip.

(ii) The best performances as been measured for a Fabry-Perot cavity 1.5mm long in a longitudinal geometry leading to emission bandwidth lower than $0.6nm$ and threshold lower than to $1.8\mu J/mm^2$. These digits are far below from any optofluidic laser based on Fabry-Perot cavity proposed up to now. In our case we were able to achieve a quality factor as high as Q~10^3. This result was possible thanks to the robustness of the glass support and to the high geometrical precision of the fabrication technique.

Nevertheless, there are some issues to be addressed to improve the optofluidic lasers performance in order to make them really suitable for lab-on-chip applications. The main issue concerns lowering the pumping threshold of about one order of magnitude to make suitable the use of a laser diode as pumping source. To this aim further investigation is necessary along different directions. First of all, it concerns the fabrication method: realization on smoother mirror surfaces, optimization of mirror reflectivity, test of different geometry for the optical resonators.

For what concerns the laser materials investigation should be carried on testing quantum dots as active media in order to look for higher efficiency in light emission. A second point will be the use of a suitable high index solvent in order to realize waveguide conditions to reduce the losses in the optical cavity.

It is also worth testing cavity designs and methods necessary to get wavelength tuning of the laser emission. In order to achieve this goal different methods can be proposed such as the use of birefringent layers in the cavity, liquid crystal mixture, etc.

References

[1] O. Svelto, Principle of lasers 1976 Plenum press, New York

[2] A. Yariv, Optical Electronics Fourth edition, 1991, Saunders College Publishing

[3] Z. Li, D. Psaltis, Optofluidic dye lasers, Microluid Nanofluid (2008) 4:145-158

[4] H. Becker, C. Gartner Polymer microfabrication technologies for microfluidic systems, Anal Bioanal Chem (2008) 390:89-111;

[5] M. Altissimo E-beam lithography for micro-/nanofabrication, Biomicrofluidics **4**, 026503 (2010); doi: 10.1063/1.3437589

[6] M. Austina, H. Geb, W. Wub, M. Lib, Z. Yub, D. Wasserman, S. A. Lyon, and Stephen Y. Choub Fabrication of 5nm linewidth and 14nm pitch features by nanoimprint lithography. Applied Physics Letters, 84 (26):5299-5301.2004.

[7] K. Sugioka and Y. Cheng Femtosecond laser processing for optofluidic fabrication Lab Chip 12 3576-3589 (2012)

[8] S. Lo Turco, Femtosecond laser micromachining for advanced manufacturing of microfluidics devices Ph.D. Thesis Politecnico di Milano 2011-2014

[9] R. Taylor, C. Hnatovsky, and E. Simova, Applications of femtosecond laser induced self-organized planar nanocracks inside fused silica glass. Laser & Photonics Reviews, 2(1-2):26–46, 2008.

[10] S. G. Bucella, G. Nava, K. C. Vishunubhatla, and M. Caironi, High-resolution direct-writing of metallic electrodes on flexible substrates for high performance organic field effect transistors. Organic Electronics, 14(9):2249–2256, 2013

[11] B. Helbo, A. Kristensen, and A. Menon, “A micro-cavity fluidic dye laser,” J. Micromech. Microeng. 13(2), 307–311 (2003)

[12] Y. Cheng, K. Sugioka, and K. Midorikawa, Microfluidic laser embedded in glass by three dimensional femtosecond laser micro processing, Opt. Lett. 2004 29, 2007-2009.

[13] Q. Kou, I. Yesilyurt, and Y. Chen, Collinear dual-color laser emission from a microfluidic dye laser, Applied Physics Letters 88, 091101 (2006); doi: 10.1063/1.2179609

[14] W.Song and D. Psaltis, Pneumatically tunable optofluidic dye laser, Applied Physics Letters 96, 081101 (2010); doi: 10.1063/1.3324885

[15] Kyoung-Sik MoonHai DongRadenka MaricSuresh PothukuchiAndrew HuntYi LiC. P. Wong,Thermal behavior of silver nanoparticles for low-temperature interconnect applications, Journal of Electronic Materials, February 2005, Volume 34, Issue 2, pp 168–175

[16] M. Altissimo E-beam lithography for micro-/nanofabrication Biomicrofluidics **4**, 026503 (2010); doi: 10.1063/1.3437589

[17] C. Tsao and D. L. DeVoe. Bonding of thermoplastic polymer microfluidics Microfuidics and Nanofuidics, 6(1):1-16, 2008. doi:10.1007/s10404-008-0361-x

[18] *K. Sugioka, Y. Hanada and K. Midorikawa, Three-dimensional femtosecond laser micromachining of photosensitive glass for biomicrochips, Laser & Photonics Reviews 2010, 4, 386–400*

[19] H. Chandrahalim, Q. Chen, A.A. Said, M. Dugan and X.Fan, Monolithic optofluidic ring resonator lasers created by femtosecond laser nanofabrication, Lab Chip 2015, 15, 2335-2340.

[20] G. Aubry, S. Meance, A.-M. Haghiri-Gosnet, Q.Kou, Microelectronic Eng. 2010, 87, 765-768

[21] Y. Yang, A. Q. Liu, L. Lei, L. K. Chin, C. D. Ohl, Q. J. Wang and H. S. Yoon, A tunable 3D optofluidic waveguide dye laser via two centrifugal Dean flow streams, Lab Chip 2011, 11, 3182-7.

[22] D.V. Vezenov, B.T. Mayers, R.S. Conroy, G.M. Whitesides, P.T. Snee, Y.Chan, D.G. Nocera, and M.G. Bawendi, A Low-Threshold, High-Efl ciency Microfluidic Waveguide Laser, J.Am.Chem.Soc. Comm. 2005, 127, 8952-8953

Appendix A

Visiting periods spent in other University

During this three years project, I had the opportunity of participating in two summer schools and to carrying out some research activities in two different Universities, allowing me to learn and better understand other technologies related to micro-and nanofabrication.

Summer schools

The summer schools that I attended were focused on the introduction to current and promising technologies available for the fabrication of polymeric optofluidic sensor systems. Sensors which can be used in many fields of research and real life. For instance, the following sensors have been considered: device for manipulation of red blood cell, device to detect glucose concentration in blood.

Visiting periods

Part of my research activity was carried out in the group of Prof. Christian Karnutsch at the Institute of Optofluidics and Nanophotonic (IONAS) of the Applied Science University (Karlsruhe, Germany November 2015) and in the group of Prof. Anders Kristensen at the Department of Micro and Nanotechnology (DTU Nanotech) at Technical University of Denmark (Lyngby, Denmark, August-September 2016 and September 2017).

Activity at IONAS

During the four weeks at IONAS I worked on the realization of air suspended polymer structures by using a bonding technique with a silicone stamp. The process involved the lamination of layers of SU-8 onto a KMPR microstructure. The two materials are both polymers but characterized by different refractive index, in particular SU-8 has higher refractive index. The validation of this fabrication process allowed the development and the successive realization of a sensor in which a thin layer of air suspended SU-8 acts as optical guide. The two major goals achieved are: (i) the demonstration of the potential and a real application of the lamination process by realizing a vertical microfluidic mixer on silica and glass substrates and (ii) the realization of samples to qualify the resulting mechanical bond strength of the membranes of different thickness covering microfluidic channels of different widths from $50\mu m$ to $250\mu m$. The thickness of the membranes itself is ranging from $5\mu m$ down to $0.5\mu m$. Figure A1.

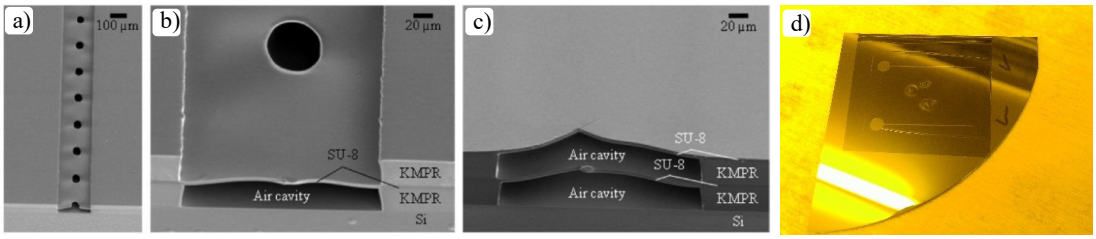

Figure A1 SEM images of the microfluidic vertical mixer during the fabrication steps. (a) Laminated SU-8 layer with opening on top of the first KMPR microfluidic channel; (b) magnification of the laminated layer and the structure of the second microfluidic channel (c) section of the sealed 3D microfluidic mixer fabricated by combining photolithography and lamination processes. (d) Picture of one of the samples used during the mechanical bond strength of the SU-8 membrane sealed on top of KMPR microfluidic channel.

During the fabrication of the samples for the bond strength qualification tests, we found some issue about the lamination of the thin films because they sometime appeared broken. It is well known that polymerization process is sensitive to clean room climate parameters (temperature and relative humidity) and process parameters (post exposure bake at room temperature or at high temperature). Attention has been focused to the plasma treatment used to temporary increase the adhesion between SU-8 and PDMS, considering (i) how much and how long it affects the adhesion enhancement; and (ii) if the control of the plasma treatment atmosphere can simplify the demoulding process between PDMS carrier and the SU-8 layer.

The first experiment was done to monitor the PDMS surface wettability when one droplet of SU-8 2000.5 was daily left in two PDMS samples: one where the surface was previously treated by plasma and another without any treatment. It was observed that, after three days, the wettability of the PDMS surfaces becomes comparable with the not

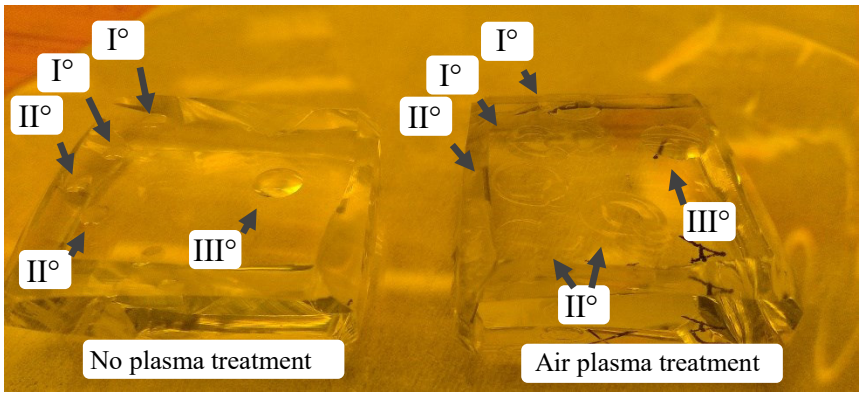

Figure A2 picture at the end of the PDMS surface wettability evolution. On the left the sample without plasma treatment, on the right the sample with plasma treatment.

treaded one. This allows pointing out the key role played by the plasma treatment in the lamination process. (see Figure A2).

In the second experiment three PDMS molds were laminate by a $7\mu m$ thick layer of SU-8 over three KMPR microfluidic channels (width 250 μm) following the same procedure. The first sample was laminated without any pre-treatment, the second after pure N_2 plasma treatment of the silicone mold, while the third one after environmental air plasma treatment. The following table summarizes the results.

PDMS treatment	**Adhesion forces**
No	**Low**
Pure N_2	**Medium**
Environmental air	**High**

This visiting period gave me the opportunity of gaining experience with photolithography and lamination processes.

Activities at DTU Nanotech

During the visiting periods at Nanotech the Ink-Jet technology was tested for the plasmonic colour generation. Prof. Kristensen and its group is working on the generation of colours by localized surface plasmon resonator (LSPR) using the hybridization between LSPR modes in aluminium nanodisks and nanoholes to design and fabricate bright colours in the whole visible spectrum.

In order to realize plasmonic resonances, a nanostructure with cylindrical pillars was realized by replication of a master mold with nanoholes realized by electron beam lithography. Aluminium is evaporated on top, creating the disk-hole structure thereby revealing colours due to the underlying polymer topography. The structure was coated with a protective transparent material. (see Figure A3).

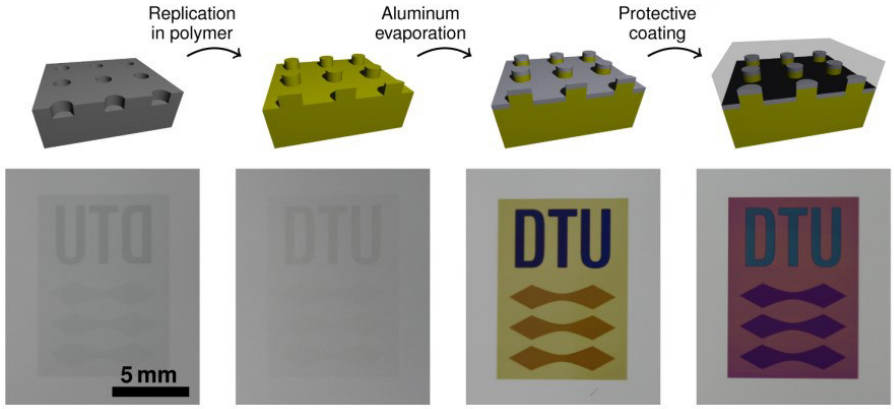

Figure A3 - Basic concept of fabrication and working mechanism; from the left, master mould used to realize nanopillars by replication method. Nanostructured after aluminium evaporation from the top of the surface that generate nanodisks and nanoholes; the final structure covered by a transparent protective coating.

Thanks to the aluminium evaporation it is possible have a precision thickness control that allows an electrical separation between the deposition on top and on the bases of pillars. However this process is expensive and requires a vacuum chamber. For these

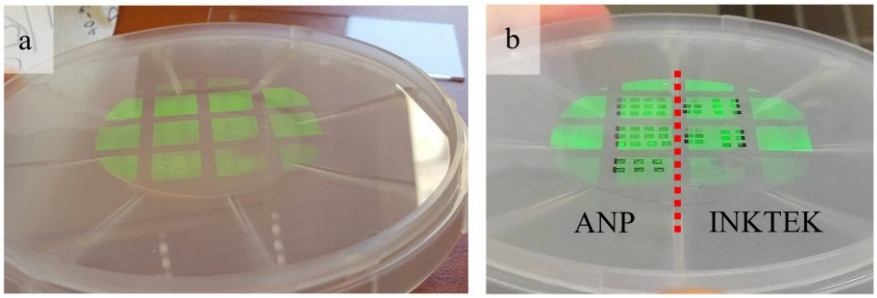

Figure A4 Picture of the sample used to study the plasmonic resonance. Sample before (a) and after (b) the printing process. Squares of 1.5mm^2 size were printed using Silver-based ink from two different companies: ANP and INKTEK.

reasons we tried a different technique using inks for printable electronic to realize the nanoholes structure. This activity was performed in collaboration with the FemtoFab in the Centre for Nano Science of the Italian Institute of Technology (CNST-IIT). Two commercial inks (Inktech ij010 and ANP silverjet DGP-40LT15C) were used to realize a coating of $1.5mm^2$ on a nanostructure. The nanostructure was an array of pillars with height of $30nm$, variable diameter in the range of between $60 - 100nm$ and pitch of $200nm$.

Replacing the aluminium evaporation process with the metallic Ink-Jet printing has the advantage of printing only the required areas. For the considered sample, the smaller printable area of about $27\mu m^2$ (one 10pL sintered droplet).

The characterization test was performed checking the metallic squares quality in terms of uniformity and homogeneity by optical microscope observations (Nikon Eclipse Ti) and acquiring the reflection spectrum of the most interesting samples by a CCD spectrometer (Andor Shamrock).

The most interesting results were achieved in an area where some droplets were missing, generating an edge with a gradual reduction of the printed ink that generates green light, as shown in Figure A5. In this area was measured a selective absorption in

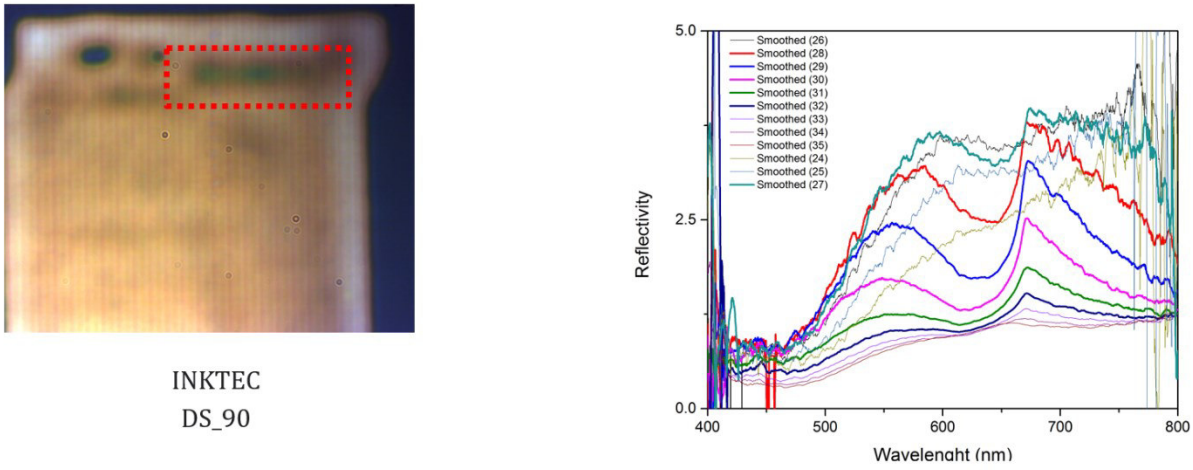

Figure A.5 Microscope image and reflectivity spectrum of the defect at the printed area. The graph reports some selected spectrum from different positions. Spectra showing a higher reflectivity around the green wavelength region are evident.

between $630 - 670nm$. This test pointed out that in general the thickness of the ink coating was too high to give rise to the required colours.

An alternative way to realise metallic layer was proposed with the use of a different ink (mts-jl, Harma) coupled to laser sintering. This material was spin coated in order to get a thin and uniform layer and then sintered by focused laser light at 1032nm. Several silver layers (thickness in range of $30 - 100nm$) where realized over the pillars height. Figure A6 shows a SEM image of the sintered metallic square achieved by moving the sample during the light exposure. As visible in the inset, the metallic film follows the nanotexture topography. We tried to obtain uniform metallic film with different thickness changing the laser energy dose. In general, we obtained different kind of aggregations that correspond to different reflection spectra, as reported in Figure A7. The picture shows that the same sintering parameters produce different absorptions, then the sintering process needs to be further investigated in order to achieve a higher control of the process. In any case these results represent a first step in order to control the light absorption of structured surfaces with the aim of using silver based ink to realize plasmonic colours.

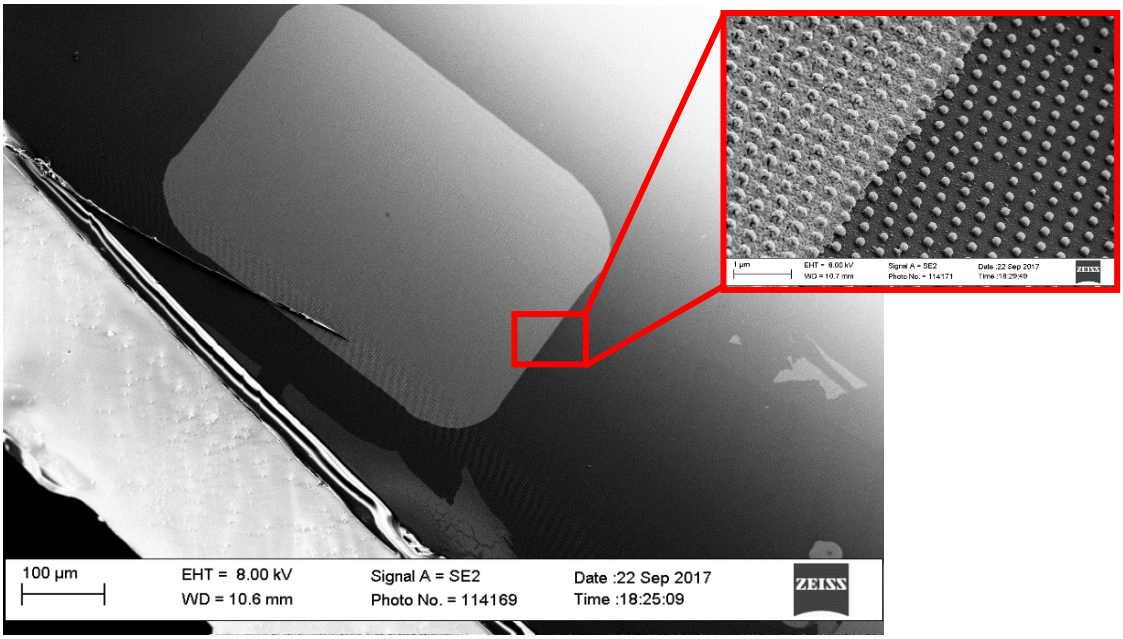

Figure A6 – SEM images of Sample 2, square 2 fabricated with oscillator power 1657mW + Att. 7%, 50X microscope objective, ink surface down, writing speed o 5mm/s

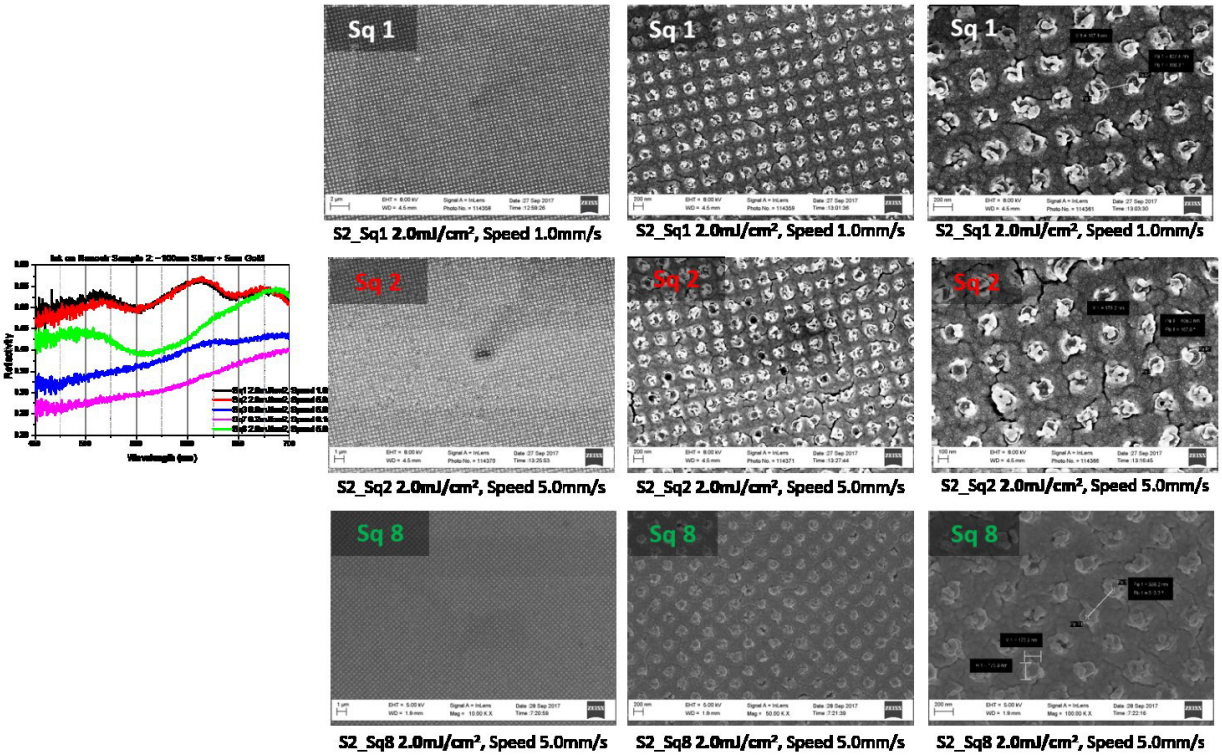

Figure A7- Reflected spectra and SEM images of three samples treat with different energy dose.

Appendix B

Publication in international journals

Research Article | Vol. 24, No. 15 | 25 Jul 2016 | OPTICS EXPRESS 17416
Optics EXPRESS

Low threshold Fabry-Perot optofluidic resonator fabricated by femtosecond laser micromachining

F. SIMONI,[1] S. BONFADINI,[2,3] P. SPEGNI,[1] S. LO TURCO,[3] D.E. LUCCHETTA,[1] AND L. CRIANTE[3,*]

[1]*Department of Scienze e Ingegneria della Materia, dell'Ambiente ed Urbanistica, Università Politecnica delle Marche, 60131 Ancona, Italy*
[2]*Department of Physics, Politecnico di Milano, Piazza Leonardo da Vinci 32, 20133 Milano, Italy*
[3]*Center for Nano Science and Technology CNST-IIT@PoliMi, Istituto Italiano di Tecnologia, via Pascoli 70/3, 20133 Milano, Italy*
[*]*luigino.criante@iit.it*

Abstract: We report the realization and characterization of an optofluidic microlaser based on a Fabry-Perot resonator fabricated by exploiting two direct writing fabrication techniques: the femtosecond laser micromachining and the inkjet printing technology. In this way a standard Fabry-Perot cavity has been integrated into an optofluidic chip. When using rhodamine 6G dissolved in ethanol at concentration of $5 \cdot 10^{-3}$ mol/l, laser emission was detected at a threshold energy density of 1.8 μJ/mm^2 at least one order of magnitude lower than state-of-the-art optofluidic lasers. Linewidth below ~0.6 nm was measured under these conditions with a quality factor Q~10^3. These performances and robustness of the device makes it an excellent candidate for biosensing, security and environment monitoring applications.

OCIS codes: (140.0140) Lasers and laser optics; (230.0230) Optical devices; (140.2050) Dye lasers.

References and links

1. B. Helbo, A. Kristensen, and A. Menon, "A micro-cavity fluidic dye laser," J. Micromech. Microeng. **13**(2), 307–311 (2003).
2. G. Aubry, Q. Kou, J. Soto-Velasco, C. Wang, S. Meance, J. J. He, and A.-M. Haghiri-Gosnet, "A multicolor microfluidic droplet dye laser with single mode emission," Appl. Phys. Lett. **98**(11), 111111 (2011).
3. W. Song, A. E. Vasdekis, Z. Li, and D. Psaltis, "Low-order distributed feedback optofluidic dye laser with reduced threshold," Appl. Phys. Lett. **94**(5), 051117 (2009).
4. M. Gersborg-Hansen and A. Kristensen, "Tunability of optofluidic distributed feedback dye lasers," Opt. Express **15**(1), 137–142 (2007).
5. X. Fan and S.-H. Yun, "The potential of optofluidic biolasers," Nat. Methods **11**(2), 141–147 (2014).
6. H. Chandrahalim, Q. Chen, A. A. Said, M. Dugan, and X. Fan, "Monolithic optofluidic ring resonator lasers created by femtosecond laser nanofabrication," Lab Chip **15**(10), 2335–2340 (2015).
7. Y. Cheng, K. Sugioka, and K. Midorikawa, "Microfluidic laser embedded in glass by three-dimensional femtosecond laser microprocessing," Opt. Lett. **29**(17), 2007–2009 (2004).
8. Q. Kou, I. Yesilyurt, and Y. Chen, "Collinear dual-color laser emission from a microfluidic dye laser," Appl. Phys. Lett. **88**(9), 091101 (2006).
9. G. Aubry, S. Meance, A.-M. Haghiri-Gosnet, and Q. Kou, "Flow rate based control of wavelength emission in a multicolor microfluidic dye laser," Microelectron. Eng. **87**(5-8), 765–768 (2010).
10. Y. Yang, A. Q. Liu, L. Lei, L. K. Chin, C. D. Ohl, Q. J. Wang, and H. S. Yoon, "A tunable 3D optofluidic waveguide dye laser via two centrifugal Dean flow streams," Lab Chip **11**(18), 3182–3187 (2011).
11. D. V. Vezenov, B. T. Mayers, R. S. Conroy, G. M. Whitesides, P. T. Snee, Y. Chan, D. G. Nocera, and M. G. Bawendi, "A low-threshold, high-efficiency microfluidic waveguide laser," J. Am. Chem. Soc. **127**(25), 8952–8953 (2005).
12. M. Beresna, M. Gecevičius, and P. G. Kazansky, "Ultrafast laser direct writing and nanostructuring in transparent materials," Adv. Opt. Photonics **6**(3), 293–339 (2014).
13. R. Osellame, H. J. W. M. Hoekstra, G. Cerullo, and M. Pollnau, "Femtosecond laser microstructuring: an enabling tool for optofluidic lab-on-chips," Laser Photonics Rev. **5**(3), 442–463 (2011).
14. R. Taylor, C. Hnatovsky, and E. Simova, "Applications of femtosecond laser induced self-organized planar nanocracks inside fused silica glass," Laser Photonics Rev. **2**(1-2), 26–46 (2008).
15. S. LoTurco, R. Osellame, R. Ramponi, and K. C. Vishnubhatla, "Hybrid chemical etching of femtosecond laser irradiated structures for engineered microfluidic devices," J. Micromech. Microeng. **23**(8), 085002 (2013).
16. A. Kiraz, Q. Chen, and X. Fan, "Optofluidic lasers with aqueous quantum dots," ACS Photonics **2**(6), 707–713 (2015).

#268449 http://dx.doi.org/10.1364/OE.24.017416
Journal © 2016 Received 16 Jun 2016; revised 18 Jul 2016; accepted 18 Jul 2016; published 22 Jul 2016

Optics EXPRESS

17. R. M. Gerosa, A. Sudirman, L. S. Menezes, W. Margulis, and C. J. S. de Matos, "All-fiber high repetition rate microfluidic dye laser," Optica **2**(2), 186 (2015).

1. Introduction

The story of optofluidic lasers started more than a decade ago with a nice demonstration given by Helbo et al. who were able to show lasing action from a microchannel where Rh6G was slowly flowing, getting a linewidth of 5.7 nm with a threshold of few hundreds of $\mu J/mm^2$ [1]. After that time a lot of work has been done on this topic leading to different solutions to get single mode emission [2], low threshold [3], tunability [4]. Some of these configurations have been successfully exploited for biosensing [5]. The interest in developing such devices relies in the great potential of being used in lab-on-chip (LOC) technology because integrable coherent light sources are essential for those kind of applications, mainly in biomedical, security and environment monitoring field. The first issue to be addressed to make them attractive for large scale fabrication is avoiding a complex manufacturing composed of many different steps. This concept has been recently underlined by demonstrating the monolithic nanofabrication of an optofluidic ring resonator by femtosecond laser writing [6]. A reliable and robust ring microlaser has been realized achieving a threshold fluence of $\approx 15\ \mu J/mm^2$ and a quality factor $Q \approx 3.3 \cdot 10^4$. This demonstration comes after more than ten years after the first attempt to realize a laser cavity using a similar fabrication technique [7]. In this case the fabricated optical cavity was realized by four 45° micromirrors vertically buried inside the glass substrate formed by hollow structures and working as total internal reflectors. A 80 μm diameter microchannel crossing the cavity provided the active medium flow (Rh6G dye in ethanol). Laser action was observed above an energy density threshold of $\approx 16.6\ \mu J/mm^2$ with a linewidth of about 5 nm. As a matter of fact the most simple laser cavity based on a Fabry-Perot resonator has not yet been realized exploiting this fabrication method so far due to the difficulty of getting suitable high reflectivity mirrors that are both perfectly aligned independently of the length of the cavity and not in contact with the active medium solution avoiding any degradation phenomenon.

Besides the first report [1] a few examples of Fabry-Perot cavity in optofluidic microlaser have been reported realizing reflecting mirrors by coating with metallic films either the edge of fibers used to collect the signal [8,9] or the side of the microfluidic channel [10,11]. In all these cases multi-steps soft lithography was used to realize the microfluidic structures, their perfect alignment is not easy especially for long cavity and usually the metallic mirror was put into contact with the dye solution. Most of these devices were mainly addressed to demonstrate multicolor emission and tunability rather than to improve threshold conditions and emission linewidth, that was in all cases larger than 3-4 nm. These last two laser peculiarities are the key requirements to be fulfilled in order to increase the measurement sensitivity in LOC platform systems.

In this paper we report the first demonstration of an optofluidic laser based on a Fabry-Perot optical cavity "fully embedded" in the glass substrate realized by coupling the ink-jet technology, necessary to get a fine control of surface coating using a highly reflective metallic ink, with the femtosecond laser processing. By using a solution of Rh6G as active medium we were able to get reliable laser emission above a threshold of $1.8\ \mu J/mm^2$ and a linewidth as low as ≈ 0.6 nm getting a quality factor $Q \approx 10^3$.

2. Experimental methods

2.1 Design and fabrication

The devices realization takes advantage from an innovative combination of two direct writing fabrication techniques: the femtosecond laser micromachining and the inkjet printing technology.

Optics EXPRESS

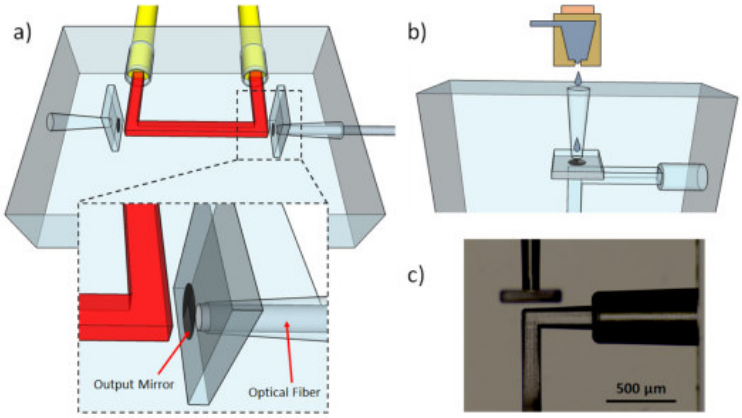

Fig. 1. Sketch of the device. a) Fabry-Perot long cavity geometry; b) micro mirror fabrication procedure c) optical microscope image of the zoom section.

Different geometries have been fabricated and investigated although the most basic configuration of the proposed optofluidic microlaser is shown in Fig. 1. It is composed by a central microfluidic channel where the active material flows and two square section empty "basins" – located close to the dye recirculation microchannel – where metallic mirrors will be directly printed in a second step, Fig. 1(b). Since the aim of these "basins" is to facilitate the mirror printing, its size and shape have been chosen in order to facilitate the ink wettability of the inner surface (avoiding phenomena of clogging before the annealing procedure) and to ensure a printed mirror diameter at least double with respect to the fiber core. Integrated broad band optical fiber, inserted in the partial reflector side, and two microtubes (inlet and outlet) complete the microcircuit design in order to out-couple the emitted light and connect the chip to the macroscopic external world. In order to insert the optical fiber (as well as the microtube), the structure includes two conical channels reaching the basins and the microfluidic channel. The special conical geometry of these channels ensures optimum fiber (and tubes) alignment with the internal part of the chip, already during the insertion.

The microfluidic structure is completely buried inside a pure fused silica substrate (JGS1, FOCtek), obtained after ultrafast laser irradiation followed by chemical etching [12–15]. As well-known this technique is based on the multiphoton absorption and consequent modification of the physical-chemical properties of the substrate. In a particular irradiance regime, a self-organized internal structure (nanograting) is formed with a period of $\lambda/2n$ (n integer) depending on the wavelength λ and polarization writing pulse. Moreover these assemblies are generated in the perpendicular direction with respect to the polarization of the laser beam. Since the femtosecond laser pulse writing affects a small volume of the material (only in the beam focus) without thermal effects, it is possible to create inside the substrate structures with arbitral 3D geometry.

When the written microchip is put in a chemical etching solution (typically HF), it digs the irradiated zone more rapidly respect to the non-irradiated ones creating the microfluidic circuit (the reasons of this selective action are mainly due to the chemical and physical modification the material achieved by the femtosecond laser treatment).

The used laser micromachining system is equipped with a regenerative amplified mode-locked femtosecond laser source based on Yb:KGW active medium (PHAROS - Light Conversion) whose pulses at the fundamental wavelength of 1030 nm are characterized by duration of 240 fs, repetition rate up to 1 MHz and pulse energy up to 0.2 mJ. In order to work in the "nanograting regime" [12] the second harmonic at λ = 515 nm and 500 kHz repetition rate has been used with average power set at 200 mW. The laser light is statically

Optics EXPRESS

focused inside the substrate (1 mm thickness) through a microscope objective (50X, Mitutoyo, NA 0.42) and the 3D structure is achieved moving the sample, placed on an high precision three axis air-bearing translation stage (Aerotech, ABL 1000 series) with a resolution of 2 nm, at the speed of 1 mm/s.

Concerning the etching step the irradiated sample is placed in HF aqueous solution at 20% concentration at controlled temperature (35 °C) for few hours. The obtained small device (4 mm x 4 mm) represents the microfluidic chip as shown in Fig. 2(b).

Taking advantage from the optical fiber access, two broadband micro reflectors are fabricated in bulk structure by means of a controlled dispensing of silver organic complex inks (TEC-IJ-010 InkTec Co., Ltd.) using an inkjet printer (DIMATIX - Fujifilm). By adjusting the volume of the dispensed inks, one mirror was realized as completely reflective while the other one, to be used as output mirror, was realized has partial reflector, with a possible fine-tuning of the reflectivity in the range from 60% to 95%. In order to remove the solvents and make sintering of the silver film the sample is heated at 150 °C for 5 minutes on a hotplate. Finally the device must be connected to the external world, so two microfluidic tubes (external diameter 360 μm) are inserted into their specific compartments and fixed with UV-curable glue (NOA 65). Following the same procedure, an optical fiber is inserted and fixed in the semitransparent mirror arm in order to directly collect and out-couple the laser light. In this way a ready-to-use monolithic device has been obtained. In the case here reported the optical cavity length is of 1.6 mm, the average square channel section is of 200 μm and the output mirror reflectivity is about 92% at 570 nm. The actual device is shown in Figs. 2(a) and 2(b).

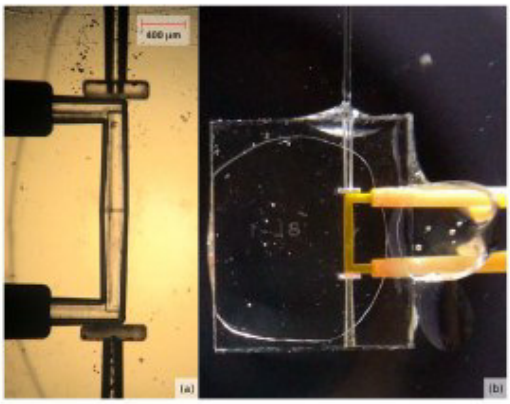

Fig. 2. a) Optical micrograph of the top view of the microfluidic laser; b) photo showing the fabricated chip and the cavity with the laser dye.

2.2 Optical characterization

In order to test the optofluidic laser performances, the glass chip was fixed on a x-y-z translation stage and properly plugged with inert tubes connected to a high performance syringe pump. It was providing a stable flow (3.3 μl/minute) of the solution made by RhG6 dissolved in ethanol at concentrations ranging from $1 \cdot 10^{-2}$ to $1 \cdot 10^{-4}$ mol/l. The used flow rate guarantees complete replacement of new dye molecules in the cavity volume between two succesive pumping pulses, in order to avoid any bleaching or quenching effect. The fiber optic coming from the glass chip was connected to an Ocean Optics spectrometer with resolution of 0.2 nm and the signal analyzed by a computer. The optofluidic laser was pumped by the second harmonic of a pulsed Nd-YAG laser at 532 nm and pulse duration ~5 ns. The pump beam power was controlled by means of neutral density filters and fine-tuned by rotating a half-wave plate placed before a polarizer providing vertical polarization of the

Optics EXPRESS

beam. A beam splitter was used to monitor the intensity of each laser pulse by a fast photodetector. After the beam splitter, a cylindrical lens (focal length f = 5 cm) and a diaphragm allowed getting a focal spot suitable to overlap the optofluidic laser cavity. The reference photodetector was previously calibrated through measurements of the beam power by a power meter located in the position of the glass chip. In this way it was possible to monitor the energy of each pumping pulse. A careful measurement of the laser spot size was carried out by the knife-edge technique using a razor blade in front of a detector. The focused spot resulted to have a dimension of 2.2 × 0.09 mm^2 ≈0.2 mm^2. A sketch of the experimental set-up is given in Fig. 3.

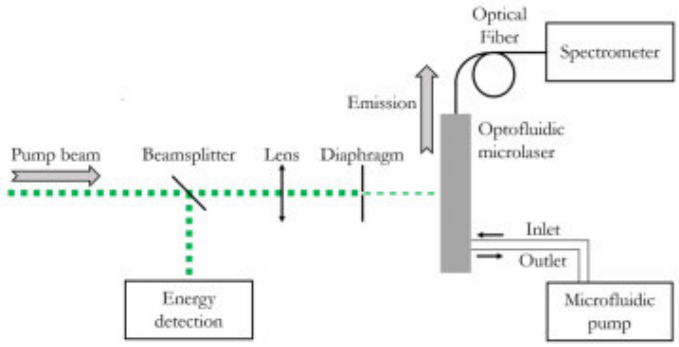

Fig. 3. Experimental set-up for optofluidic micro laser analysis.

3. Results and discussion

Measurements were performed at different pumping power and different dye concentrations. An example of the appearance of the laser action over the dye spontaneous emission band is given in Fig. 4.

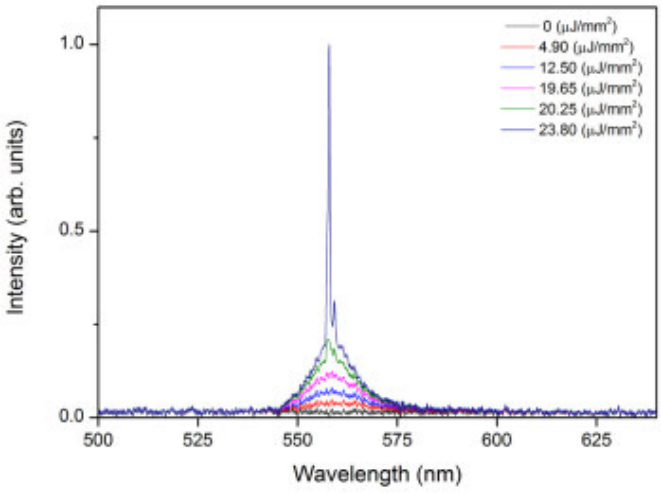

Fig. 4. Typical emission spectrum increasing the pump power. Data correspond to dye concentration of 10^{-4} mol/l.

Actually the transition from the spontaneous to the laser emission can be easily observed in the less efficient cases, while when the laser threshold is very low, spontaneous emission

Optics EXPRESS

cannot be easily observed since it is mixed with the detection noise. Figure 5 depicts the evolution of the spectrum linewidth showing the narrowing effect at the threshold of ~22 μJ/mm^2. An optimal performances of this device were obtained with a careful alignment to get the best matching between the pump beam spot size and the dye microfluidic channel. Under these conditions the measured threshold values ranged from 1.8 μJ/mm^2 to 22 μJ/mm^2 depending on the dye concentration.

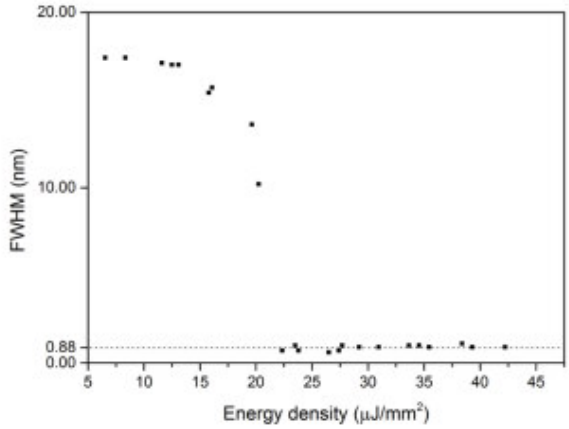

Fig. 5. Full width half maximum of the stimulated emission bandwidth vs pumping energy density. Data correspond to dye concentration of 10^{-4} mol/l.

Figure 6 displays the laser output vs the energy density of the pumping pulse for a Rh6G concentration of $5\cdot10^{-3}$ mol/l that showed the lowest threshold of 1.8 μJ/mm^2. In Fig. 7 it is shown the typical emission spectrum above threshold for this concentration: such narrow linewidth ($\Delta\lambda < 0.6$ nm) slightly increases to values $\Delta\lambda < 0.9$ nm by increasing the pump power.

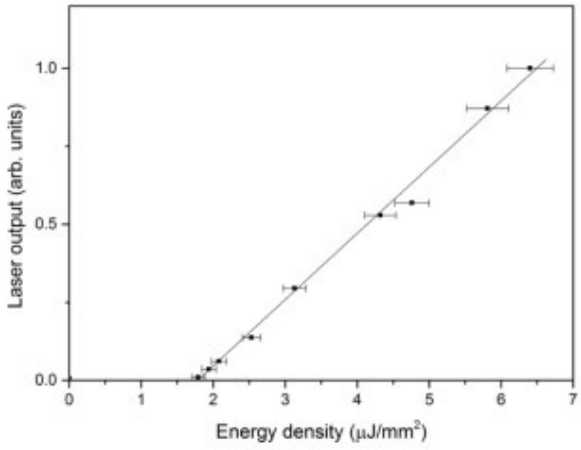

Fig. 6. The laser emission spectrum for the same device above threshold for dye concentration of $5\cdot10^{-3}$ mol/l.

Optics EXPRESS

Concerning the spectral behavior in some cases we have even observed a narrower linewidth of $\Delta\lambda \approx 0.4$ nm, but at the moment this result is not reliable as those reported in Figs. 4 and 7. In fact we should stress that these results have been obtained several times.

However, the measured threshold in all cases ranges from values lower than 2.0 μJ/mm^2 to 25 μJ/mm^2 with linewidth generally below 1 nm. The corresponding threshold energy of the pumping pulse ranges from 350 nJ to 5 μJ. Actual threshold is one order of magnitude or more lower than the typical one of the state-of-the-art optofluidic lasers regardless of the cavity design.

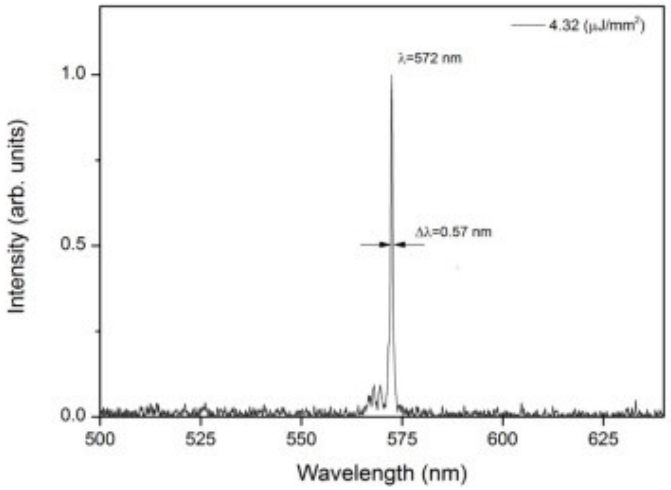

Fig. 7. Laser output vs energy density of the pumping pulse for dye concentration of $5 \cdot 10^{-3}$ mol/l.

In one single case a lower threshold of 0.1 μJ/mm^2 has been reported for an optofluidic ring resonator using aqueous quantum dots as active medium [16]. While concerning the linewidth is definitely much narrower than in the other mentioned Fabry-Perot based optofluidic lasers (0.5 nm against 3-5 nm). It leads to evaluate the quality factor Q in the range $0.5 \div 1 \cdot 10^3$ depending on the dye concentration. This result points out the advantage of the femtosecond micromachining technology for the cavity fabrication. In fact the high value of the quality factor means low losses due to the high precision achieved in the parallelism of the mirrors surfaces without the need of further adjustement. The all-fiber laser recently reported [17] allows high repetition rate with emission performances similar to our device. However, the fabrication steps look quite complex compared to our system and it appears of difficult integration with LOC technology.

For all these reasons the present device, not only overcome the performances of any up-to-date Fabry-Perot based micro-lasers cavities, but it is also competitive with most of the optofluidic lasers realized in the last decade. The obtained very narrow linewidth as well as its robustness allows to foreseeing possible integration the device for high sensitivity optical sensor. Moreover the Fabry-Perot cavity can work in a wide range of optofluidic laser emission wavelengths to be easily chosen by selecting the appropriate dye circulating in the microfluidic channel. The threshold around 2.0 μJ/mm^2 is very close to enter in the regime of inexpensive high power LED pumping.

The novelty is also the use of the ink-jet technology for realizing the inner mirrors, that are not in contact with the fluid active medium as in many optofluidic Fabry-Perot configurations, thus they are not subject to degradation due to chemical interaction with such a fluid.

Optics EXPRESS

The monolithic microfabrication combined with the huge flexibility shown by the two coupled technique allow adjusting the device performance for a wide range of applications which otherwise would require cumbersome integrations and alignment of each component (optical, microfluidic, ….) at every specific use.

4. Conclusions

We have successfully designed and fabricated an optofluidic laser Fabry-Perot resonator in fused-silica glass substrate. Such achievement has been possible by exploiting two direct writing fabrication techniques: the femtosecond laser micromachining and the inkjet printing technology. In this way a standard Fabry-Perot cavity has been integrated into an optofluidic chip.

The manufacturing procedure of this device satisfactorily addresses the main issue to make it attractive LOC technology: multi-step and complex procedures are replaced by an easy fabrication and robustness of the device.

The excellent results obtained in the performances of the optofluidic laser in term of emission linewidth and threshold confirm the recent claim that the femtosecond writing technology can be successfully used to create high quality optical cavities. In addition the use of high resolution inkjet printing technology allows realizing passive optical elements for optofluidic circuits providing a novel tool for their fabrication.

The flexibility is the strength of these coupled techniques, allowing testing different laser cavity geometries and size. Further developments of this analysis involve optimization of mirrors performances, optimum coupling investigation and use of different active media. Exploitation of this device in optical sensing is also planned.

Acknowledgments

The Authors wish to thank Maddalena Binda, Ph.D. for deep and thorough inkjet facilities training and the initial support with the mirror printing.

Research Article **Open Access**

F. Simoni*, P. Spegni, S. Bonfadini, D.E. Lucchetta, S. Lo Turco, and L. Criante

Optofluidic Microlasers based on Femtosecond Micromachining Technology

https://doi.org/10.1515/optof-2017-0002
Received December 12, 2016; revised February 8, 2017; accepted March 20, 2017

Abstract: We present the different optofluidic lasers which have been realized using the Femtosecond Micromachining technique to fabricate the monolithic optofluidic structures in glass chips. We show how the great flexibility of this 3D technique allows getting different kind of optical cavities. The most recent devices fabricated by this technique as ring shaped and Fabry-Perot resonators show excellent emission performances. We also point out how the addition of the inkjet printing technique provides further opportunities in realizing optofluidic chips.

Keywords: Optofluidics, Microlaser, Femtosecond Micromachining

1 Introduction

A milestone for the present research on optofluidic devices is represented by the work reported in 2003 by the group of Kristensen presenting the first example of "micro cavity fluidic dye laser" [1]. In that case the laser cavity was realized inside a microfluidic channel using metallic mirrors coated on the top and bottom of glass substrates which were sealed together. A multi-step process based on UV-lithography was used to build the microfluidic channels in the photoresist SU8. After this work several demonstrations of optofluidic lasers have been reported. In many cases the distributed feedback configuration (DFB) has been exploited to achieve challenging features such as low pump thresholds [2], tunable wavelengths [3], and single mode of operations [4]. In general the realization of these devices requires several processing steps, usually combining electron-beam and photo-lithography with soft lithography. Fabry-Perot resonators have also been realized by coating metallic mirrors on the edge of optical fibers or on the sides of the microfluidic channel [5–8]. Also in these cases the fabrication of the microfluidic structure required many steps resulting in a critical alignment of the laser cavity sub-parts.

High quality factor Q optical resonators have been realized as ring-shaped cavities fabricated on chip [9, 10]. Their resonances are given by the whispering gallery modes and allow lasing on a broad range of emission wavelengths. However these devices were realized with soft materials (like polydimethylsiloxane-PDMS) with limited chemical compatibility and hydrophobic behavior, that makes difficult their use in practical systems. Moreover, in such a case, the gain medium delivered into the resonator can degrade the quality factor of the cavity and the overall optical performance of the device.

On the other hand the actual spread of optofluidic lasers in the lab-on-chip (LOC) systems will be possible if they can be realized by using a simple process requiring few fabrication steps and offering a high flexibility concerning the resonator design. Additionally the final device should be robust from a mechanical point of view, with high chemical compatibility and good thermal stability and, ideally, the mirrors should not be in contact with the active medium solution avoiding any degradation phenomenon.

A method that may fulfill all these requirements is provided by femtosecond laser micromachining [11–14]. This is a simple and mask-less technique that allows a 3D fast prototyping thanks to its inherent ability to fabricate buried microstructures in transparent materials. Taking advantage from the high fluence delivered by ultrashort pulses, an extremely localized material modification is made possible with reduced thermal effects. In detail, considering transparent dielectric substrates, this is due to the non-linear effects that occur during light matter interaction, as the pulse width results shorter than typical thermal relaxation time of several materials. In particular, for *fused silica* glass it as been demonstrated that by playing with the laser fluence it is possible to obtain a

***Corresponding Author: F. Simoni:** Department SIMAU, Universitŕ Politecnica delle Marche, Ancona, Italy, E-mail: f.simoni@univpm.it
P. Spegni, D.E. Lucchetta: Department SIMAU, Universitŕ Politecnica delle Marche, Ancona, Italy
S. Bonfadini, S. Lo Turco, L. Criante: Center for Nano Science and Technology, Istituto Italiano di Tecnologia, Milano, Italy

smooth increase of the refractive index, hence directly embedded waveguides, as well as internal nano-cracks which basically constitute the skeleton of the microfluidic platform [12].

The full control of the laser "direct writing" of the chip structure is guaranteed through a computer-controlled advanced micromachining workstation. This Femtosecond Micromachining Technique (FMT) has several advantages over the conventional micro-channel molding: (i) it is very suitable for rapid prototyping; (ii) it has great flexibility since it is resistless and mask-less; (iii) it allows a precise and easy alignment of the entire microfluidic structure, at different depths inside the glass sample.

Since the same tool can be used to fabricate both the microfluidic channels and waveguides in the same glass substrate, it is easy to create monolithic optofluidic chips which are free of misalignment or vibrations during operation. After laser irradiation, the optofluidic circuit is obtained by chemical etching removing selectively the areas modified by the laser spot.

In the next section we will briefly review: the first demonstration of an optofluidic resonator realized by FMT given more than a decade ago [15] and a recently reported optofluidic ring resonator fabricated by femtosecond laser nanofabrication in two glass substrates melted together as post-process [16]. In the third section we will summarize our recent results by coupling FMT with high resolution ink-jet printing to realize low threshold Fabry-Perot resonators in monolithic microfluidic platforms

2 Previous resonator designs

The first demonstration of an optical micro-resonator fabricated by FMT inside a microfluidic platform has been reported by Midorikawa and co-workers in 2004 [15]. In this work the authors exploited the laser writing technique to integrate in a photo-sensitive glass substrate (Foturan) a micro-resonator cavity with a microfluidic circuit obtaining an optofluidic laser fully embedded in a glass chip. In this case, being the substrate a metal-ions rich structure, a further baking step between the laser irradiation and the chemical etching is required to complete the formation of the modified areas with enhanced etching selectivity [14]. Finally, a post baking of the sample was beneficial for smoothing the internal surfaces of the obtained hollow structures.

The realized device is shown in Fig. 1. A close inspection of the micro-resonator (Fig. 1(a)) reveals a square section chamber built crossing the microfluidic channel necessary to provide the gain medium solution. The optical resonator is realized by four mirrors placed at 45° with respect to the oscillating beam, as depicted in Fig. 1(c), constituted by empty hollow structures in order to induce total internal reflection at the glass-air interface. Therefore we actually have a ring cavity realized by the four mirrors and the gain medium in the chamber of about 1 mm^2 square section and 200 μm thickness, while the micro-channel in its center has an average diameter of 80 μm.

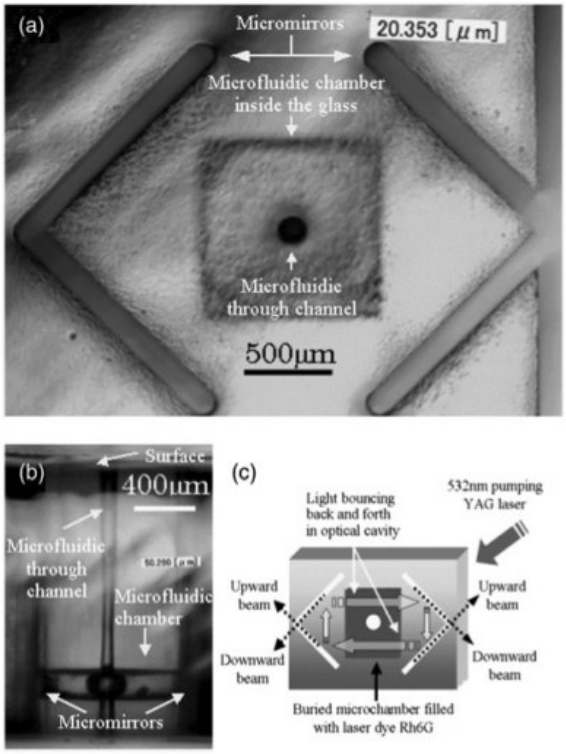

Figure 1: The first optofluidic laser realized by FMT: (a) Optical micrograph of the top view of the resonator, (b) optical micrograph of the side view of the whole structure including the cavity chamber and the microfluidic channel, (c) sketch of the ring cavity resonator with light path and output beams. (after Ref. [15])

Critical issues in this design are the smoothness of micromirror surface and their reciprocal alignment, since deviation from 45° and mutual orthogonal orientation increases optical losses thus reducing the quality factor of the resonator. On the other hand, in this first demonstration the laser output was detected by exploiting the light leakages tangential to the mirror surfaces as shown in Fig. 1(c).

The resonator performances were tested using a solution of dye Rh6G in ethanol ($2 \cdot 10^{-2}$ mol/l) pumped by the

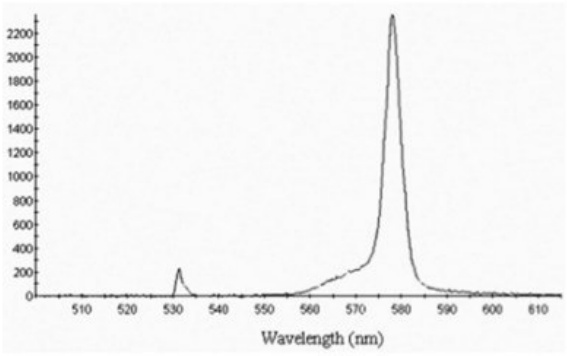

Figure 2: Typical emission spectrum of the microfluidic laser described in the text (after Ref. [15]). The peak at 532 nm is due to scattering from the pump beam.

second harmonic (λ = 532 nm) of a Nd:YAG laser pulse of 5 ns. The authors reported the detection of laser emission at a pump energy density of 16.6 μJ/mm^2 with an emission spectrum above threshold shown in Fig. 2, where an emission linewidth of about 5 nm can be observed.

While the threshold value is quite satisfactory as compared to most optofluidic lasers, the main drawbacks rely on the broad emission band and a poorly efficient output coupling. However it is an important demonstration of the potential of FMT for the realization of optical resonators embedded in glass. Nevertheless only recently interesting comparative works have come out, thanks to the progress and high performances achieved in these years by FMT.

In 2015 the design, fabrication, and characterization of a monolithically integrated optofluidic ring resonator using FMT has been reported [16].

In this case, the resonator is defined by a ring-shaped channel, that is connected to conventional microfluidic channels necessary to flow the gain medium solution. Again the all components were buried into a glass chip. Sketches of the resonator design are shown in Fig. 3. The sizes are the following: inner ring radius 150 μm; outer ring radius 170 μm, depth 40 μm.

EXploiting the 3D capability of fmt the microfluidic channels have been connected to the inner ring of the resonator, therefore not affecting the whispering gallery modes and not degrading the Q factor of the cavity. The ring resonator and the microchannels to flow the gain medium were fabricated in two different substrates using laser writing and chemical etching; a third step consisted in fusing the two substrate together in a high temperature furnace in order to get a single monolithic optofluidic platform, shown in Fig. 4.

This optofluidic laser was tested with a solution of Rhodamine 6G (Rh6G) in quinoline (n = 1.62) as solvent

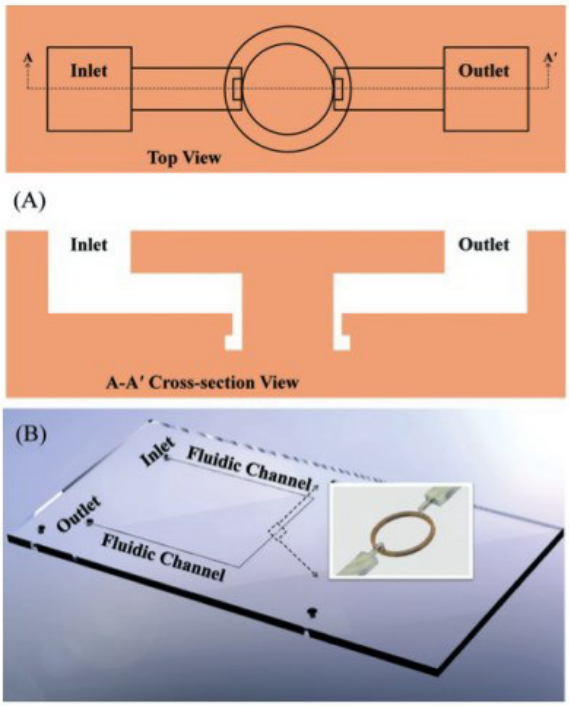

Figure 3: Design of the ring resonator based on the Whispering Gallery Modes realized by FMT: top view (A) , cross section (A-A') and overall scheme (B) (after Ref. [16]).

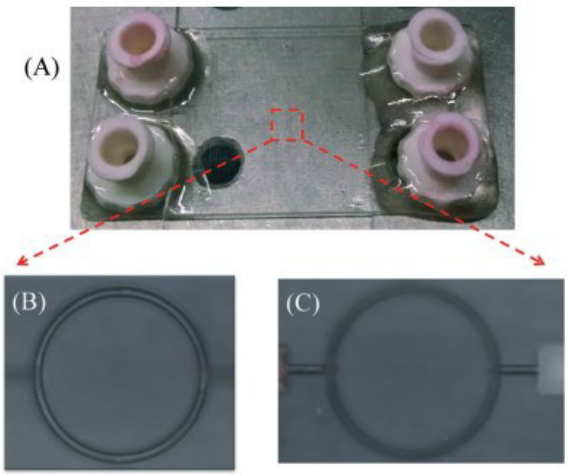

Figure 4: Practical realization of the ring resonator described in the text: (A) the whole optofluidic chip ; (B) the ring resonator embedded in glass; (C) microchannels providing the gain medium. (After Ref. [16]).

using an optical parametric oscillator as pumping source providing nanosecond pulses at 532 nm.

The characteristic emission is shown in Fig. 5. Data correspond to lasing of Rh6G in quinoline at concentration of $1{\cdot}10^{-3}$ *mol/l* and a flow rate of 3 µl/min. The lasing threshold was found at about 15 µJ/mm^2 with quality factor as high as $Q{\sim}3.3{\cdot}10^4$. These excellent results show the capability of FMT as powerful tool to fabricate optofluidic microlasers with state-of-the-art performances.

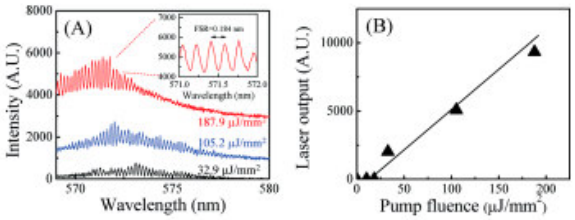

Figure 5: Laser emission from the optofluidic ring resonator based on the WGM: (A) spectrum above threshold; (B) plot of laser output vs pump fluence showing the threshold energy density. (After Ref. [16]).

3 Fabry-Perot resonators

The difficulty in realizing a Fabry-Perot microresonator depends on the critical alignment of the two mirror surfaces with respect to each other and on mechanical stability of such alignment. This is one of the main reasons why all the optofluidic microlaser based on Fabry-Perot cavity, which have been fabricated up to now, could not achieve a high quality factor providing emission linewidth of about 3–4 nm. These lasers were fabricated by coating with a metallic film on the side of microfluidic channel or the edge of the fibers used to collect the signal and using the soft-lithography technique to realize the microfluidic circuit [5–8].

It is evident that the alignment problems can be overcome if the cavity is fabricated as a rigid structure embedded in glass, since these problems can be solved during the cavity fabrication, without further need of adjustment. As previously reported, FMT provides the capability of realizing 3D structures completely buried in glass with high geometrical resolution thus fulfilling the above mentioned conditions. Since in this case the conventional coating approach is not possible, obtaining reflective surfaces in the realized structures is not an easy task. The solution is found by using a high resolution ink-jet printing technique in order to provide droplets of metallic ink on the suitable surfaces. In this way two metallic mirrors of controlled reflectivity and different geometry can be obtained in the glass embedded structure, thus realizing the required Fabry-Perot resonator.

The micromachining system used in this case is based on a regenerative amplified mode-locked femtosecond laser (Yb:KGW) with pulse duration of 240 fs at the fundamental wavelength of 1030 nm. The recording second harmonic (515 nm) was working at a repetition rate of 500 KHz and average power of 200 mW in order to get the nanograting writing regime [12]. The laser beam was focused in the bulk of the fused silica substrate to create a 3D structure by fine scanning of the sample, with resolution of 100 nm. The following step was chemical etching (HF acid, 20%, 35°C, 3–4 hours) to wash out the irradiated areas and create the microfluidic circuit. In this way different geometrical configurations have been realized. In the first one, depicted in Fig. 6a, two square section empty basins were fabricated on opposite sides of the microfluidic channel to realize a resonator with axis perpendicular to the gain medium flow (transversal cavity). In the second configuration (Fig. 6b) the empty basins were built close to the edges of the microchannel in order to realize the laser cavity along the gain medium flow (longitudinal cavity).

In both cases the final step was the completion of the mirrors fabrication. At this purpose an inkjet printer was used to provide droplets of silver organic ink on one surface of each basin through the previously realized open inlet for the optical fiber. The mirror reflectivity was adjusted by controlling the total volume of the ink droplets in such a way to get a high reflectivity mirror (∼95%) and an output mirror with reflectivity in the range 65%–95%. As final treatment the sample was heated at 150°C for 5 minutes on an hotplate, to let the solvent evaporate and obtain a solidified thin metallic layer.

The final device is completed by integration of an optical fiber close to the output mirror and two microtubes for inlet and outlet of the fluid gain medium. All the correspondent channels were made with conical shape in order to ensure best alignment during integration. Microscope photographs of the realized resonators are shown in Fig. 6 and typical final chips are shown in Fig. 7.

The performances of the Fabry-Perot resonators as laser sources were tested using as gain medium Rh6G in ethanol at concentrations in the range $1 \cdot 10^{-2}$ to $1 \cdot 10^{-4}$ mol/l and constant flow of 3.3 µl/min. Pumping was provided by the Second Harmonic of a pulsed Nd-YAG laser at 532 nm and pulse duration ∼ 5 ns. The signal collected by the optical fiber next to the output mirror was analyzed by a spectrometer with resolution of 0.13 nm.

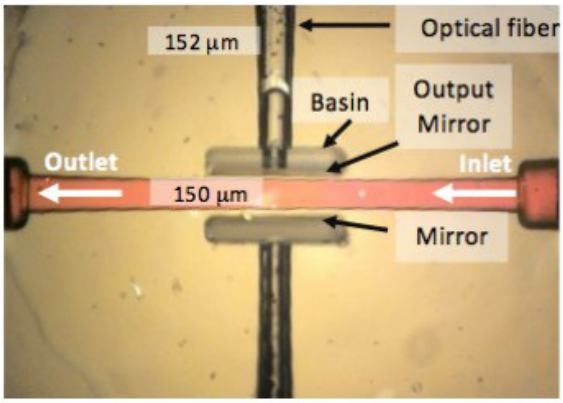

(a)

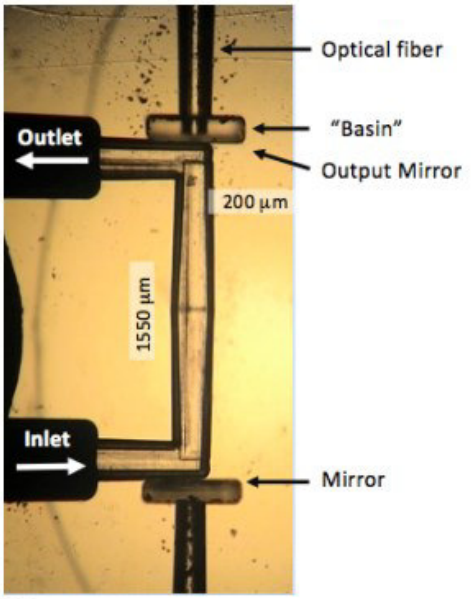

(b)

Figure 6: Microscope pictures of the Fabry-Perot resonators realized in glass chip: (a) transversal cavity; (b) longitudinal cavity.

Different focusing geometries were used for the case of transversal and longitudinal cavities respectively in order to optimize overlapping of the pump beam spot with the gain medium volume in the optical resonator. The power of the pump beam was finely controlled by rotating a half-wave plate placed before a polarizer and by neutral density filters. A reference beam was detected by a calibrated photodiode in order to measure the pumping energy of each pulse.

A sketch of the experimental apparatus used for testing the optofluidic laser performances is reported in Fig. 8

(a)

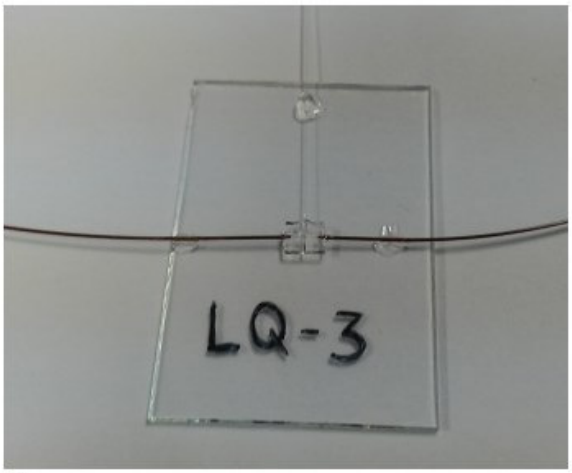

(b)

Figure 7: Glass chips including a Fabry-Perot resonator (a) and one chip integrated with microtubes and optical fiber and mounted on a glass substrate.

The performances of the optofluidic microlaser based on the transversal cavity are reported in Figs. 9–10. The lasing effect is clearly observed in the emission spectrum showing a peak growing over the fluorescence above a threshold for the energy of the pumping pulse. Such a threshold behavior (signature of the onset of the laser emission) is highlighted by plotting the full width at half maximum (FWHM in Fig. 10a) and the output signal (Fig. 10b) versus the energy density of the pumping pulse.

We observe a line width of about 2.5 nm above a threshold of 350 $\mu J/mm^2$. these results are interesting since they demonstrate the possibility of realizing an optofluidic microlaser based on Fabry-Perot resonator using the above described technology, however the threshold looks high with respect to previous examples of

optofluidic lasers based on fabry-perot cavity while the linewidth is of the same order of magnitude.

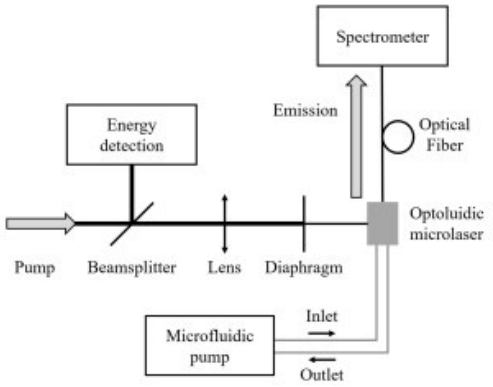

Figure 8: Sketch of the experimental set-up used to monitor the optofluidic laser performances.

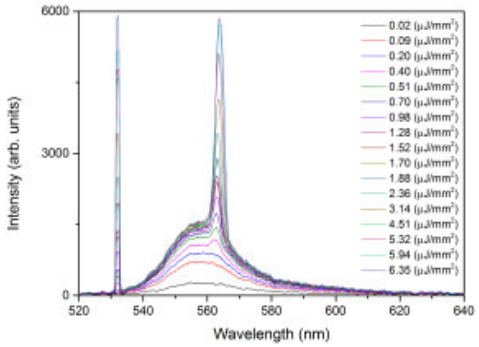

Figure 9: Emission spectrum of an optofluidic laser based on transversal F-P cavity with Rh6G in ethanol as gain medium ($1 \cdot 10^{-3}$ mol/l).

On the contrary the performances of the longitudinal cavity are very good for a simple fabry-perot resonator since they show a quality factor Q $\sim 10^3$ [17]. In this case using Rh6G in ethanol as active medium at a concentration of $5{\cdot}10^{-3}$ mol/l we get a threshold even below 2 μJ/mm^2 and a laser line width of ~0.5 nm as shown in Figs. 11–12.

These results show a behavior extremely better than any previously realized optofluidic laser based on Fabry-Perot resonator. On the other hand these performances also overcome the ones of many other optofluidic laser for what concern the pumping threshold, that is a critical parameter for practical applications of this device. In fact

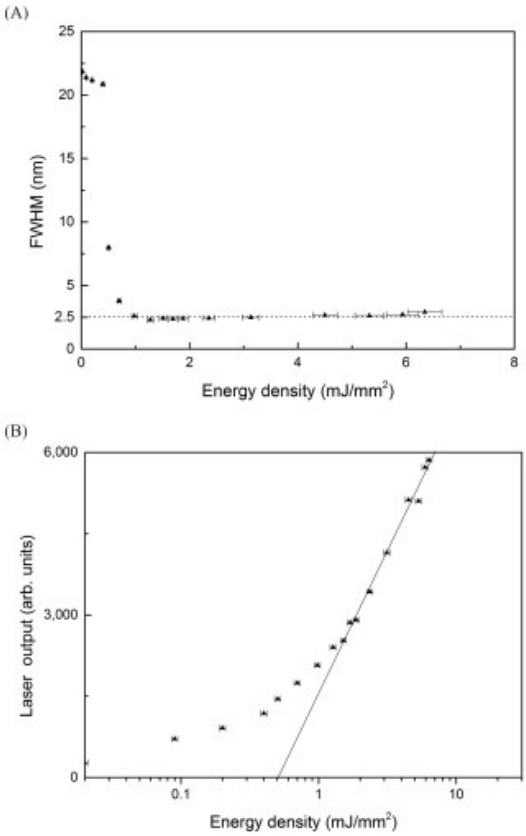

Figure 10: Linewidth of the emisson spectrum (A) and output signal (B) vs the energy density of the pump beam for the transversal F-P cavity. Gain medium was Rh6G in ethanol ($1 \cdot 10^{-3}$ mol/l).

most of the state-of-the-art optofluidic lasers manifest a threshold at least one order of magnitude higher than the one presented here. This result has been made possible by the larger gain volume due to the extended cavity length (1.55 mm) and by the precise fabrication technique offered by FMT allowing the required alignment of the two cavity mirrors.

4 Conclusions

We have presented different optofluidic laser resonators realized by FMT pointing out the great flexibility of this 3D technique to design and fabricate different kind of optical cavities. We have shown that devices with excellent performances can be realized both as ring shaped and Fabry-Perot resonators. The addition of the inkjet printing technique provides further opportunities in realizing optofluidic chips.

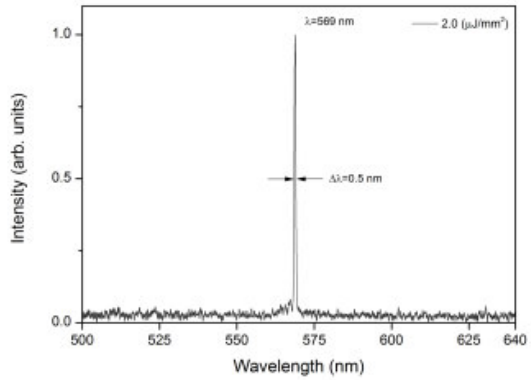

Figure 11: Emission spectrum of an optofluidic laser based on longitudinal F-P cavity with Rh6G in ethanol as gain medium ($5{\cdot}10^{-3}$ mol/l).

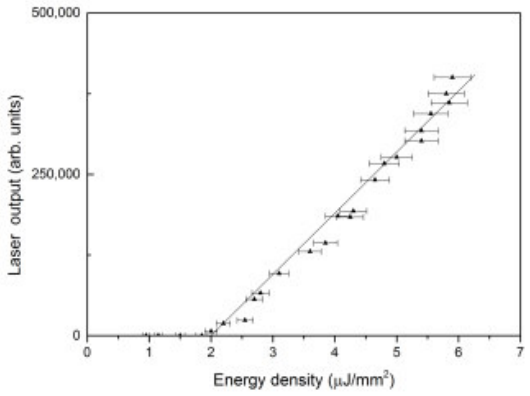

Figure 12: Output signal vs the energy density of the pump beam for the longitudinal F-P cavity. Gain medium was Rh6G in ethanol ($5{\cdot}10^{-3}$ mol/l).

The realized Fabry-Perot resonator fully embedded in glass achieved record performances with respect to any other optofluidic laser based on this cavity configuration. In fact the emission bandwidth of ~0.5 nm of the longitudinal cavity has to be compared to emission linewidth of 3–4 nm previously reported for optofluidic laser based on Fabry-Perot cavity. This result is due to the fabrication method allowing good and robust mirrors alignment during the femtosecond laser writing process. Moreover the threshold of 2 μJ/mm^2 is hardly obtained also with other cavity configurations. These performances are stable in time and can be found again checking the laser operation after several days.

In conclusion the FMT approach allows realizing robust devices through an easy fabrication method avoiding multistep and complex procedure, thus fulfilling one major requirement of lab-on-chip technology.

References

[1] B. Helbo, A. Kristensen and A. Menon, A micro-cavity fluidic dye laser, J. Micromech. Microeng. 2003, 13, 307–311.

[2] W.Song, A.E. Vasdekis, Z.Li and D. Psaltis, Low-order distributed feedback optofluidic dye laser with reduced threshold, *App. Phys. Lett.* 2009, **94**, 051117-3.

[3] M. Gersborg-Hansen and A. Kristensen, Tunability of optofluidic distributed feedback dye lasers, *Opt.Express* 2007, **15**, 137-142.

[4] G. Aubry, Q.Kou, J. Soto-Velasco, C. Wang, S. Meance, J. J. He and A.-M. Haghiri-Gosnet, A multicolor microfluidic droplet dye laser with single mode emission, *App. Phys. Lett.* 2011, **98**, 111111-3.

[5] Q. Kou, I. Yesilyurt and Y. Chen, Collinear dual-color laser emission from a microfluidic dye laser, *App.Phys.Lett.* 2006, **88**, 091101-3.

[6] G. Aubry, S. Meance, A.-M. Haghiri-Gosnet, Q.Kou, *Microelectronic Eng.* 2010, **87**, 765-768.

[7] Y. Yang, A. Q. Liu, L. Lei, L. K. Chin, C. D. Ohl, Q. J. Wang and H. S. Yoon, A tunable 3D optofluidic waveguide dye laser via two centrifugal Dean flow streams, *Lab Chip* 2011, **11**, 3182-7.

[8] D.V. Vezenov, B.T. Mayers, R.S. Conroy, G.M. Whitesides, P.T. Snee, Y.Chan, D.G. Nocera, and M.G. Bawendi, A Low-Threshold, High-Efficiency Microfluidic Waveguide Laser, *J.Am.Chem.Soc. Comm.* 2005, **127**, 8952-8953.

[9] X. Fan and S.-H. Yun, The potential of optofluidic biolasers, *Nature Methods* 2014, **11**, 141-147.

[10] A. Kiraz, Q. Chen, and X. Fan, Optofluidic Lasers with Aqueous Quantum Dots, *ACS Photonics* 2015, **2**, 707–713.

[11] Martynas M. Beresna, M. Gecevičius and P.G. Kazansky, Ultrafast laser direct writing and nanostructuring in transparent materials, *Advances in Optics and Photonics* 2014, **6**, 293–339.

[12] Roberto R. Osellame, H.JWM. Hoekstra, G. Cerullo and M. Pollnau, Femtosecond laser microstructuring: an enabling tool for opto?uidic lab-on-chips, *Laser & Photonics Reviews* 2011, **5**, 442–463.

[13] Rod R. Taylor, C. Hnatovsky and E. Simova, Applications of femtosecond laser induced self-organized planar nanocracks inside fused silica glass, *Laser & Photonics Reviews* 2008, **2**, 26–46.

[14] K. Sugioka, Y. Hanada and K. Midorikawa, Three-dimensional femtosecond laser micromachining of photosensitive glass for biomicrochips, *Laser & Photonics Reviews* 2010, **4**, 386–400.

[15] Y. Cheng, K. Sugioka, and K. Midorikawa, Microfluidic laser embedded in glass by three-dimensional femtosecond laser microprocessing, *Opt. Lett.* 2004 **29**, 2007-2009.

[16] H. Chandrahalim, Q. Chen, A.A. Said, M. Dugan and X.Fan, Monolithic optofluidic ring resonator lasers created by femtosecond laser nanofabrication, *Lab Chip* 2015, **15**, 2335-2340.

[17] F. Simoni, S.Bonfadini, P.Spegni, S. Lo Turco, D.E.Lucchetta and L.Criante, Low threshold Fabry-Perot optofluidic resonator fabricated by femtosecond laser micromachining, *Opt Exp* 2016, **24**, 17416-17423.

Glass-embedded Optofluidic Lasers

P. Spegni[1], **D. Tricarico**[1], **S. Bonfadini**[2],
S. Lo Turco[2], **L. Criante**[2], **and F. Simoni**[1]

[1]Department SIMAU, Università Politecnicadelle Marche, Ancona, Italy
[2]Center for Nano Science and Technology, Istituto Italiano di Tecnologia, Milano, Italy

Abstract— We report the realization and characterization of optofluidic lasers fully embedded in glass chips. By coupling femtosecond micromachining technology for writing the microfluidic circuit with high resolution inkjet technology to fabricate the cavity mirrors, it was possible to get robust Fabry-Perot resonators suitable for low threshold optofluidic lasers. Using as active medium a solution of Rh-6G in ethanol, linewidth as low as 0.5 nm has been obtained with a threshold for oscillation at a pump fluence of 2 $\mu J/mm^2$.

Different resonant cavities have been tested obtaining record performances for what concern pumping threshold and emission linewidth for Fabry-Perot based optofluidic lasers, achieving a quality factor $Q \sim 10^3$.

1. INTRODUCTION

The critical alignment of the two mirror surfaces with respect to each other the mechanical stability of such alignment is a major issue in realizing a Fabry-Perot microresonator suitable for laser cavity. For this reason the reliability of the optofluidics laser based on this cavity design has been limited, since they have been fabricated by coating a metallic film on the side of microfluidic channel or the edge of the fibers used to collect the signal and using the soft-lithography technique to realize the microfluidic circuit [1–4]. In any case a low quality factor was achieved not allowing emission linewidth narrower than 3–4 nm. On the other hand Femtosecond Micromachining Technology (FMT) has been proved to be an efficient method to realize robust optofluidic circuit in 3D according to a variety of possible designs [5–8] and to obtain high Q ring resonators [9]. Based on these previous achievements we have coupled FMT with ink jet printing technology to realize optofluidic laser fully embedded in glass based on Fabry-Perot resonator. Due to the high precision of the channels fabrication and the robustness of the realized mirrors we have been able to achieve record performances optofluidic laser with a Fabry-Perot cavity [10]. We summarize in the following the main characteristics of the device and the different configuration investigated.

2. DEVICE FABRICATION

The optofluidic device was realized exploiting FMT with equipment based on a regenerative amplified mode-locked femtosecond laser (Yb:KGW) with pulse duration of 240 fs at the fundamental wavelength of 1030 nm. For the recording process second harmonic (515 nm) was used at a repetition rate of 500 kHz and average power of 200 mW; these parameters allowed to work in the nanograting writing regime [6] necessary to have efficient chemical etching The laser beam was focused in the bulk of the fused silica substrate, the designed 3D structure was obtained through a fine scanning of the sample, with resolution of 100 nm. After laser recording chemical etching (HF acid, 20%, 35°C, 3–4 hours) was necessary to wash out the irradiated areas in order to get the microfluidic circuit. Using this method it was possible to realize and study two different geometrical configurations They are defined as (i) transversal cavity and (ii) longitudinal cavity, taking into account the flow direction of the gain medium. In the first case the optical cavity is realized in a direction perpendicular to it, while in the second case it is along the same direction. The schemes of such cavities are shown in Fig. 1.

In both cases two basins were realized suitable for mirror fabrication. To this aim an inkjet printer was used to provide droplets of silver organic ink on one surface of each basin through the previously realized open inlet indicated in the figure. The mirror reflectivity could be controlled being dependent on the total volume of the ink droplets. In this way we got a high reflectivity mirror ($\sim 95\%$) and an output mirror with reflectivity in the range 65%–95%. The final treatment was the sample heating at 150°C for 5 minutes placing it on a hotplate; it allows the solvent evaporation and solidification of the thin metallic layers.

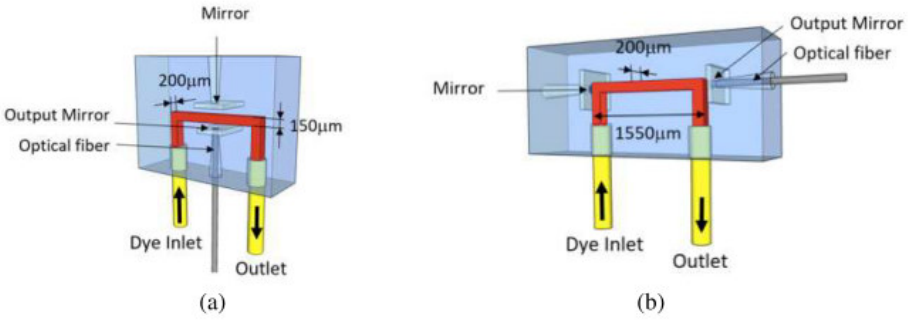

Figure 1: (a) Scheme of the transversal cavity; (b) scheme of the longitudinal cavity.

The final step was the integration of an optical fiber close to the output mirror necessary to collect the laser signal and the connection of two microtubes for the inlet and outlet of the fluid gain medium.

The longitudinal cavity was realized with different lengths: 0.7 mm, 1.5 mm, 2.5 mm. The gain media investigated were the following laser dyes dissolved in ethanol: Rhodamine 6G, DCM, Pyrromethene-597.

3. RESULTS AND DISCUSSION

Firstly the different optical resonators were studied and compared by using Rh6G as active medium. Pumping beam was given by the second harmonic of a pulsed Nd-YAG laser at 532 nm and pulse duration 5 ns. The focusing geometry controlled by cylindrical lens and diaphragm was adapted to the cavity configuration in order to have the best overlap between pump spot size and optical cavity.

The pump power was finely controlled by half-wave plate, polarizer and neutral density filter and the spot size accurately measured.

The signal collected by the optical fiber integrated in the chip was analyzed by a spectrometer having a resolution of 0.13 nm.

Laser emission was easily detected from the transversal cavity laser when using Rh6G in ethanol at concentration 10^{-3} mol/l, however the pumping threshold was pretty high ($\sim 400\,\mu J/mm^2$) with emission bandwidth only slightly lower than previously reported optofluidic laser based on Fabry-Perot resonator. On the contrary when studying the behavior of the longitudinal cavity laser we have found excellent performances with threshold decreasing to value below $2\,\mu J/mm^2$ by increasing the cavity length and bandwidth of about 0.5 nm that corresponds to quality factor $Q > 10^3$.

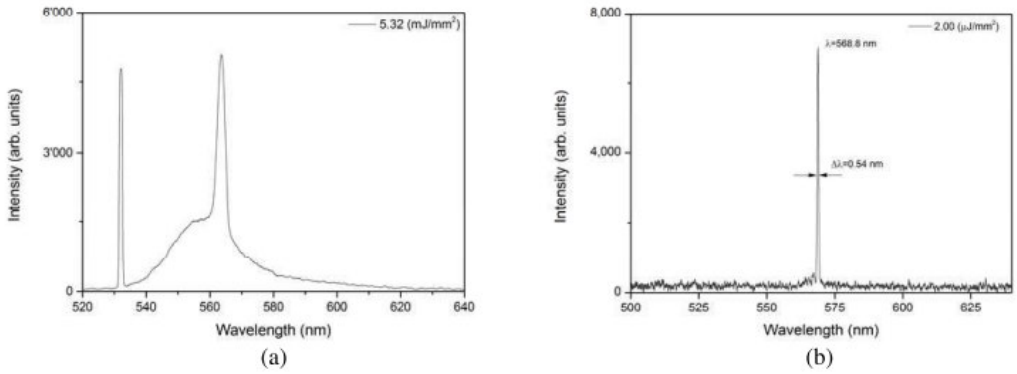

Figure 2: Emission spectrum of glass embedded optofluidic laser: (a) transversal cavity; (b) longitudinal cavity 1.5 mm long.

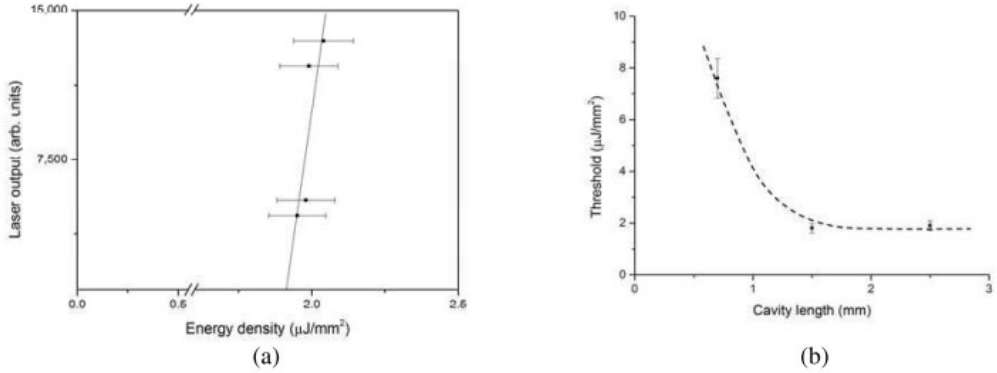

Figure 3: (a) Output laser peak vs pumpenergy density for the longitudinal cavity 2.5 mm long (Rh6G, $5 \cdot 10^{-3}$ mol/l); (b) Threshold for laser emission vs resonator length for the longitudinal cavities (Rh6G, $5 \cdot 10^{-3}$ mol/l).

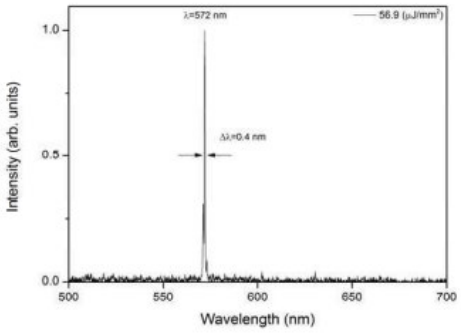

Figure 4: Emission spectrum of glass embedded optofluidic laser: longitudinal cavity 1.5 mm long. Gain medium: PM-597 solution in ethanol (10^{-3} mol/l).

The Fig. 2 reports the optimized emission spectrum of the transversal cavity (a) and of the longitudinal cavity with length 1.5 mm (b).

In the following Fig. 3 we show the characteristic output signal vs the pump energy density for the longitudinal cavity 2.5 mm long (a) and the decrease of threshold with the length of the resonator (b). We observe a remarkable decrease by increasing the length from 0.7 to 1.5 mm and a negligible one for further increase of the length. Actually the strongest effect of the length increase from 1.5 mm to 2.5 mm is the increase of the active region volume with a further increase of the involved cavity modes; this leads to an emission not so sharp as the one shown in Fig. 2.

The best performing longitudinal cavity 1.5 mm long has been tested by using different gain media as already mentioned. Somewhat higher threshold was measured both using DCM and Pyrromethene-597, however in the latter case very narrow and reliable peak was easily found as shown in Fig. 4.

4. CONCLUSIONS

The presented results point out the possibility of efficiently exploiting FMT and inkjet printing to develop Fabry-Perot laser resonators for the optofluidic chip technology. The reported devices represent the first examples of fully glass embedded lasers. They show record performances with respect to any other optofluidic laser based on this type of resonator with emission band as low as 0.5 nm to be compared to the emission linewidth of 3–4 nm of previously reported devices. This result was made possible by the fabrication method allowing good and robust mirrors alignment in the femtosecond recording process. The achieved threshold is among the best obtained in optofluidic

devices. The stability in time of the performances of our lasers is also remarkable.

Further development involve investigation of more complex cavity geometry and inclusion of tuning mechanisms.

REFERENCES

1. Kou, Q., I. Yesilyurt, and Y. Chen, "Collinear dual-color laser emission from a microfluidic dye laser," *App. Phys. Lett.*, Vol. 88, 091101-3, 2006.
2. Aubry, G., S. Meance, A.-M. Haghiri-Gosnet, and Q. Kou, *Microelectronic Eng.*, Vol. 87, 765–768, 2010.
3. Yang, Y., A. Q. Liu, L. Lei, L. K. Chin, C. D. Ohl, Q. J. Wang, and H. S. Yoon, "A tunable 3D optofluidic waveguide dye laser via two centrifugal Dean flow streams," *Lab. Chip.*, Vol. 11, 3182–7, 2011.
4. Vezenov, D. V., B. T. Mayers, R. S. Conroy, G. M. Whitesides, P. T. Snee, Y. Chan, D. G. Nocera, and M. G. Bawendi, "A low-threshold, high-efficiency microfluidic waveguide laser," *J. Am. Chem. Soc. Comm.*, Vol. 127, 8952–8953, 2005.
5. Beresna, M. M., M. Gecevičius, and P. G. Kazansky, "Ultrafast laser direct writing and nanostructuring in transparent materials," *Advances in Optics and Photonics*, Vol. 6, 293–339, 2014.
6. Osellame, R. R., H. J. W. M. Hoekstra, G. Cerullo, and M. Pollnau, Femtosecond laser microstructuring: An enabling tool for optofluidic lab-on-chips," *Laser & Photonics Reviews*, Vol. 5, 442–463, 2011.
7. Taylor, R. R., C. Hnatovsky, and E. Simova, "Applications of femtosecond laser induced self-organized planar nanocracks inside fused silica glass," *Laser & Photonics Reviews*, Vol. 2, 26–46, 2008.
8. Sugioka, K., Y. Hanada, and K. Midorikawa, "Three-dimensional femtosecond laser micromachining of photosensitive glass for biomicrochips," *Laser & Photonics Reviews*, Vol. 4, 386–400, 2010.
9. Chandrahalim, H., Q. Chen, A. A. Said, M. Dugan, and X. Fan, "Monolithic optofluidic ring resonator lasers created by femtosecond laser nanofabrication," *Lab. Chip.*, Vol. 15, 2335–2340, 2015.
10. Simoni, F., S. Bonfadini, P. Spegni, S. Lo Turco, D. E. Lucchetta, and L. Criante, "Low threshold Fabry-Perot optofluidic resonator fabricated by femtosecond laser micromachining," *Opt. Exp.*, Vol. 24, 17416–17423, 2016.